Boundary Layer flow of a Casson Fluid Past a Thin Needle

A thesis submitted to
NATIONAL INSTITUTE OF TECHNOLOGY WARANGAL, (T.S.)
for the award of the degree of
DOCTOR OF PHILOSOPHY
in
MATHEMATICS

by
SARITHA GORANTALA
(Roll No. 720104)

UNDER THE SUPERVISION OF
Prof. D. SRINIVASACHARYA

DEPARTMENT OF MATHEMATICS
NATIONAL INSTITUTE OF TECHNOLOGY
WARANGAL - 506 004, INDIA

MAY 2024

C E R T I F I C A T E

This is to certify that the thesis entitled " **Boundary Layer Flow of a Casson Fluid Past a Thin Needle** " submitted to National Institute of Technology Warangal, for the award of the degree of ***Doctor of Philosophy***, is the bonafide research work done by **Mrs. SARITHA GORANTALA** (ROll No 720104) under my supervision. The contents of this thesis have not been submitted elsewhere for the award of any degree.

Dr. D. Srinivasacharya
Professor
Department of Mathematics
National Institute of Technology,
Warangal, T.S., INDIA

.

DECLARATION

This is to certify that the work presented in the thesis entitled **"Boundary Layer Flow of a Casson Fluid Past a Thin Needle"**, is a bonafide work done by me under the supervision of **Prof. D. SRINIVASACHARYA** and has not been submitted elsewhere for the award of any degree.

I declare that this written submission represents my ideas in my own words and where others' ideas or words have been included, I have adequately cited and referenced the original sources. I also declare that I have adhered to all principles of academic honesty and integrity and have not misrepresented or fabricated or falsified any idea / data / fact /source in my submission. I understand that any violation of the above will be a cause for disciplinary action by the Institute and can also evoke penal action from the sources which have thus not been properly cited or from whom proper permission has not been taken when needed.

Saritha Gorantala

Roll No. 720104

Date:_____

Dedicated to

My Parents

&

Mr.P.Balabhaskar and P.Megha Chandrika

ACKNOWLEDGEMENTS

It is a rare privilege and boon that I could associate myself with Dr. D. Srinivasacharya, Professor of Mathematics, National Institute of Technology Warangal, India, for pursuing my research work. I sincerely record my gratitude for his invaluable guidance and constant encouragement throughout the preparation of this thesis and his involvement and meticulous supervision while my work was in progress. With his inimitable qualities as a good teacher, he chiseled my path towards perfection. He has been a perpetual source of inspiration, spiritual guidance, encouragement, and enlightenment since I first met him. He is the one who ensured that the duration of my research work was both educational and fun. He has been a great source of motivation and inspiration. The thesis would not have seen the light of the day without his unrelenting support and cooperation. I deem it a privilege to have worked under his amiable guidance. My vocabulary is inadequate to express my gratitude. I also thank madam Smt. D. Jaya Srinivasacharya for her hospitality and patience during our elongated discussions with my supervisor.

I am grateful to Prof.A.Benerji Babu, Head, and Prof.H.P.Rani, Dr. P. Muthu, former Heads, Department of Mathematics for providing necessary help and support throughout my research period.

I take this opportunity to thank Prof. Y. N. Reddy, Prof. K. N. S. Kasi Viswanadham, Prof. Debashis Dutta, and Department of Mathematics for their valuable suggestions, moral support and encouragement.

I thank the members of the Doctoral Scrutiny Committee, Prof. J. V. Ramana Murthy, Dr. Ch. Ramreddy and Dr. K. Kaladhar, Department of Mathematics, and Dr. G. Uday Bhaskar Babu, Department of Chemical Engineering for their valuable suggestions, moral support, and encouragement while my work was in progress.

I place on record my gratitude to all the faculty members of the Department of Mathematics, for their constant encouragement.

I express my sincere thanks to the Director, National Institute of Technology, Warangal for providing me QIP Fellowship (AICTE, GoI) to carry out my research work.

I thank Dr. K. Sita Ramana, Dr. R. Shravan Kumar,Dr. B. Rajender, Ms. Nidhi Humnekar, Mr. Pankaj Barman, Mr. Sarthak Sharma and all other research colleagues in the Department of Mathematics and my friends, who helped me during my Ph.D. for being cooperative and also for making my stay in the NITW campus fruitful and enjoyable every moment.

My heartfelt gratitude goes to my parents, late G. Kedari and Smt.Rajeshwari, in-laws, P.Rajanarasihma and Smt.Lakshmi and My Sisters and Brother-in-laws whose encouragement and blessings inspired me to finish my job ahead of schedule. I am overjoyed to thank my family members for their contributions to the completion of this job. All of their prayers, support, love, and affection have been the driving force behind what has happened.

Also, most importantly, I would like to thank my better half, Mr. P.Bala Bhaskar and my child P. Megha Chandrika for their support,prayers,patience and understanding that were vital to complete this thesis. Without their help and encouragement, I would not have been finished this thesis.

Saritha Gorantala

Contents

[1]Accepted for publication in "**WSEAS Transactions on Heat and Mass Transfer "**
[2]Accepted for publication in "**Discontinuity, Nonlinearity, and Complexity "**,
[3]Communicated to "**International Journal of Applied and Computational Mathematics**
[4]Publication in"**Journal of Xidian University"**

[5] Accepted to "**Journal of Advanced Research in Fluid Mechanics and Thermal Sciences**"
[6] Communicated to "**Journal of Applied and Computational Mathematics**"

[7] Communicated to "**Heat Source**"

[8] Communicated to "**Mathematics and Computers in Simulation**"

Part I

INTRODUCTION

Chapter 1

Preliminaries and Review

1.1 Introduction

The connection between fluid dynamics and nature, as well as its numerous applications and real-world problems, has made fluid dynamics a passionate, thought-provoking, and challenging field of modern science. The quest for a deep comprehension of the subject has advanced related mathematical sciences as well as the field itself, including applied mathematics, numerical computing, physical and mechanical sciences, and applied mathematics. A listing of all fluid dynamics applications in technology would be impossible due to the wide use of fluids in technological devices.

Pure science fields such as atmospheric sciences (global circulation, global warming, mesoscale weather patterns), oceanography (pollution effect on living organisms, ocean circulation patterns), geophysics (study of plate tectonics, earthquakes, volcanoes, magnetic fields), astronomy (galactic structure, clustering, stellar evolution, supernovae), and biological sciences (circulatory, cellular processes, and respiratory systems in animals) can all benefit from the axioms and principles of fluid dynamics.

The literature on fluid dynamics has been greatly enriched by studies of convective heat and mass transfer across different geometries and cross sections. The patterns of fluid flow around surfaces of different cross-sections, such as spheres, cylinders, and cones, are real-

istic to examine. These flows have gained strong interest in view of their wide range of applications in a broad variety of engineering processes. These include fiber technology, high-speed thermal aerodynamics, nuclear cooling systems, surface treatment, spray deposition processes, polymer engineering, etc. In the past, simplified formulations were used to analyze fluid flow behavior analytically.

1.2 Casson fluid

Fluids that obey Newton's Law of Viscosity are known as Newtonian fluids. Some examples of Newtonian fluids include water and organic solvents. For those fluids, the viscosity is only dependent on temperature.

Non-Newtonian fluids are a type of fluid that doesn't follow Newton's law of viscosity, which states that the rate of deformation (shear strain) of a fluid is directly proportional to the applied shear stress. In simpler terms, the viscosity of Newtonian fluids remains constant regardless of the applied force or shear rate.

However, non-Newtonian fluids change their viscosity when a force is applied to them. This means their flow behavior depends on factors such as shear rate, stress, temperature, and time.

The Casson fluid model was proposed by Casson [1]. The fluid is shear-thinning. These fluids exhibit no viscosity at infinite shear rates and infinite viscosity at zero shear rates. It is noteworthy that this model reduces to a Newtonian liquid if yield stress is less than shear stress. For use in practical applications, it offers a simple way to calculate the two parameters: apparent yield stress and Casson viscosity. As a consequence of its applications in the fields of drilling operations, metallurgy, food processing, polymer processing industries, synthetic lubricants, biomedical fields, printing ink preparation, and so forth, the Casson fluid model is being employed in a broad spectrum of theoretical and computational studies. Casson fluid the rheological equation of the state are

$$\tau_{ij} = \begin{cases} 2(\frac{\tau_y}{\sqrt{2\pi}} + \mu_B)e_{ij} & for \quad \pi > \pi_c \\ 2(\frac{\tau_y}{\sqrt{2\pi_c}} + \mu_B)e_{ij} & for \quad \pi < \pi_c \end{cases} \tag{1.1}$$

where τ_y is yield stress, μ_B is plastic dynamic viscosity of the Casson fluid, e_{ij} represent the $(i,j)^{th}$ component of the rate of deformation, $\pi = e_{ij}e_{ij}$, π_c is the critical value π.

The momentum equation for Casson Fluid

$$\rho(\bar{q}\cdot\nabla)\bar{q} = -\nabla P + \mu_B(1+\frac{1}{\beta})\nabla^2\bar{q} + \rho\bar{f} \tag{1.2}$$

where $\beta = \dfrac{\mu_B\sqrt{2\pi_c}}{\tau_y}$ is the Casson fluid parameter.

1.3 Basic Terminology

Boundary Layer Theory

The boundary layer theory was proposed by Prandtl in 1904 [2].The main idea is to divide the flow into two major parts. The larger portion is concerned with a free stream of fluid that is farther away from the wall and is deemed inviscid. The smaller portion is a thin layer near the wall that experiences the effects of viscosity. This thin layer where friction effects cannot be ignored is called the **boundary layer**. Through experimental observations, Prandtl found that large velocity gradients normal to the streamlines occur only in regions close to the wall. Using this, one can obtain a simplified form of governing equations by estimating the order of magnitude of the various terms in the conservation equations. Hence, the derived equations are called boundary layer equations [3].

There are many reasons why boundary layer theory is used very frequently in solving fluid flow and heat transfer problems (Bradshaw and Cebeci [4], Bejan [5]). The most important reason is that the boundary layer equations are parabolic, while the full Navier-Stokes equations are elliptic or sometimes even hyperbolic, which are of considerable complexity. Thus, parabolic partial differential equations can be solved much easier. Further, boundary layer theory also gives more information about the flow separation from the surface of a body than full Navier-Stokes equations. However, the boundary layer equations are available only up to the separation point, and beyond this point, the full Navier-Stokes equations have to be solved with much complexity.

Heat Transfer

When internal energy is transferred between areas or components within a medium, heat transfer occurs. It often occurs from a region with higher temperatures to one with lower

ones. There are three modes in which heat transfer takes place. Convection, radiation, and conduction are them. In a thermodynamic system, conduction is the molecular transfer of heat within or between bodies. The fluid in the medium, or the fluid medium itself, is the subject of convection. Convection is the term used to describe the heat transfer that occurs when a fluid moves from one area of the medium to another. The process by which a substance's internal energy is transformed into radiant energy is known as radiation heat transfer. Convective heat is heat transferred by both convection and conduction.

Mass Transfer

Mass transfer is the tendency of a component in a mixture to move from a region of high concentration to a region of a region of low concentration. There are two ways that mass is transferred: diffusion mass transfer and convective mass transfer. A concentration gradient, temperature gradient, or pressure gradient can all lead to diffusion mass transfer. A phenomenon known as convective mass transfer occurs when matter moves from a fluid to a solid surface or back, transferring mass between the fluid and the surface.

Mixed Convection

Mixed convection is a heat transfer phenomenon that occurs when both natural convection and forced convection mechanisms contribute to heat transfer in a fluid (liquid or gas). In natural convection, heat transfer is driven by buoyancy forces that arise due to temperature differences in the fluid, causing the fluid to move and transfer heat. Forced convection, on the other hand, involves the movement of fluid induced by external means such as a pump or a fan.

In mixed convection, both natural and forced convection effects are present simultaneously, and their relative importance depends on various factors such as the geometry of the system, flow conditions, and the magnitude of external forces.

Cross Diffusion Effects

The flow in simultaneous heat and mass transfer mechanisms is driven by density variations induced by a temperature or concentration gradient and material composition at the same time.

The mass flux generated by temperature gradients is known as thermal diffusion, also identified as thermo-diffusion or the Soret effect [6]. The Dufour effect, also known as the diffusion-thermo effect, describes the heat flux generated by a concentration gradient.

Variable fluid properties

In most of the studies, the thermophysical properties of fluids were assumed to be constant. However, it is known that these properties may change with temperature, especially for fluid viscosity and thermal conductivity. For example, the absolute viscosity of water decreases by 240% when the temperature increases from 10^oC to 500^oC. The increase in temperature in lubricating fluids causes internal friction, which changes the viscosity of the fluid, which no longer remains constant. The increase in temperature accelerates the transport process by lowering viscosity throughout the temperature boundary layer, influencing the heat transfer rate. Therefore, to predict the heat transfer rate accurately, it is necessary to take into account this variation in viscosity and thermal conductivity.

Kays and Crawford [7] presented many correlations between fluid physical characteristics and temperature. The first researchers to look at the impact of variable fluid characteristics on laminar boundary layer flow were Herwig and Gersten [8]. Applications include the drawing of plastic films and glass fiber, the study of spilling pollutant crude oil over the surface of seawater, the cooling of nuclear reactors, petroleum reservoir operations, food processing, welding and casting in manufacturing processes, wire drawing, paper production, glass fiber production, the glueing of labels on hot bodies, etc. Despite its importance in many applications, this effect has received little attention. In recent years, fewer researchers have analyzed the influence of variable properties on convective flows over stretched surfaces.

Thermal Radiation

Applications for the radiative effect are numerous in the domains of physics and engineering, space technology, high-temperature processes, power generation, cooling nuclear reactors, and liquid metal fluids. However, the impact of radiation on boundary layer flows is largely unknown. Thermal radiation has a considerable impact on heat transfer and temperature distribution in the boundary layer flow when temperatures are high. When heat-controlling factors have a partial influence on the final product's quality, thermal radiation influence may be a major factor in managing heat transfer. The radiation term is linearized in the

majority of studies that are presently available in the literature.

Chemical Reaction

A chemical reaction is the process by which a mixture of chemical components is changed into something else. Traditionally, chemical reactions have been defined by a chemical equation and have included just the locations of electrons in the formation and breaking of chemical bonds between atoms; no modifications were made to the elements present or to the nuclei. A branch of science known as "nuclear chemistry" studies the chemical interactions between radioactive and unstable materials, which can result in both nuclear and electronic changes. The influence of chemical reactions is a crucial aspect in analyzing heat and mass transport in many disciplines of engineering, industry, and science.

Viscous Dissipation

Viscous dissipation refers to the conversion of mechanical energy into heat due to internal friction or viscosity within a fluid. This phenomenon occurs when a fluid, such as a liquid or gas, experiences deformation or flow, and the viscous forces within the fluid lead to the generation of heat. It is required in viscous fluids such as polymers and oils. It has numerous uses in industry and technology. Viscous dissipation is commonly used in electrical equipment like light bulbs, electric heaters, electric stoves, and electric fuses.

1.4 Successive Linearization Method

The Successive Linearisation Method (SLM) is one of the linearization methods and it is proposed and developed by Makukula *et al.* [9] and Motsa and Sibanda [10]. This procedure has been used effectively to linearize several boundary value problems in heat and mass transfer investigations ([11, 12], [13], [14] erc.).

To solve the nonlinear boundary value problem in an unknown function $z(x)$ using SLM, we assume that $z(x)$ is approximated by

$$z(x) = z_r(x) + \sum_{m=0}^{r-1} z_m(x) \tag{1.3}$$

where $z_r(x)$ is an unknown function and $z_0(x)$, $z_1(x) \cdots z_{r-1}(x)$ are known approximate solutions. The unknown function $z_r(x)$ can be determined by solving the linearized differential equation in $z_r(x)$ obtained by substituting (1.3) in the given nonlinear differential equation and linearizing the resulting differential equation using Taylor's series expansion. Hence, the subsequent solutions $z_r(x), r \geq 1$, are obtained by successively solving the linear equations for $z_r(x), r \geq 1$ given that the previous guess $z_{r-1}(x)$ is known. The initial guess $z_0(x)$ is taken such that it satisfy the given conditions on the boundary.

Any numerical scheme can used to solve the above iterative sequence of linearized differential equations. The SLM method has been successfully applied to a wide variety of scientific models over finite and semi-infinite intervals. The SLM approximation was applied to boundary value problems which possess smooth solutions.

1.5 Chebyshev Collocation Method

The Chebyshev collocation method ([15, 16, 17, 18]) is based on the Chebyshev polynomials defined on the interval $[-1, 1]$. To solve a differential equation, in an unknown function $z(x)$, on $[-1, 1]$, the interval $[-1, 1]$ is to be descritized at $N+1$ Gauss-Lobatto collocation points, which are given by

$$\xi_j = \cos \frac{\pi j}{N}, \quad j = 0, 1, 2, ..., N \tag{1.4}$$

Next, the unknown function $z(x)$ and its derivatives are guestimated at the collocation points as follows

$$z(\xi) = \sum_{k=0}^{N} z(\xi_k) T_k(\xi_j) \quad \frac{d^{\boldsymbol{r}} z}{dx^{\boldsymbol{r}}} = \sum_{k=0}^{N} \left[\frac{2}{(b-a)} \mathbf{D}_{kj} \right]^{\boldsymbol{r}} z(\xi_k), \tag{1.5}$$

where $T_k(\xi) = \cos(k \cos^{-1} \xi)$ is the k^{th} Chebyshev polynomial and $\mathbf{D}$ being the Chebyshev spectral differentiation matrix whose entries are defined as ([15, 17, 18]) "

$$\left.\begin{array}{l} \mathbf{D}_{00} = \frac{2N^2+1}{6} \\ \mathbf{D}_{jk} = \frac{c_j}{c_k} \frac{(-1)^{j+k}}{\xi_j - \xi_k}, \;\; j \neq k; \;\; j, k = 0, 1, 2 \cdots, N, \\ \mathbf{D}_{kk} = -\frac{\xi_k}{2(1-{\xi_k}^2)}, \;\; k = 1, 2 \cdots, N-1, \\ \mathbf{D}_{NN} = -\frac{2N^2+1}{6} \end{array}\right\} \tag{1.6}$$

" Substituting equations (1.4)-(1.5) into the given differential equation, we obtain the system

of the algebraic equation gven by

$$\mathbf{A}_{r-1}\mathbf{X}_r = \mathbf{R}_{r-1}, \tag{1.7}$$

in which A_{r-1} is a square matrix of order $(N+1)\times(N+1)$ while X_r and R_{r-1} are $(N+1)^{th}$ order coloumn vectors. Writing the boundary conditions in terms of Chebyshev polynomials, incorporating them in the above system of equations and solving the reduced system of algebraic equations, we obtain the solution of the given differential equation. If the domain is $[a, b]$, then it will be transformed to the domain $[-1, 1]$ by using the using suitable transformation.

1.6 Literature Review

The examination of non-Newtonian fluid flow intrigued many investigators on account of its applicability to a variety of engineering problems. These include crystal growth, tarry fuel abstraction from petroleum-based goods, the freezing of nuclear reactors, the manufacture of plastic materials, etc. Numerous analytical and numerical analyses have been reported in the literature for the examination of the boundary layer flow of Newtonian and non-Newtonian fluids over different body shapes, such as a flat plate, a stretching sheet, an elastic sheet with variable thickness, a horizontal cylinder, a stretching cylinder, a stretching disk, a sphere, a Riga plate, etc. The boundary layer flow and heat transfer generated by a thin needle have significance for hot wire anemometers, wire coating, biomedicine, blood flow, aerodynamic extrusion of plastic sheets, lubrication, and power generation. Thin needle problems have implications for microstructured electronic gadgets, blood transportation, microscale cooling gadgets, cancer therapy, and many others. A parabola that is rotated along its axis creates a smearing surface known as thin-needle geometry. Lee [19] proposed a boundary layer flow around a moving needle in a parallel free stream and discussed the asymptotic behaviour of an approximation solution. The similarity solutions for convective flow over a needle were then found by Narain and Uberoi [20, 21, 22]. Later, several investigators analyzed Newtonian and non-Newtonian fluid flows over a thin needle. Soid et al. [23] investigated the forced convective nanofluid flow around a horizontal needle. The flow around a tiny needle with variable thermal conductivity and viscosity was studied by Qasim *et al.* [24]. Prashar *et al.* [25] have reported on the effects of hybrid nanoparticles on the flow across a heated needle. Nazar *et al.* [26] investigated the effects of radiation, magnetic fields, and viscous dissipation on fluid flow across a moving needle in a fluid containing hybrid nanoparticles. Despite the

importance of Casson fluid flow over a thin, moving needle, not much has been published in this field of study. Souayeh *et al.* [27] analyzed the impact of cross diffusion and non-linear radiation on the MHD Casson nanofluid across tiny needles. Ibrar *et al.* [28] considered the effect of Navier slip on the nano Casson fluid towards a tiny needle in the presence of thermal radiation and magnetic fields. Hamid [29] examined the magnetic field heat source/sink and non-linear thermal radiation effects on a 2-dimenisonal mixed convection flow of Casson nanofluid over a thin needle moving vertically. Akinshilo *et al.* [33] scrutinized internal heat generation and non-linear radiation on the nanofluid flow past a thin needle in a Casson flow. Bilal and Urva [30] analyzed the consequences of nonlinear radiation on the mixed convective Casson nanofluid over a thin needle. Naveen Kumar *et al.* [31] studied the flow of a Casson fluid down a horizontal, thin moving needle using the Soret/Dufour effect and thermophoretic particles. Prashar [32] examined the Blasius and Sakiadis hybrid Casson nanofluid flow over a tiny heated needle.

It is well known that fluid characteristics, like viscosity and thermal conductivity, fluctuate with temperature. By reducing viscosity over the entire thermal barrier layer, temperature enhancement accelerates the transport phenomenon, which affects how quickly heat transfers. The increased internal friction caused by the increased temperature of lubricating fluids changes the fluid's viscosity, causing it to no longer be constant. The impact of variable fluid characteristics on boundary layer flow was investigated by Herwig and Gersten [34]. Since then, several investigators have looked at the results of changeable thermal conductivity and varying viscosity on the Casson fluid stream in various physical configurations. Animasaun *et al.* [35] investigated how the natural convective Casson fluid stream over an exponentially extending sheet is affected by magnetic fields, suction, heat generation, thermal conductivity, and temperature-dependent viscosity. Mondal *et al.* [36] analyzed the viscous dissipative chemically reacted Casson fluid across a vertical sheet having temperature-dependent viscosity. Sivaraj *et al.* [37] quantitatively examined the implications of cross-diffusion on the Casson fluid stream in the presence of varied fluid characteristics. The peristaltic flow of a Casson fluid in an inclined channel was examined by Prasad *et al.* [38] in relation to the impacts of variable transport parameters and a magnetic field. Govindaraj *et al.* [39] examined the magnetic, Soret, and Dufour effects on the flow of Casson fluid with thermal radiation and changing physical parameters.

Temperature gradients can cause mass flux, which is known as thermal diffusion, thermodiffusion, or the Soret effect. The heat flux caused by a concentration gradient is known as the Dufour effect or diffusion-thermo effect. These impacts are usually regarded as a second-order effect and may become important in fields such as petrology, geosciences, hydrology, and so

on. Eckert and Drake [40] presented several Dufour effect applications.. The Soret effect was employed to divide isotopes and gas mixtures of intermediate (N_2, air) and exceedingly light (H_2, He) molecular weights[41]. There has been a significant amount of study published in the literature on Newtonian and non-Newtonian fluid streams in several geometries, with an emphasis on the Soret and Dufour effect. Shojaei *et al.* [42] inspected the flow of a non-Newtonian liquid through a cylinder influenced by Soret, Dufour, and warm radiation effects. Waini *et al.* [43] investigated the implications of Soret and Dufour on the stream of Al2O3-water nanoliquid through a narrow needle. Salleh *et al.* [44] scrutinized the consequences of Soret and Dufour on the convective stream near a moving, slender needle. Rehman *et al.* [**?**] examined cross diffusive streams on a moving tiny needle, focusing attention on the consequences of Soret and Dufour, heat absorption and generation, nonlinear heat radiation, thermal activation, and chemical reaction properties. Reddy *et al.* [46] used the stream of hybrid (Al_2O_3-Cu/Ethylene glycol) Casson nanofluids over a moving tiny needle to analyze MHD, thermal radiation, and Dufour and Soret effects.

The increase in fluid temperature caused by flow-induced friction at the surface is referred to as viscous dissipation. It is required in viscous fluids such as polymers and oils. It has numerous uses in industry and technology. Viscous dissipation is commonly used in electrical equipment like light bulbs, electric heaters, electric stoves, and electric fuses. Furthermore, the influence of chemical reactions is a crucial aspect in analyzing heat and mass transport in many disciplines of engineering, industry, and science. Khan *et al.* [47] examined the effects of chemical reaction on Casson fluid flowing on a stretched sheet. Sulochana *et al.* [49] covered viscous dissipation and non-uniform heat source/sink in a 2-D forced convective MHD ferrofluid stream upon a horizontally moving needle. Afridi *et al.* [48] examined the Rosseland radiation and entropy generation of a moving tiny needle on self-similar surfaces in the existence of viscous dissipation. Raju *et al.* [50] studied effect of Darcy-Forchheimer flow on a tiny needle in viscoelastic fluid. Upreti and Kumar [51] checked For moving a tiny needle, the flow behavior over a tiny needle under joule heating, thermal radiation, and viscous dissipation. Hamid [29] used a chemical reaction and non-linear thermal radiation to analyze the MHD Casson nanofluid stream upon a tiny needle located vertically. Nayak *et al.* [52] concentrated on examining the effects of heat generation, viscous dissipation, Joulian dissipation, buoyancy, variable Prandtl number, and transverse magnetic field on a stream of nanofluids across a tiny needle moving in a parallel stream. Khan *et al.* [53] analyzed the effects of a magnetic field, a hall current, and viscous dissipation on a chemically reactive nanofluid stream past a tiny moving needle. Sulatana *et al.* [54] analyze the simulations effects of exponential solar radiation and dissipative transport of a steady mixed convective

hybrid nanofluid stream past a non-isothermal moving tiny needle. The interactions of thermal radiation and viscous dissipation on a steady MHD stream through a moving tiny needle in hybrid nanofluid were covered by Nazar *et al.* [26]. Ali *et al.* [55] covered the effects of nanoparticle aggregation, MHD, and viscous dissipation on nanofluid over a tiny needle.

A combination of forced and free convection occurring at the same time, mixed convection has applications in most modern industries and technological processes. Examples include heat exchangers that are kept in a low-velocity condition in order to cool nuclear reactors during emergency interruptions, as well as fan-driven cooling systems for electrical equipment. Wang [56] performed a numerical analysis of mixed convection over a vertical needle and discovered that opposing flows can have single, dual, or no results, whereas assisting flows can only have unique solutions. Ahmed *et al.* [57] examined the mixed convection flow of a viscous fluid along a moving vertical tiny needle. Ahmed *et al.* [58] investigated the impact of changeable heat flux on the mixed convection of a viscous fluid across vertically moving tiny needles. Trimbitas *et al.* [59] considered the mixed convective flow of nanofluid across a vertical needle with a changeable wall temperature. Salleh *et al.* [60] discussed the mixed convection flow of nanofluid caused by the motion of a tiny vertical needle. Qasim and Afridi [61] studied the entropy generation in mixed convection flow across a thin needle.

Many investigators have explored the effect of an applied magnetic field on both Newtonian and non-Newtonian streams across different geometries in the instance of an electrically conducting fluid. Raza [63] investigated the various responses of a mixed convection stream of Casson fluid in a porous channel beneath the force of a magnetic field. The impacts of a consistent transverse magnetic field, heat radiation, and chemical reaction on the erratic Casson fluid stream flowing past an upright plate that oscillates and is utilized in a porous medium were estimated by Kataria and Patel [64]. Ahmed [65] analyzed the MHD narrowing stream of a Casson fluid presented among parallel plates. Jain and Parmar [66] examined the slip stream of Casson fluid across a stretching sheet with magnetic implications. Senapati *et al.* [67] numerically looked at the Casson nanofluid stream beyond the stretching sheet. In a study conducted by Raghunath and Obulesu [68], the investigation involved the analysis of the unsteady magnetohydrodynamic oscillatory flow of Casson fluid past an inclined upright porous plate. The study considered the continuation of chemical reactions along with heat consumption and soret effects. The magnetohydrodynamic Casson fluid flowed steadily and incompressibly in two dimensions over an extended sheet placed in an absorbent medium, as demonstrated by Saeed *et al.* [69]. With the assistance of thermal radiation and chemical reaction, Rasheed *et al.* [70] provided a numerical explanation of the steady two-dimensional MHD free convective stream of Casson fluid above the upright surface. Umavathi *et al.*

[71] concluded magnetohydrodynamic narrowing of Casson nanofluid streams among parallel convectively heated disks. Nandhini *et al.* [72] investigate the consequences of ethyl alcohol, a universal solvent, on radiation absorption and chemical reactions when combined with Casson fluid via an exponentially stretched sheet. The existence of a heat sink or source can significantly affect a stream of Casson fluid, leading to changes in temperature, velocity, and shear stress distribution within the fluid.

Casson fluid flow with a heat source includes various industrial processes, such as polymer processing, food processing, and oil and gas production, where the occurrence of a heat source is prevalent and can severely impair the functioning of the system. Mythili and Sivraj [73] examined the implications of an uneven heat source on an unsteady chemically reacted Casson fluid stream above an upright cone and flat plate with thermal conductivity and viscosity variations. Makinde and Rundora [74] explored time dependent convective streams of a chemically reactive Casson fluid in an upright channel with permeable walls containing the porous medium. Zia *et al.* [75] hypothesized the consequences of cross diffusion, radiation, and exponential heat sources on three-dimensional mixed convective Casson fluid streams by a heated surface. Goud *et al.* [76] provided the implication of heat source on motion of a Casson fluid through an upright fluctuating permeable plate. Awais *et al.* [77] analyzed the implications of magnetic field on the stream of Casson fluid in a porous medium caused by a shrinking surface subjected to heat absorption or germination.

1.7 The Aim of the Thesis

The aim of the present thesis is to study the boundary layer flow of a Casson fluid past a thin, moving needle. This study examines characteristics such as Soret and Dufour effects, magnetic fields, thermal radiation, chemical reactions, and variable properties.

The problems studied concern the geometry of horizontally moving needles in natural and mixed convection.

1.8 Overview of the Thesis

This thesis consists of four parts and ten chapters.

Chapter 1 is an introduction and gives motivation for the investigations carried out in

the thesis. An overview of relevant literature is provided, highlighting the significance of the problems considered in the thesis. This chapter presents the basic equations governing the casson fluid.

Part-II deals with the natural convective boundary layer flow of Casson fluid across a horizontally moving thin needle. This consists of four chapters, i.e., chapters 2 through 5. In these chapters, the governing equations, which are nonlinear in nature, and their accompanying conditions on the boundary are initially transformed into dimensionless form using suitable transformations. Subsequently, successive linearization is used to linearize the resulting nonlinear set of ordinary differential equations, and then Chebyshev spectral collocation is employed to solve it. In several cases, the resulting numerical results agree well with previously reported data.

Chapter 2 describes the boundary layer flow over a thin, horizontal needle moving in a Casson fluid. Initially, similarity transformations are used to transform the governing equations into a set of ordinary differential equations. A graphic representation and analysis are provided for the impact of the needle size and Casson fluid parameter on the temperature and velocity profiles, as well as the skin friction coefficient and Nusselt number.

Chapter 3 deals with the flow past a horizontally moving needle submerged in Casson fluid. The viscosity and thermal conductivity are assumed to be dependent on temperature. The effects of the Casson fluid parameter, needle size, and viscosity parameter on velocity and temperature, along with the coefficient of skin friction and local heat transfer rate, are analyzed.

Chapter 4 studies Soret and Dufour effects on steady two-dimensional laminar boundary layer flow past a horizontal, thin needle immersed in a Casson fluid. The influences of needle size, Casson fluid parameter, Soret, and Dufour parameters on the velocity, temperature, and concentration profiles, as well as on the skin friction coefficient, heat, and mass transfer rates, are studied.

Chapter 5 considers the stream of Casson fluid past a horizontal, tiny needle under the influence of thermal radiation, viscous dissipation, and chemical reaction. A numerical solution has been obtained for velocity, temperature, and concentration through successive linearizing techniques followed by the Chebyshev method. The effect of dimensionless parameters on velocity, temperature, concentration, skin friction coefficient, Nusselt number, and Sherwood number is scrutinized in detail.

Part III deals with the mixed convective boundary layer flow of Casson fluid past a

horizontal, thin, moving needle. This consists of four chapters, i.e., chapter 6 to 9. In these chapters, the nonlinear governing equations and their associated boundary conditions are initially cast into dimensionless forms using similarity transformations.

Chapter 6 deals with Casson fluid flow with mixed convection past a thin, horizontal needle. Graphical representations of the local heat transfer rate and coefficient of skin friction are shown, along with the effects of needle size and mixed convection parameters on temperature and velocity.

Chapter 7 examines the significance of magnetic field, chemical reaction and heat source on a mixed convection stream through a horizontal, tiny needle consumed in Casson fluid. The effects of pertinent parameters, including needle size and Casson fluid parameters, on the stream and thermal fields are concluded. The effects of needle size and Casson fluid parameters on stream and heat transfer in terms of velocity and temperature should be investigated.

Chapter 8 examines the impact of variable properties on a mixed convection stream along a horizontal, thin, moving needle immersed in Casson fluid. The effects of needle size and Casson fluid parameters on velocity and thermal fields are included.

Chapter 9 studies the Soret and Dufour effects on a mixed convection flow along a horizontal, thin needle moving in a Casson fluid. The effects of the mixed convection parameter, needle size, Casson fluid parameter, Soret, and Dufour parameters on the velocity, temperature, and concentration profiles, as well as on the skin friction coefficient, heat, and mass transfer rates, are studied.

Part IV consists of a single chapter, i.e., Chapter 10. In this chapter, the main conclusions of the earlier chapters and the directions for further investigations are indicated.

In all the above chapters (Chapter 2 to Chapter 9), similarity transformations are employed to convert the governing system of partial differential equations to nonlinear ordinary differential equations. The resulting equations were linearized using the successive linearization method [78]. Thus, the obtained linear equations are solved using the Chebyshev pseudo-spectral collocation method [79].

A list of references is given at the end of the thesis and is arranged in alphabetical order.

A considerable part of the work in the thesis has been published or accepted for publication in reputed international journals. The remaining part is communicated for publication. The details are presented below.

List of papers Published

1. "Casson Fluid Flow Past a Thin Needle with Radiation, Viscous Dissipation and Chemical Reaction Effects ", ***Journal of Xidian University***, Vol 18 (3), 981-990, 2024

2. "Flow Over a Thin Needle Moving in a Casson Fluid ", ***WSEAS Transactions on Heat and Mass Transfer***, Vol 19, 27 - 32, 2024

List of papers Accepted

3. "Mixed Convection Flow of a Casson Fluid Past a Thin Needle "***Journal of Advanced Research in Fluid Mechanics and Thermal Sciences***

4. "Effect of Variable Properties on The Flow Past a Needle Moving in a Casson Fluid ", ***Revision submitted to Discontinuity, Nonlinearity, and Complexity***

List of papers communicated

5. "Casson Fluid Flow past a Thin Needle with Cross Diffusion Effects", ***International Journal of Applied and Computational Mathematics***

6. "Heat source and Chemical reaction effects on a MHD mixed convection of a Casson fluid flow over a thin needle ", ***Journal of applied and computational Mathematics***

7. "Mixed Convection Flow Past a Thin Needle in a Casson Fluid ", ***Computational Thermal Sciences: An International Journal***

8. "Effects of Variable Properties on Mixed Convection of a Casson Fluid Flow Over a Thin Needle ", ***Heat Transfer***

9. "Cross Diffusion Effects on Mixed Convection of a Casson Fluid Flow Over a Thin Needle ",***Mathematics and Computers in Simulation.***

Part II

NATURAL CONVECTION IN BOUNDARY LAYER FLOW OF CASSON FLUID PAST A THIN NEEDLE

Chapter 2

Casson Fluid Flow Over a Moving Thin Needle [1]

2.1 Introduction

Several researchers were intrigued in Casson fluid flow because of its potential application to a wide range of engineering problems. These include in drilling operations, metallurgy, food processing, polymer processing industries, synthetic lubricants, biomedical fields, the preparation of printing ink, etc. A few studies, for example, Souayeh *et al.* [27], Bilal *et al.* [30], Ibrar [28], Akinshilo *et al.* [33] etc. on the Casson nanofluid flow over a thin needle with different physical effects have been published.

This chapter examines the steady flow of a Casson fluid across a horizontal moving thin needle. The flow equations are first transformed into a system of ordinary differential equations, which are then solved using the Chebyshev collocation method after sequential linearization has been applied.

2.2 Formulation of the Problem

Consider the steady, laminar and incompressible flow of Casson fluid over a horizontally moving thin needle. Assume that the uniform velocity of the fluid be U_∞ and the moving velocity of the needle be U_w. Figure 2.1 shows the schematic of the problem along with

[1] Accepted for publication in "**WSEAS Transactions on Heat and Mass Transfer "**

coordinate system. The radius of the needle is given by $r = R(x)$. The needle is assumed to be thin, with a thickness smaller than that of the boundary layer that surrounds it. Let T_w and T_∞ where $T_w > T_\infty$ are the temperatures the needle and surrounding fluid.

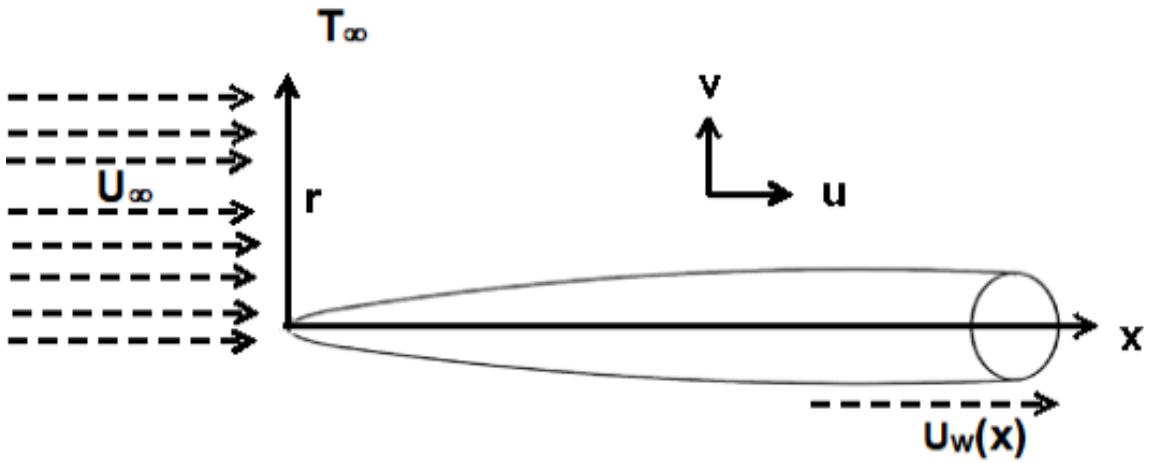

Figure 2.1: "Coordinate system and physical flow model".

The flow equations are obtained by using the boundary layer postulations and the aforementioned assumptions.

$$\frac{\partial(ru)}{\partial x} + \frac{\partial(rv)}{\partial y} = 0 \tag{2.1}$$

$$u\frac{\partial u}{\partial x} + v\frac{\partial u}{\partial r} = \nu\left(1 + \frac{1}{\beta}\right)\frac{1}{r}\frac{\partial}{\partial r}\left(r\frac{\partial u}{\partial r}\right) \tag{2.2}$$

$$u\frac{\partial T}{\partial x} + v\frac{\partial T}{\partial r} = \alpha\left(\frac{1}{r}\frac{\partial}{\partial r}\left(r\frac{\partial T}{\partial r}\right)\right) \tag{2.3}$$

where u denote the axial velocity component, v denote radial velocity component, T represents the fluid temperature, ρ represents the fluid density, ν represents the kinematic viscosity, β represents Casson fluid parameter, and α represents the thermal conductivity.

The boundary conditions are

$$\begin{aligned} u = u_w, \quad v = 0, \quad T = T_w \ \ at\ r = R(x) \\ u \to u_\infty, \quad T \to \infty \ \ at\ r \to \infty \end{aligned} \tag{2.4}$$

The similarity Transformations are defined as:

$$\psi = \nu x f(\eta), \quad \theta(\eta) = \frac{T - T_\infty}{T_w - T_\infty}, \quad \eta = \frac{Ur^2}{\nu x} \tag{2.5}$$

using Eq. (2.5), the equation for the surface of the needle $\eta = a$, (where a is dimensionless constant), can be written as $R = (\frac{\nu a x}{U})^{\frac{1}{2}}$ which characterizes the size and shape of the needle.

Making use of similarity transformations given in (2.5) in equation (2.1) to (2.3) we get

$$2\eta[1 + \frac{1}{\beta}]f''' + 2[1 + \frac{1}{\beta}]f'' + ff'' = 0 \tag{2.6}$$

$$\eta\theta'' + \frac{Pr}{2}\theta' f + \theta' = 0 \tag{2.7}$$

The modified conditions on boundary are

$$\begin{aligned} f'(\eta) = \frac{\lambda}{2}, f(\eta) = \frac{\lambda a}{2}, \theta(\eta) = 1 \quad at \quad \eta = a \\ f'(\eta) \to \frac{1-\lambda}{2}, \quad \theta(\eta) \to 0 \quad at \quad \eta \to \infty \end{aligned} \tag{2.8}$$

where λ is the velocity ratio parameter,$Pr = \frac{\mu}{\alpha_0}$ denotes the Prandtl number.

The non-dimensional form of coefficient of skin friction (C_f) and the heat transfer rate (Nusselt number (Nu)) are

$$Re^{\frac{1}{2}} C_f = 8a^{\frac{1}{2}}(1 + \frac{1}{\beta})f''(a), \quad Re^{\frac{-1}{2}} Nu = -2a^{\frac{1}{2}}\theta'(a) \tag{2.9}$$

2.3 Solution of the Problem

The system of differential Eqns. (2.6) and (2.7) are solved by using successive linearization method (SLM) along with the Chebyshev collocation method.

It is assumed in SLM that the unknown functions $\mathbf{F}(\eta) = [f(\eta), \theta(\eta)]$ can be represented as

$$\mathbf{F}(\eta) = \mathbf{F}_j(\eta) + \sum_{m=0}^{j-1} \mathbf{F}_m(\eta), \tag{2.10}$$

where the unknown function $\mathbf{F}_j(\eta)$ $(j = 1, 2, ...)$ is an approximation. The linearized set of equations obtained by putting on equation (2.10) to the equations (2.6) and (2.7) and can

be solved to determine this estimate. The fundamental principle is that, even as j grows enormous, F_j shrinks dramatically, allowing non-linear factors in F_j and their differential to be ignored.

Using Eq.(2.10) in the Eqs. (2.6) to (2.7) and ignoring nonlinear terms containing f_j,θ_j and ϕ_j , we get

$$a_1 f_i^{'''} + a_2 f_i^{''} + a_3 f_i = r_1 \tag{2.11}$$

$$b_1 f_i + b_2 \theta_i^{''} + b_3 \theta_i{}' = r_2 \tag{2.12}$$

where

$$a_1 = 2\eta\left(1+\frac{1}{\beta}\right), \quad a_2 = 2\left(1+\frac{1}{\beta}\right) + \sum f_m, \quad a_3 = \sum f_m''$$

$$r_1 = -2\eta\left(1+\frac{1}{\beta}\right)(\sum f_m''') - 2\left(1+\frac{1}{\beta}\right)(\sum f_m'') - (\sum F_m)(\sum f_m'')$$

$$b_1 = \frac{Pr}{2}(\sum \theta_m'), \quad b_2 = \eta, \quad b_3 = \frac{Pr}{2}(\sum f_m) + 1$$

$$r_2 = -\eta(\sum \theta_m'') - \frac{Pr}{2}(\sum \theta_m')(\sum f_m) - (\sum \theta_m')$$

The set of linearized Eqs.(2.11) - Eq.(2.12) is solved by using the Chebyshev collocation method [79].

The solution region for this problem is changed to $[a, B]$; B is chosen to acquire the conditions that are far from the body. In order to use this technique, the following transformation is once again used to turn $[a, B]$ to $[-1, 1]$.

$$\eta = \frac{(a+B)-(a-B)\xi}{2}, \quad -1 \le \xi \le 1 \tag{2.13}$$

The unknown functions f_i and θ_i are approximated at the Gauss-Lobatto collocation points on $[-1, 1]$

$$\xi_i = \cos\frac{\pi i}{N}, \quad i = 0, 1, 2, 3.....N \tag{2.14}$$

as

$$f_j(\xi) = \sum_{k=0}^{N} f_j(\xi_k) T_k(\xi_i),\ \theta_j(\xi) = \sum_{k=0}^{N} \theta_j(\xi_k) T_k(\xi_i),\ i = 0, 1, 2...N \tag{2.15}$$

where$T_k(\xi)$ is the k^{th} Chebyshev polynomial.

Similarly, the r^{th}differentials of f_i and θ_i and are guesstimated as

$$\frac{d^r F_j}{d\eta^r} = \sum_{k=0}^{N} D^r_{ki} F_j(\xi_k), \quad \frac{d^r \theta_j}{d\eta^r} = \sum_{k=0}^{N} D^r_{ki} \theta_j(\xi_k), \quad i = 0, 1, 2...N \tag{2.16}$$

where $D = \frac{2}{B}\mathfrak{D}$ with $\mathfrak{D}$ is the Chebyshev differential matrix.

Equations (2.15) - (2.16) are substituted into equations (2.11), and (2.12) to get the the following matrix equation

$$A_{i-1} X_i = R_{i-1} \tag{2.17}$$

where A_{j-1} is a $2(N+1) \times 2(N+1)$ order matrix and X_j and R_{j-1} are $2(N+1) \times 1$ column matrix given by

$$A_{i-1} = \begin{pmatrix} A_{11} & A_{12} \\ A_{21} & A_{22} \end{pmatrix}, X_i = \begin{pmatrix} F_i \\ \Theta_i \end{pmatrix}, R_{i-1} = \begin{pmatrix} r_{1,i-1} \\ r_{2,i-2} \end{pmatrix} \tag{2.18}$$

where

$$F_j = [f_j(\xi_0), f_j(\xi_1), ..., f_j(\xi_{N-1}), f_j(\xi_N)]^T,$$

$$\Theta_j = [\theta_j(\xi_0), \theta_j(\xi_1), .., \theta_j(\xi_{N-1}), \theta_j(\xi_N)]^T,$$

$$A_{11} = a_1 D^3 + a_2 D^2 + a_3 I, A_{12} = O,$$

$$A_{21} = b_1 I, A_{22} = b_2 D^2 + b_3 D,$$

$$r_1 = [r_1(\xi_1), r_1(\xi_2), r_1(\xi_3)...., r_1(\xi_{N+1})]^T,$$

$$r_2 = [r_2(\xi_1), r_2(\xi_2), r_2(\xi_3)...., r_2(\xi_N)]^T,$$

The superscript T stands for transpose, I is the identity matrix, O is the zero matrix.

Writing the boundary conditions at the collocation points, the solution is provided by

$$X_j = A_{j-1}^{-1} R_{j-1}$$

The current model concentrates mainly on the implications of three dimensionless parameters: the velocity ratio parameter (λ), the Casson fluid parameter (β), and the needle size (a). Figs. 2.2–2.6 illustrate the impacts of these parameters on temperature, velocity, skin friction coefficient, and heat transfer rate (Nusselt Number).

The effect of needle size on velocity and temperature profiles is shown in Figure 2.2. As the size of the needle lowers, the velocity increases, as shown in Fig. 2.2(a). Physically, the fluid's surface area shrinks as the thin needle's size lowers, reducing force and raising velocity in the process. Moreover, the boundary layer thickness for the velocity decreases with decreasing needle size. As can be seen in Fig.2.2(b), the temperature and its boundary layer decrease with the thin needle size.

Figure 2.3 shows how the Casson fluid parameter (β) affects temperature and velocity. As β increases, the velocity increases, as can be seen in Fig. 2.3(a). Moreover, the velocity increases with η. The temperature is seldom affected by β, as Fig. 2.3(b) illustrates. It is evident that the temperature decreases as η increases.

Figure 2.4 displays the temperature and velocity fluctuations for various velocity ratio parameter values. As one advances away from the needle's wall, the velocity drops, whereas an increase in λ increases the velocity close to the needle's wall (Figure 2.4(a)). The temperature is unaffected by the velocity ratio parameter, as Fig. 2.4(b) illustrates.

The impact of needle size on the Nusselt number and coefficient of skin friction is seen in Figure 2.5. As illustrated in Fig. 2.5(a), skin friction lowers with an improving value of β and a constant needle size. Furthermore, the skin friction coefficient falls with increasing needle size. As the needle size grows, the rate of heat transmission reduces, as Fig. 2.5(b) illustrates. As seen in Fig. 2.5(b), the Casson fluid parameter has no discernible impact on the Nusselt number.

Figure 2.6 illustrates how the velocity ratio parameter affects the coefficient of skin friction and Nusselt number. Figure 2.6(a) shows that as the velocity ratio parameter increases, the skin friction coefficient decreases. As the velocity ration parameter increases, the rate of heat transfer increases, as shown in Fig. 2.6(b).

2.4 Conclusion

This study examines the effects of parameters related to flow on the temperature, velocity, skin friction coefficient, and heat transfer rate in the flow over a thin horizontal needle moving in a Casson fluid. The following are the primary conclusions of the current investigation:

- As the needle size decreases, the velocity profile increases, and as the Casson fluid parameter increases, it decreases.
- As the thin needle's size decreases, the temperature profile decreases. The Casson fluid and velocity ratio parameters have negligible effects.

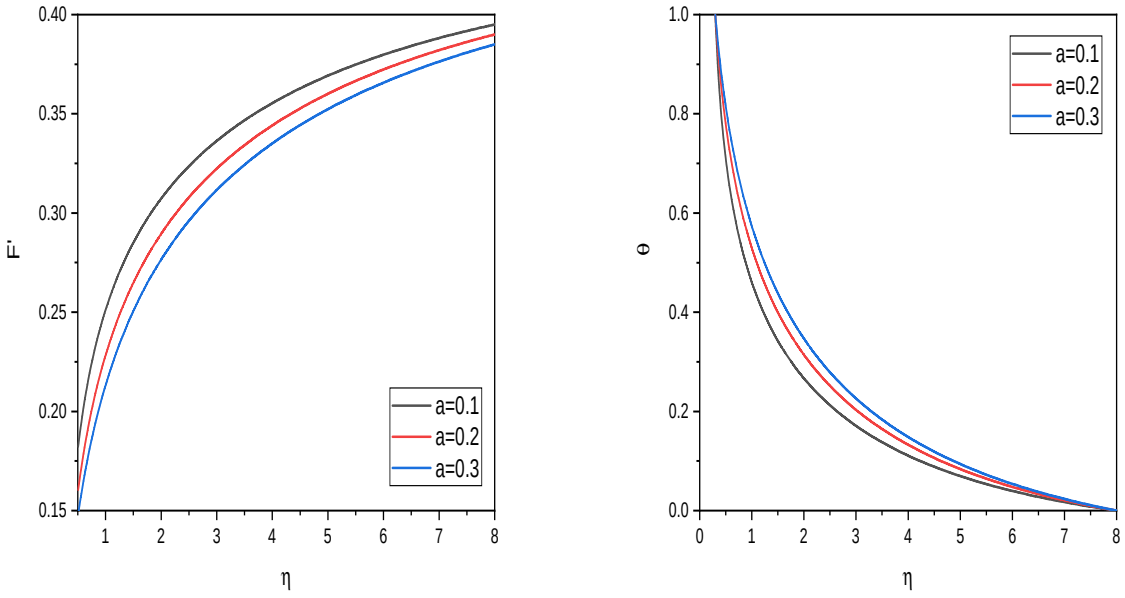

(a) (b)

Figure 2.2: "Effects of needle size on the (a) Velocity profile (b) Temperature Profile"

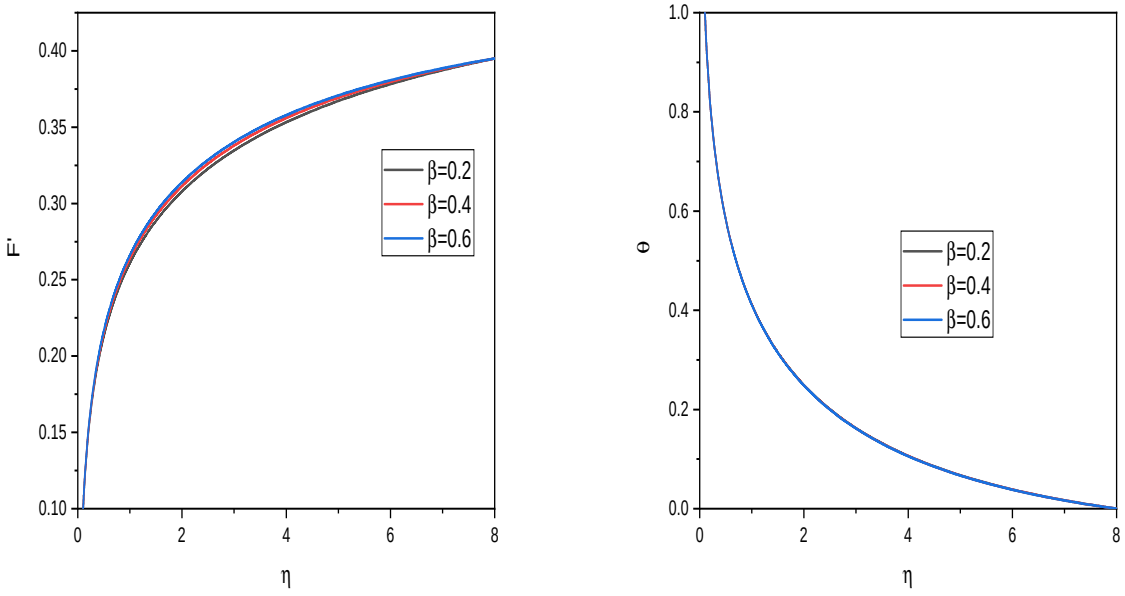

(a) (b)

Figure 2.3: "Effect of Casson fluid parameter on the (a) Velocity (b) Temperature"

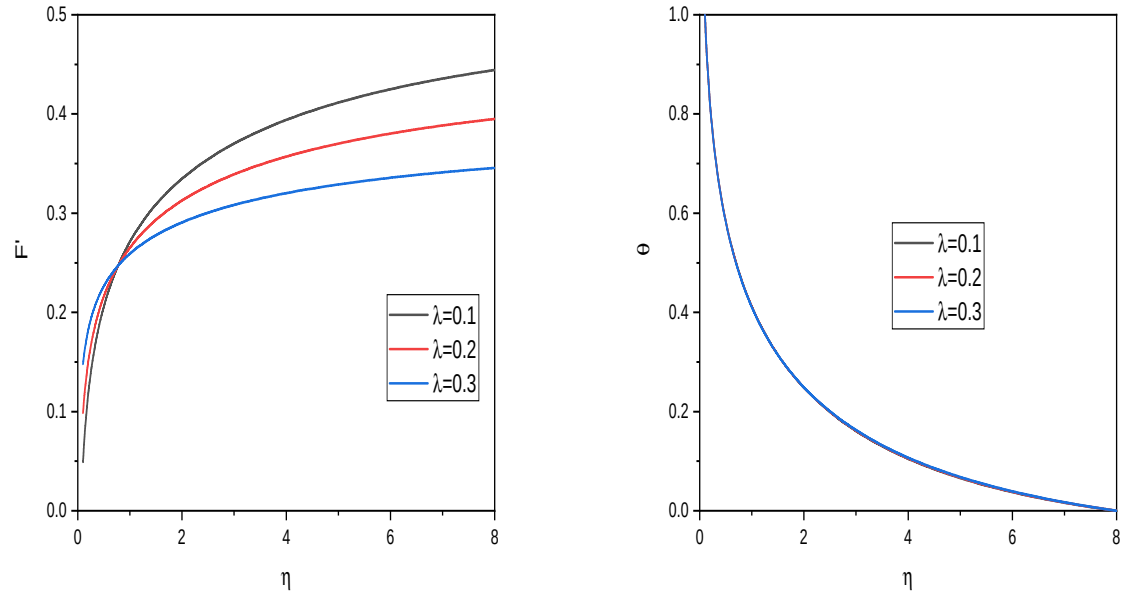

(a) (b)

Figure 2.4: "Effect of velocity ratio parameter on the (a) Velocity (b) Temperature"

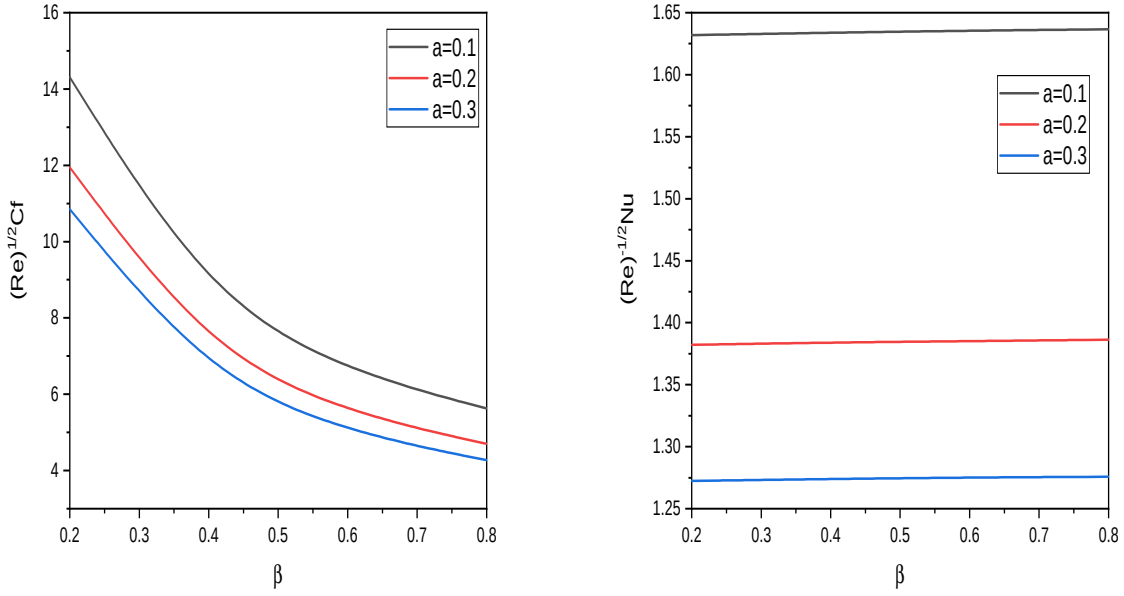

(a) (b)

Figure 2.5: "Effect of needle size on the (a) coefficient of skin friction (b) Heat transfer rate"

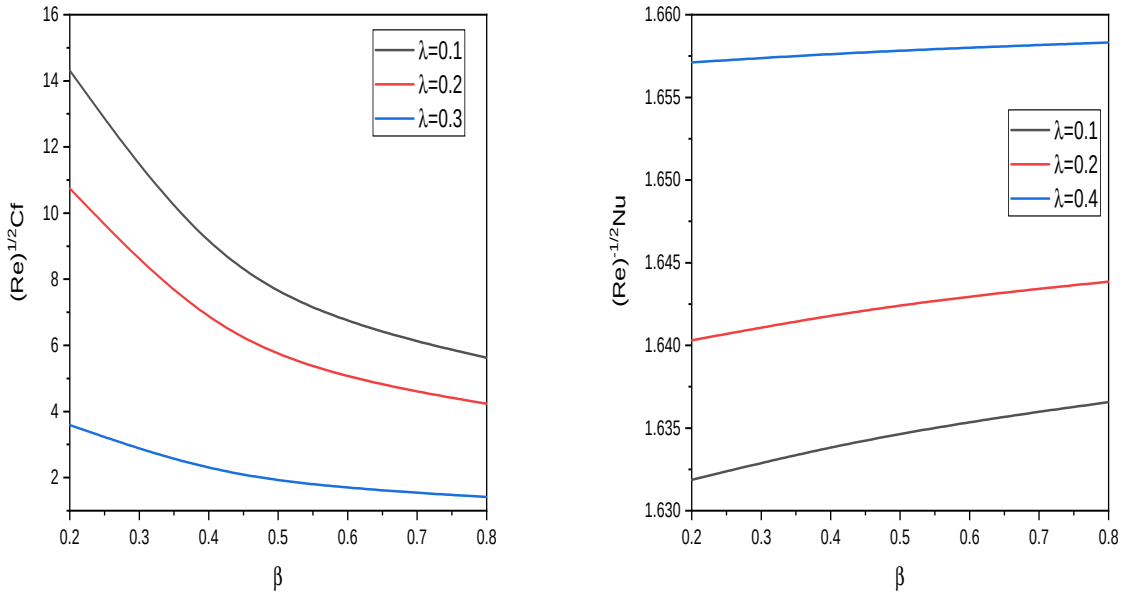

(a) (b)

Figure 2.6: "Effect of velocity ratio parameter on the (a) Skin friction coefficient (b) Heat transfer rate"

Chapter 3

Effect of Variable Properties on The Flow Past a Needle Moving in a Casson Fluid [1]

3.1 Introduction

It is well known that fluid characteristics, like viscosity and thermal conductivity, fluctuate with temperature. By reducing viscosity over the entire thermal barrier layer, the temperature enhancement accelerates the transport phenomenon, which affects how quickly heat transfers. The impact of variable fluid characteristics on boundary layer flow was investigated by Herwig and Gersten [34]. Since then, several investigators have looked at the results of changeable thermal conductivity and varying viscosity on Casson fluid stream in various physical configurations. Animasaun *et al.* [35] examined how natural convective Casson fluid stream over an exponentially extending sheet is affected by magnetic field, suction, heat generation, thermal conductivity, and temperature-dependent viscosity. Mondal *et al.* [36] analyzed the viscous dissipative chemically reacted Casson fluid across a vertical sheet having temperature dependent viscosity. Sivaraj *et al.* [37] quantitatively examined the implications of cross-diffusion on the Casson fluid stream in the presence of varied fluid characteristics. The peristaltic flow of Casson fluid in an inclined channel was examined by Prasad *et al.* [38] in relation to the impacts of variable transport parameters and a magnetic field. Govindaraj *et al.* [39] examined magnetic, Soret, and Dufour effects on the stream of

[1] Accepted for publication in "**Discontinuity, Nonlinearity, and Complexity "**,

Casson fluid with thermal radiation and changing physical parameters.

This chapter considers the flow of Casson fluid over a horizontal moving needle. The viscosity and thermal conductivity are assumed to be dependent on temperature. The governing equations of the flow are converted into a set of non-linear ordinary differential equations utilising appropriate transforms. The resulting equations are linearized by using successive linearization, and then solved by Chebyshev spectral collocation technique.

3.2 Formulation of the Problem

Consider the steady, laminar and incompressible flow of Casson fluid over a horizontally moving thin needle as shown in Figure 2.1 Apart from the assumption of Chapter - 2, here we assume that the viscosity and thermal conductivity depends on the temperature.

Hence, the equations goerning thw flow becomes

$$\frac{\partial(ru)}{\partial x} + \frac{\partial(rv)}{\partial r} = 0 \tag{3.1}$$

$$\rho u\frac{\partial u}{\partial x} + \rho v\frac{\partial u}{\partial r} = \frac{1}{r}\left(1+\frac{1}{\beta}\right)\frac{\partial}{\partial r}\left(\mu(T) r\frac{\partial u}{\partial r}\right) + g\beta_T \cos\alpha(T-T_\infty) \tag{3.2}$$

$$v\frac{\partial T}{\partial r} + u\frac{\partial T}{\partial x} = \frac{1}{r}\frac{\partial}{\partial r}\left(\alpha(T) r\frac{\partial T}{\partial r}\right) \tag{3.3}$$

where the quantities used in the above equations are already defined in Chapter - 2.

It is presumed that thermal conductivity and viscosity are linearly dependent on the temperature as

$$\alpha(T) = \alpha_0[1 + E(T - T_\infty)] \quad \text{and} \quad \mu(T) = \mu_\infty[1 + b(T_w - T)] \tag{3.4}$$

where α_0 and μ_∞ are the absolute thermal conductivity and viscosity, b and E are constants.

The boundary conditions are:

$$\begin{aligned} u = u_w, v = 0, T = T_w \ \ at\ r = R(x) \\ u \to u_\infty, T \to \infty \ \ at\ r \to \infty \end{aligned} \tag{3.5}$$

To non-dimensionlize the equations (3.1) to (3.3), we use the following similarity trans-

formations:

$$\eta = \frac{Ur^2}{\nu x}, \quad \psi = \nu x f(\eta), \quad \theta(\eta) = \frac{T - T_\infty}{T_w - T_\infty}, \tag{3.6}$$

where $U = U_w + U_\infty$ is the composite velocity and ψ is the stream function given by $u = \frac{1}{r}\frac{\partial \psi}{\partial r}$ and $v = \frac{-1}{r}\frac{\partial \psi}{\partial x}$

Using Eq. (3.6) in the equation to the surface of the wall $\eta = a$, it can be written as $R = \sqrt{\frac{\nu a x}{U}}$ which characterizes shape and size of the needle.

Substituting the similarity variables given in (3.6) in Eqns. (3.1) to (3.3), we obtain

$$\left[2\left(1 + \frac{1}{\beta}\right)(1 + A(1-\theta))\right]\left(\eta f''' + f''\right) - 2A\eta\left(1 + \frac{1}{\beta}\right)\theta' f'' + f f'' + Gr\theta = 0 \tag{3.7}$$

$$\left[2\left(\frac{1 + \epsilon\theta}{Pr}\right)\right]\left(\eta\theta'' + \theta'\right) + \frac{2\eta\epsilon}{Pr}\theta'^2 + f\theta' = 0 \tag{3.8}$$

where A is viscosity parameter, Gr is Grashof number, $Pr = \frac{\nu}{\alpha}$, is Prandtl number, $\lambda = \frac{U_w}{U}$ is velocity ratio parameter and ϵ is thermal conductivity parameter.

The modified conditions on boundary becomes

$$\begin{aligned} f'(\eta) = \frac{\lambda}{2}, f(\eta) = \frac{\lambda a}{2}, \theta(\eta) = 1 \quad at \quad \eta = a \\ f'(\eta) \to \frac{1-\lambda}{2}, \quad \theta(\eta) \to 0 \quad at \quad \eta \to \infty \end{aligned} \tag{3.9}$$

The non-dimensional form of local Nusselt number Nu and the skin friction coefficient C_f are

$$\sqrt{Re} C_f = 8\sqrt{a}\left(1 + \frac{1}{\beta}\right) f''(a), \quad \frac{Nu}{\sqrt{Re}} = -2\sqrt{a}\theta'(a) \tag{3.10}$$

3.3 Solution of the Problem

The combined Eqns. (3.7) and (3.8) and conditions on boundary (3.9) are linearized through the successive linearization method (SLM) [78]. The solution of resulting linearized equations is obtained by Chebyshev collocation method. On applying the procedure explained in Chapter 2 to the equations Eqns. (3.7) and (3.8), we get the following linearized equations.

$$a_1 f_j''' + a_2 f_j'' + a_3 f_j + a_4 \theta_j{}' + a_5 \theta_j = r_1 \tag{3.11}$$

$$b_1 f_j + b_2 \theta_j^{''} + b_3 {\theta_j}' + b_4 \theta_j = r_2 \tag{3.12}$$

where

$$a_1 = 2\eta \left(1 + \frac{1}{\beta}\right) \left(1 + A - A(\sum \theta_m)\right)$$

$$a_2 = 2 \left(1 + \frac{1}{\beta}\right) \left(1 + A - A(\sum \theta_m) - A(\sum \theta'_m)\right) + (\sum f_m)$$

$$a_3 = (\sum f''_m) \quad a_4 = -2A\eta \left(1 + \frac{1}{\beta}\right) (\sum f''_m)$$

$$a_5 = Gr - 2A \left(1 + \frac{1}{\beta}\right) \left(\eta(\sum f'''_m) - (\sum f''_m)\right)$$

$$\begin{aligned} r_1 = -2 \left(1 + \frac{1}{\beta}\right) \big(&\eta(\sum f'''_m) - A\eta(\sum f'''_m) - 2(\sum f''_m) \\ &+2A\eta(\sum \theta_m)(\sum f'''_m) - 2A(\sum f''_m) \\ &+2A(\sum \theta_m)(\sum f''_m) + 2A\eta(\sum \theta'_m)(\sum f''_m)\big) \\ &-(\sum f_m)(\sum f''_m) - Gr(\sum \theta_m) \end{aligned}$$

$$b_1 = (\sum \theta'_m) \quad b_2 = \frac{2\eta}{Pr} + \frac{2\eta\epsilon}{Pr}(\sum \theta_m)$$

$$b_3 = \frac{2}{Pr} + \frac{2\epsilon}{Pr}(\sum \theta_m) + \frac{4\eta\epsilon}{Pr}(\sum \theta'_m) + (\sum f_m)$$

$$b_4 = \frac{2\eta\epsilon}{Pr}(\sum \theta''_m) + \frac{2\epsilon}{Pr}(\sum \theta'_m)$$

$$\begin{aligned} r_2 = -\frac{2\eta}{Pr}(\sum \theta''_m) + \frac{2\eta\epsilon}{Pr}(\sum \theta_m)(\sum \theta''_m) - \frac{2}{Pr}(\sum \theta'_m) - \frac{2\epsilon}{Pr}(\sum \theta_m)(\sum \theta'_m) \\ -\frac{2\eta\epsilon}{Pr}(\sum \theta'_m)^2 - (\sum f_m)(\sum \theta'_m) \end{aligned}$$

As explained in Chapter - 2, using Chebyshev collocation method on the system of linearized equations. (3.11) and (3.12), we obtain the following equation in matrix form

$$A_{j-1} X_j = R_{j-1} \tag{3.13}$$

where A_{j-1} is a $2(N+1) \times 2(N+1)$ order matrix and X_j and R_{j-1} are $2(N+1) \times 1$ column

matrix given by

$$A_{j-1} = \begin{pmatrix} A_{11} & A_{12} \\ A_{21} & A_{22} \end{pmatrix}, X_j = \begin{pmatrix} F_j \\ \Theta_j \end{pmatrix}, R_{j-1} = \begin{pmatrix} r_{1,j-1} \\ r_{2,j-2} \end{pmatrix} \tag{3.14}$$

where

$$F_j = [f_j(\xi_0), f_j(\xi_1), ..., f_j(\xi_{N-1}), f_j(\xi_N)]^T,$$

$$\Theta_j = [\theta_j(\xi_0), \theta_j(\xi_1), .., \theta_j(\xi_{N-1}), \theta_j(\xi_N)]^T,$$

$$A_{11} = a_1 D^3 + a_2 D^2 + a_3 I, A_{12} = a_4 D + a_5 I,$$

$$A_{21} = b_1 I, A_{22} = b_2 D^2 + b_3 D,$$

$$r_1 = [r_1(\xi_1), r_1(\xi_2), r_1(\xi_3)...., r_1(\xi_{N+1})]^T,$$

$$r_2 = [r_2(\xi_1), r_2(\xi_2), r_2(\xi_3)...., r_2(\xi_N)]^T,$$

The superscript T stands for transpose, I is the identity matrix, O is the zero matrix.

Imposing the boundary conditions in terms of the collocation points, the solution is provided by

$$X_j = A_{j-1}^{-1} R_{j-1}$$

3.4 Results and Discussion

The four dimensionless parameter effects are primarily the focus of the current model. They are size of needle (a), variable viscosity parameter (A), velocity ratio parameter (λ), thermal conductivity parameter (ϵ), on velocity and temperature profiles together with the local heat transfer rate (Nusselt Number) $\frac{Nu}{\sqrt{Re}}$ and coefficient of skin friction $\sqrt{Re}C_f$. A detailed numerical parametric analysis is conducted to assure a greater comprehension of the technical issue, and the findings are presented graphically (Figs. 3.1-3.11). Numerous a, λ, A, and $\in$ values have been calculated numerically.

Figure3.1 illustrates how the needle's size affects the velocity and temperature profiles. As shown in Fig.3.1(a), enlarging a elevates the velocity. As a rises, the temperature is also increasing, as presented in Fig. 3.1(b).

The fluctuation of velocity and temperature with the Casson fluid parameter β is shown in Fig.3.2. As the Casson fluid parameter increases, velocity increases, as illustrated in Fig. 3.2(a). As depicted in Fig. 3.2(b), the impact β on the temperature profile is almost negligible.

The consequence of the thermal conductivity parameter ϵ on velocity and temperature is given in Fig. 3.3. It is represented in Fig. 3.3(a) that the velocity improves slightly as the variable thermal conductivity parameter rises. The temperature profile is also enhanced with an enhancement in ϵ, as depicted in Fig. 3.3(b).

The fluctuation of profiles of velocity and temperature with velocity ratio parameter λ is given in Fig.3.4. As presented in Fig.3.4(a), intensifying λ decreases velocity close to the needle, then increases velocity farther from the needle. The effect of the velocity ratio parameter on temperature is negligible, as depicted in Fig. 3.4(b).

Figre 3.5 represents the impact of the Grashof number on the velocity and temperature. Fig. 3.5(a) exhibits that velocity rises as Grashof number rises. The variation in the temperature profile is independent of Gr as shown in Fig. 3.5(b).

The impact of the variable viscosity parameter (A) on velocity and temperature is given in Fig. 3.6. It is detected from Fig. 3.6(a) that the velocity enhances as the variable viscosity parameter rises. As displayed in Fig. 3.6(b), the temperature profile relative to A is constant.

The effect of size of needle a on the local heat transfer rate $\frac{Nu}{\sqrt{Re}}$ and coefficient of local skin friction $\sqrt{Re}C_f$ is illustrated in Fig.3.7. As depicted in Fig.3.7(a), the skin friction coefficient is improved by increasing a. As a enhances, the local Nusselt number is also increasing, as seen in Fig. 3.7(b).

The impact of ϵ on the local rate of heat transfer $\frac{Nu}{\sqrt{Re}}$ and the coefficient of local skin friction $\sqrt{Re}C_f$ is given in Fig. 3.8. It is understood from Fig. 3.8(a) that the $\sqrt{Re}C_f$ enhances as the variable thermal conductivity parameter rises. As exhibited in Fig. 3.8(b), $\frac{Nu}{\sqrt{Re}}$ is also enhanced with an enhancement in ϵ.

Figure 3.9 presents the influence of the Grashof number Gr on the $\frac{Nu}{\sqrt{Re}}$ and $\sqrt{Re}C_f$. Fig. 3.9(a) exhibits that the $\sqrt{Re}C_f$ rises as the Grashof number rises. The variation in the $\frac{Nu}{\sqrt{Re}}$ independent of Gr is depicted in Fig. 3.9(b).

The fluctuation of $\frac{Nu}{\sqrt{Re}}$ and $\sqrt{Re}C_f$ with velocity ratio parameter λ is given in Fig.3.10. As presented in Fig.3.10(a), intensifying λ increases the skin friction coefficient. An increase in

the velocity ratio parameter increases the local Nusselt number, as depicted in Fig. 3.10(b).

The impact of the variable viscosity parameter A on $\frac{Nu}{\sqrt{Re}}$ and $\sqrt{Re}C_f$ is given in Fig. 3.11. It is noticed from Fig. 3.11(a) that the $\sqrt{Re}C_f$ enhances as the variable viscosity parameter rises. Fig. 3.11(b) exhibits that the local Nusselt number is decreasing with an increase in A.

3.5 Conclusion

The assumption that viscosity and thermal conductivity change with temperature is used to explore the boundary layer stream over a thin needle of casson fluid. The Chebyshev spectral technique is used to find the solution of the resulting set after non-dimensional equations are linearized using a successive linearized procedure.

- The velocity, temperature, skin friction coefficient, and heat transfer coefficient all rise with increasing needle size.
- The velocity rises and the heat transfer rate reduces with an improvement in the viscosity parameter.
- A rise in the thermal conductivity parameter leads to an increase in velocity, temperature, and heat transfer rate.

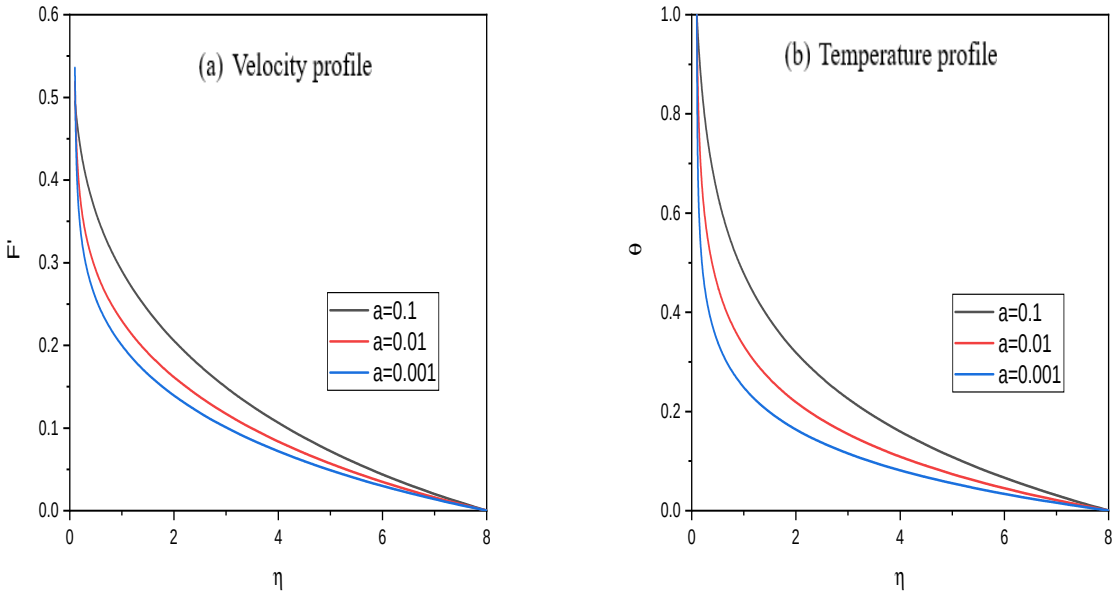

(a) (b)

Figure 3.1: "Effect of a on the (a) Velocity Profile and (b) temperature profile"

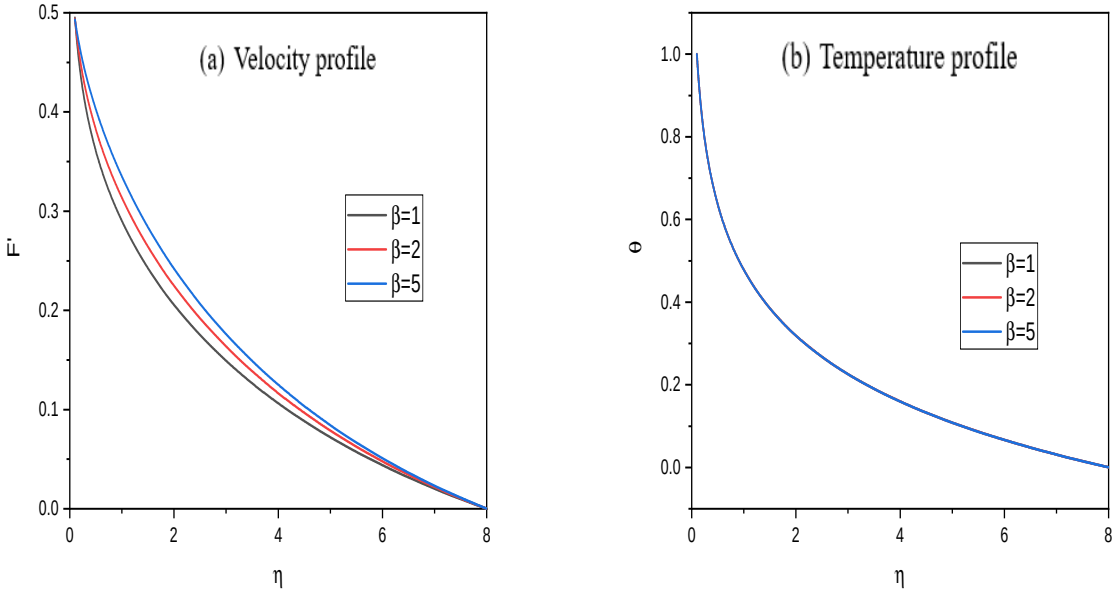

(a) (b)

Figure 3.2: "Effect of β on the (a) Velocity Profile and (b) temperature profile"

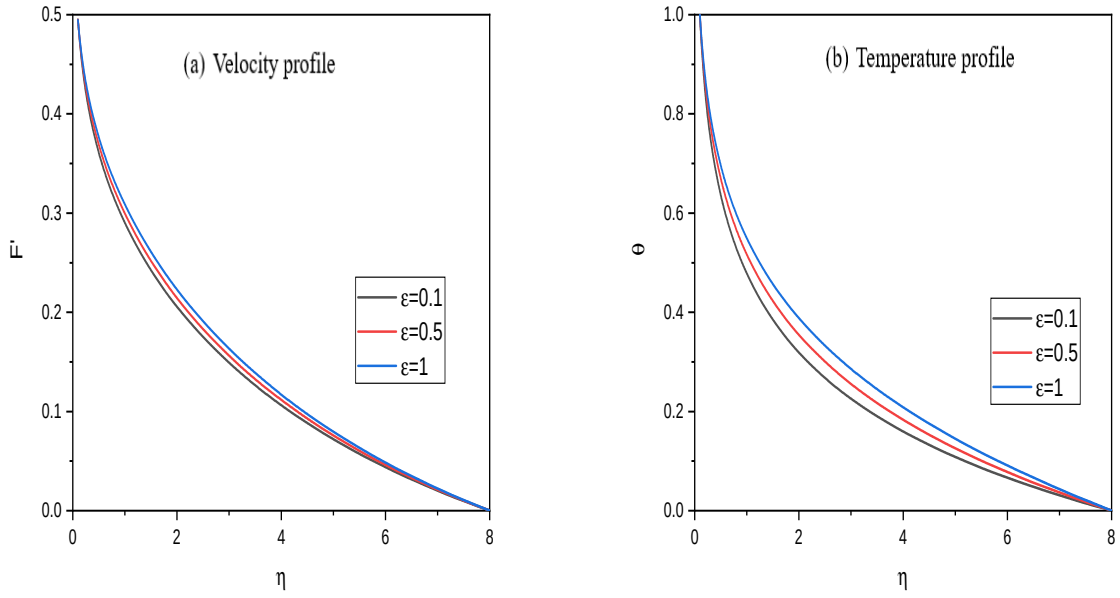

(a) (b)

Figure 3.3: "Effect of ϵ on the (a) Velocity Profile and (b) temperature profile"

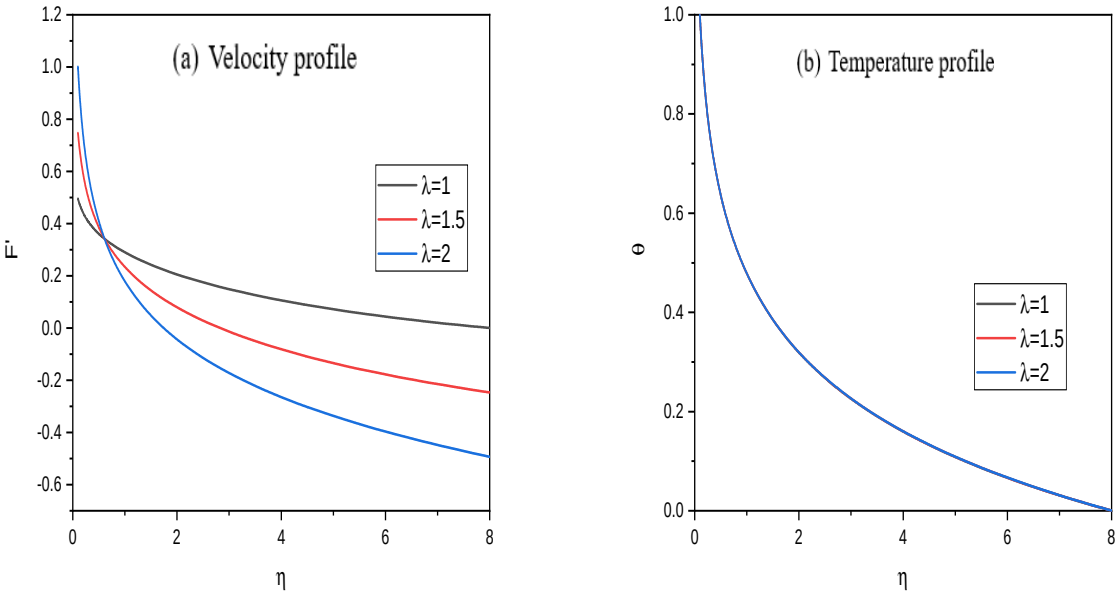

(a) (b)

Figure 3.4: "Effect of λ on the (a) Velocity Profile and (b) temperature profile"

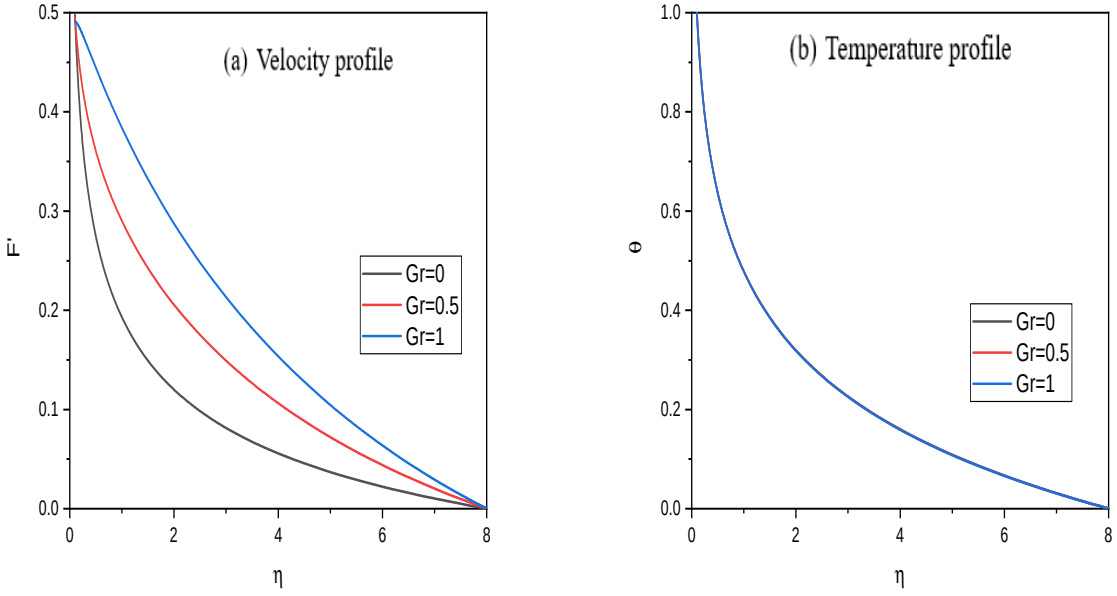

(a) (b)

Figure 3.5: "Effect of Gr on the (a) Velocity Profile and (b) temperature profile"

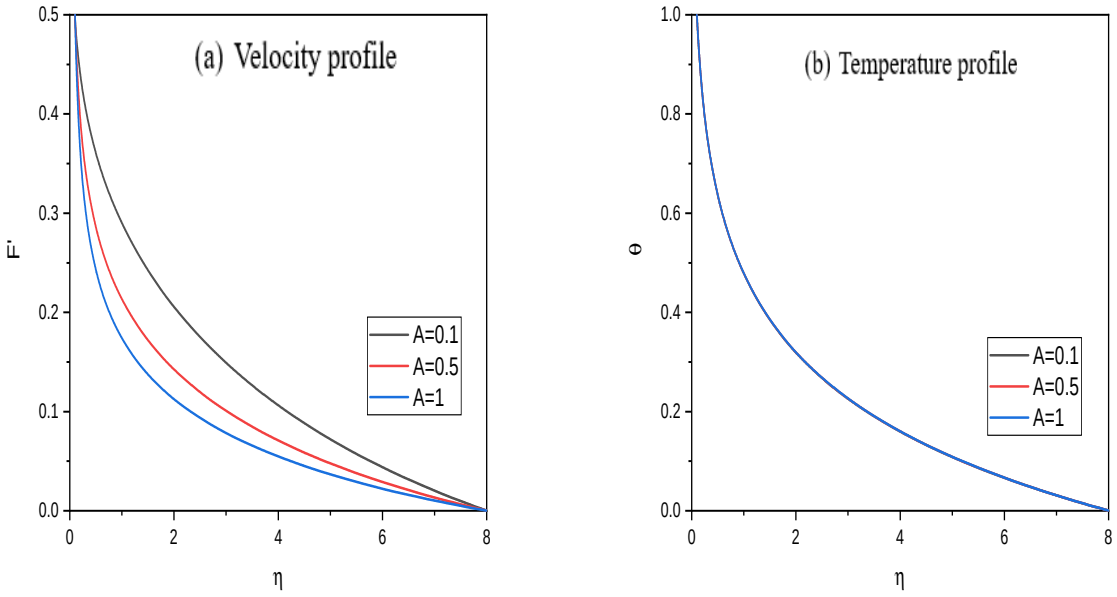

(a) (b)

Figure 3.6: "Effect of A on the (a) Velocity Profile and (b) temperature profile"

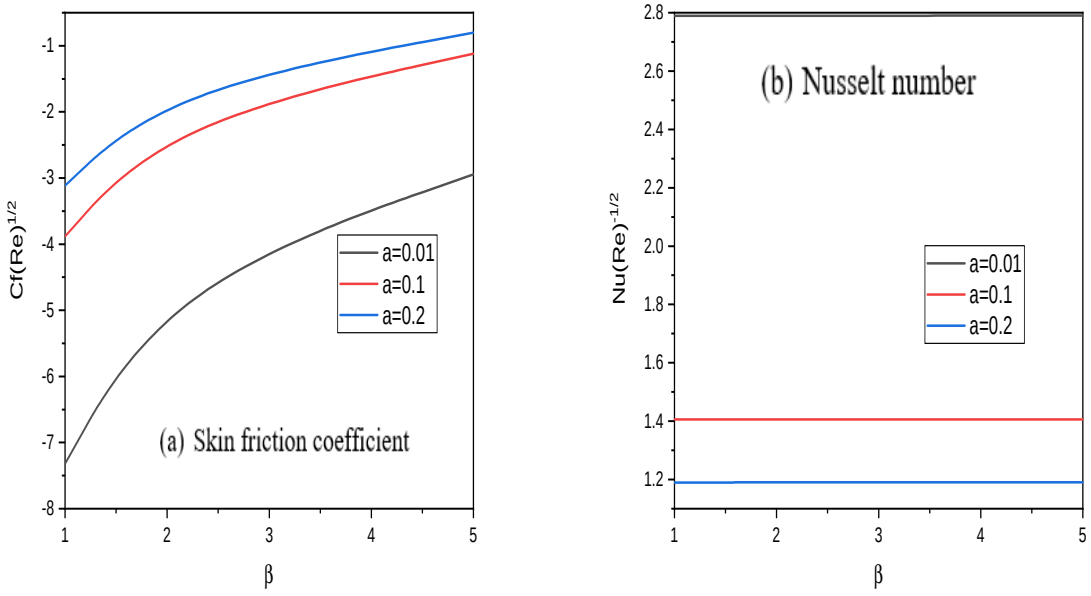

(a) (b)

Figure 3.7: "Effect of a on the (a) coefficient of Skin friction and (b) local Nusselt number "

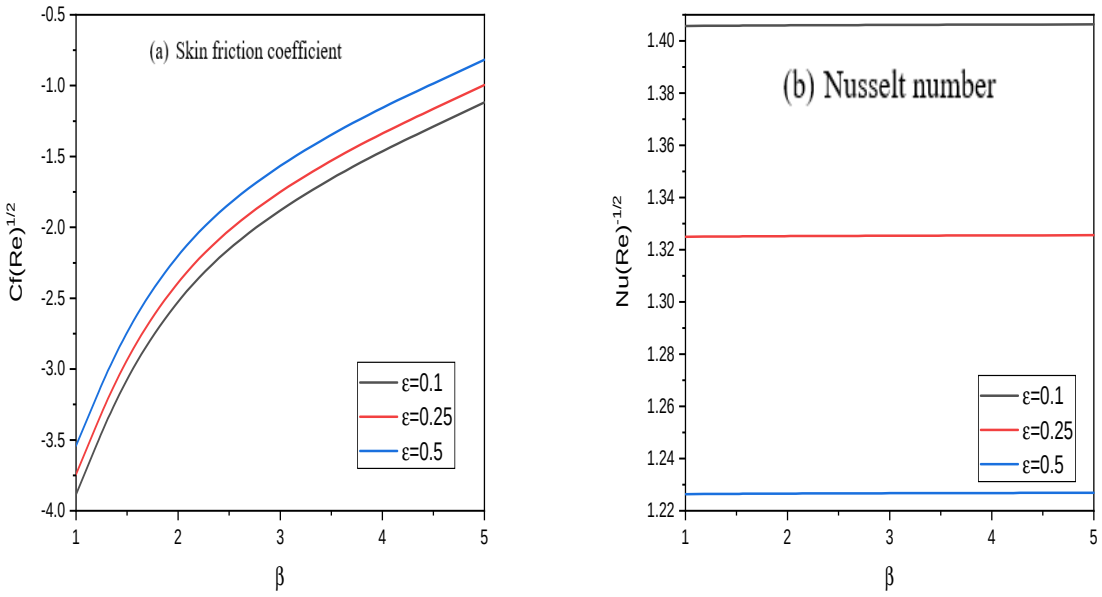

(a) (b)

Figure 3.8: "Effect of ϵ on the (a) coefficient of Skin friction and (b) local Nusselt number "

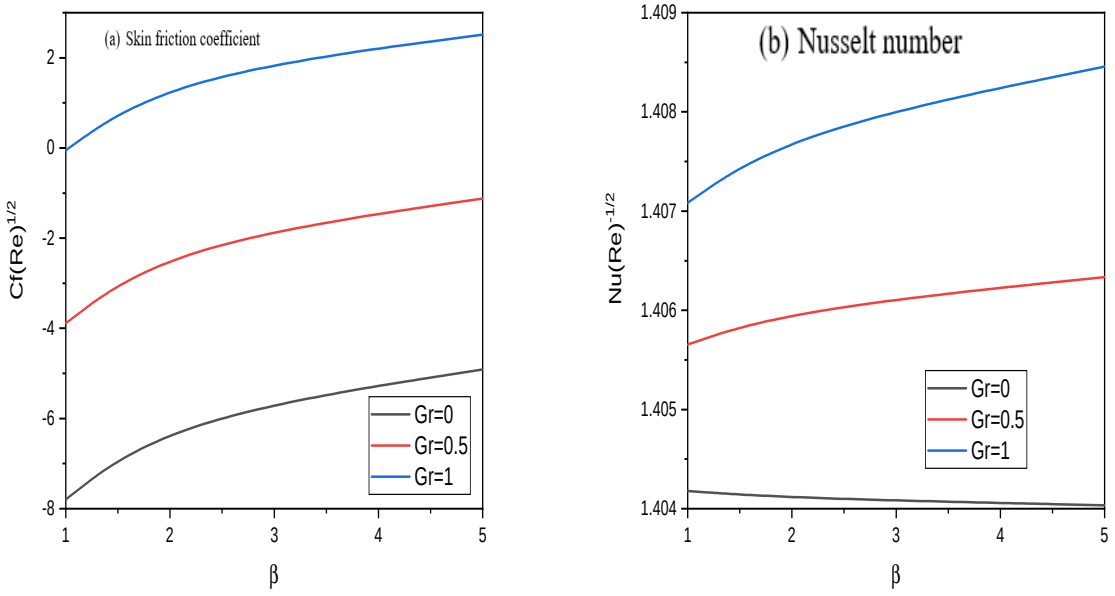

(a) (b)

Figure 3.9: "Effect of Gr on the a) coefficient of Skin friction andb) local Nusselt number"

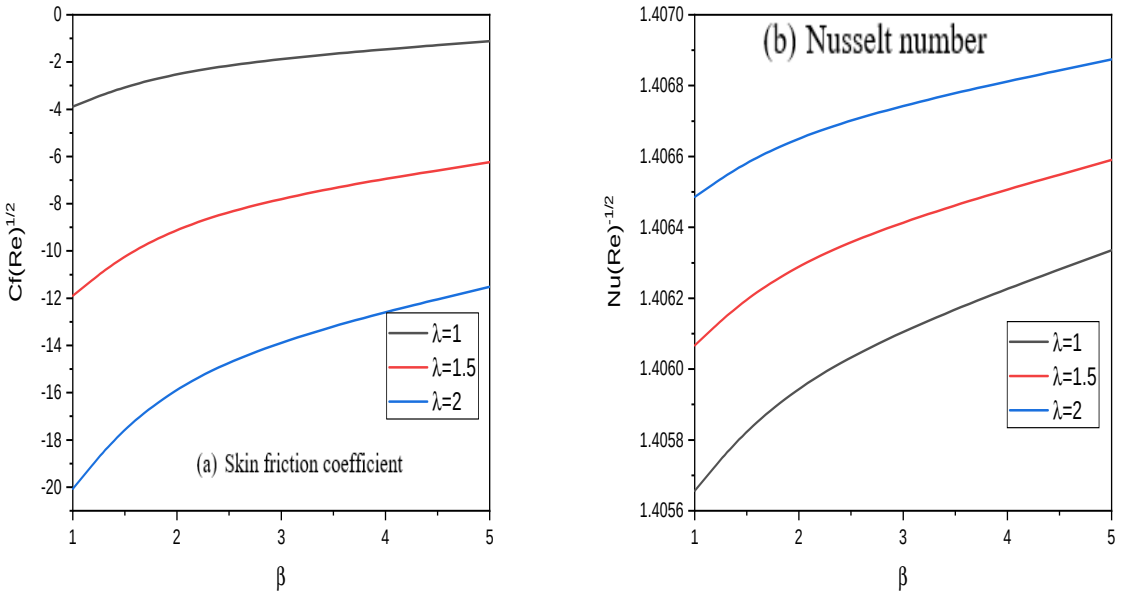

(a) (b)

Figure 3.10: "Effect of λ on the a) coefficient of Skin friction and b) local Nusselt number"

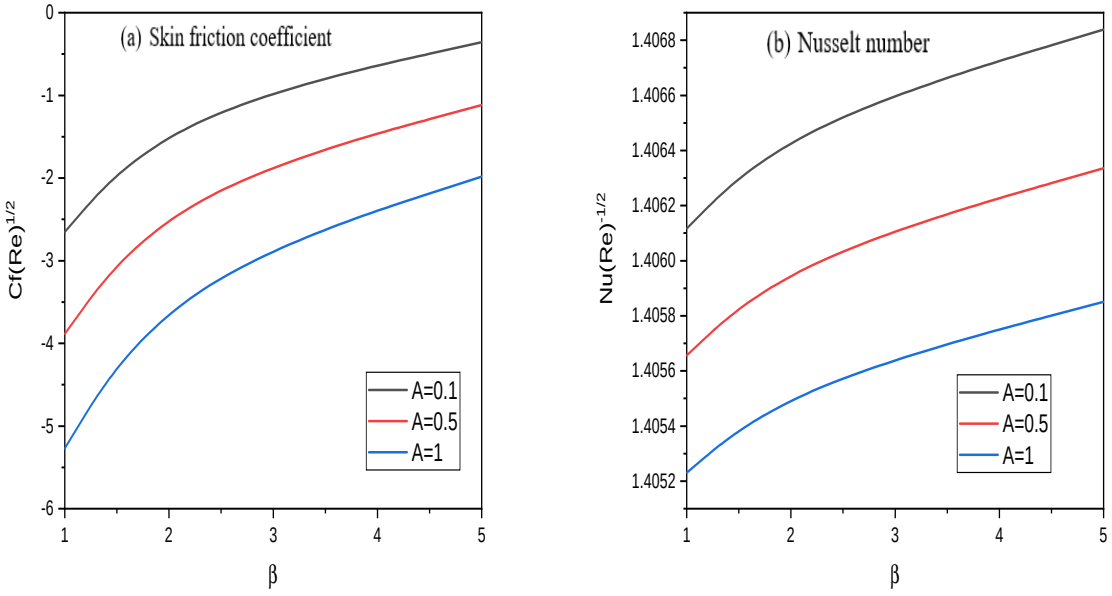

(a) (b)

Figure 3.11: "Effect of A on the a) coefficient of Skin friction and b) local Nusselt number"

Chapter 4

Casson Fluid Flow past a Thin Needle with Cross Diffusion Effects. [1]

4.1 Introduction

Temperature gradients can cause mass flux, which is known as thermal diffusion, thermo-diffusion, or the Soret effect . The heat flux caused by a concentration gradient is known as the Dufour effect or diffusion-thermo effect. These impacts are usually regarded as a second-order effect and may become important in fields such as petrology, geosciences, hydrology, and so on. Eckert and Drake [40] presented several Dufour effect applications. The Soret effect was employed to divide isotopes and gas mixtures of intermediate (N2, air) and exceedingly light (H2, He) molecular weights.[41]. There has been a significant amount of study published in the literature on Newtonian and non-Newtonian fluid streams in several geometries, with an emphasis on the Soret and Dufour effect. Shojaei et al. [42] inspected the flow of a non-Newtonian liquid thru a cylinder influenced by Soret, Dufour and warm radiation effects. Waini et al. [43] investigated implications of Soret and Dufour on the stream of Al2O3-water nanoliquid through a narrow needle. Salleh et al.[44] scrutinized the consequences of Soret and Dufour on the convective stream near a moving slender needle. Rehman et al. [62] examined cross diffusive stream on moving tiny needle, focusing attention on the consequences of Soret and Dufour, heat absorption / generation, nonlinear heat radiation, thermal activation and chemical reaction properties. Reddy et al. [46] used the stream of hybrid (Al2O3-Cu/Ethylene glycol) Casson nanofluids over a moving tiny needle

[1] Communicated to "**International Journal of Applied and Computational Mathematics**

to analyze MHD, thermal radiation, and Dufour and Soret effects.

This chapter deals with a steady two-dimensional laminar boundary layer flow along a horizontal tiny needle submerged in a Casson fluid in the presence of cross diffusion effects. The flow-governing equations are first changed into a set of nonlinear ordinary differential equations utilising appropriate transformations. The resulting equations are linearized utilising successive linearization. The linearized equations are solved using Chebyshev spectral collocation technique.

4.2 Formulation of the Problem

Consider the stream of Casson fluid with uniform velocity U_∞ over a tiny needle moving horizontally with a velocity U_w. Assume that the flow is steady, laminar, and incompressible. The x-axis runs horizontally from main edge of needle, and the radial axis runs perpendicular to it as shown in Fig. 2.1. Apart from the assumption of Chapter - 2, here we assume Soret and DuFour effects are present in the medium.

With the above assumptions and invoking boundary layer approximations, the equations governing the flow are

$$\frac{\partial(ru)}{\partial x} + \frac{\partial(rv)}{\partial y} = 0 \tag{4.1}$$

$$u\frac{\partial u}{\partial x} + v\frac{\partial u}{\partial r} = \nu\left(1 + \frac{1}{\beta}\right)\frac{1}{r}\frac{\partial}{\partial r}\left(r\frac{\partial u}{\partial r}\right) \tag{4.2}$$

$$u\frac{\partial T}{\partial x} + v\frac{\partial T}{\partial r} = \alpha\left(\frac{1}{r}\frac{\partial}{\partial r}\left(r\frac{\partial T}{\partial r}\right)\right) + \frac{D_m k_T}{c_s c_p}\frac{\partial^2 C}{\partial r^2} \tag{4.3}$$

$$u\frac{\partial C}{\partial x} + v\frac{\partial C}{\partial r} = D_m\frac{\partial^2 C}{\partial r^2} + \frac{D_m k_T}{T_m}\frac{\partial^2 T}{\partial r^2} \tag{4.4}$$

where C_p represents specific heat, D_m is the diffusivity of the solute, C_s represents concentration susceptibility,K_T represents thermal diffusion ratio and T_m is the mean fluid temperature. The remaining quantities are already defined in Chapter - 2.

The conditions on the surface of the needle are

$$\begin{aligned} u = u_w, v = 0, T = T_w, C = C_w \ \ at\ r = R(x) \\ u \to u_\infty, T \to \infty, C \to \infty \ \ at\ r \to \infty \end{aligned} \tag{4.5}$$

To non-dimensionalize the Eqs.(4.2)-(4.5), we use the following similarity transformations

$$\psi = \nu x f(\eta), \theta(\eta) = \frac{T - T_\infty}{T_w - T_\infty}, \phi(\eta) = \frac{C - C_\infty}{C_w - C_\infty}\eta = \frac{Ur^2}{\nu x} \tag{4.6}$$

where $U = U_w + U_\infty$ is the composite velocity and ψ is stream function

If the equation $\eta = a$, where 'a' is dimensionless constant, represent the needle wall, the surface of the needle, using Eq.(4.6), can be written as $R = (\frac{\nu a x}{U})^{\frac{1}{2}}$ which characterizes the shape and size of the needle.

By putting equation (4.6) in equation (4.1) to (4.4) we get

$$2[1 + \frac{1}{\beta}][\eta f''' + f''] + f f'' = 0 \tag{4.7}$$

$$\frac{\eta}{Pr}\theta'' + \frac{1}{Pr}\theta' + \frac{1}{2}f\theta' + \eta D_f \eta \phi'' + D_f \phi' = 0 \tag{4.8}$$

$$\frac{\eta}{Sc}\phi'' + \frac{1}{Sc}\phi' + \frac{1}{2}f\phi' + \eta Sr\theta'' + Sr\theta' + = 0 \tag{4.9}$$

The modified conditions on boundary are

$$\begin{aligned} f'(a) = \frac{\lambda}{2}, f(a) = \frac{\lambda a}{2}, \theta(a) = 1, \phi(a) = 1 \\ f'(\infty) \to \frac{1-\lambda}{2}, \quad \theta(\infty) \to 0, \phi(\infty) \to 0 \end{aligned} \tag{4.10}$$

where λ is the velocity ratio parameter, $Pr = \dfrac{\nu}{\alpha}$ denotes the Prandtl number, $D_f = \dfrac{D_s K_T (C_w - C_\infty)}{C_s C_p \nu (T_w - T_\infty)}$ denotes the Dufour number, $Sr = \dfrac{D_s K_T (T_w - T_\infty)}{T_m \nu (C_w - C_\infty)}$ denotes the Soret number and $Sc = \dfrac{\nu}{D_s}$ denotes the Schmidt number.

The modified conditions on boundary becomes

$$\begin{aligned} f'(\eta) = \frac{\lambda}{2}, \quad f(\eta) = \frac{\lambda a}{2}, \quad \theta(\eta) = 1 \quad \text{at} \quad \eta = a \\ f'(\eta) \to \frac{1-\lambda}{2}, \quad \theta(\eta) \to 0 \quad \text{at} \quad \eta \to \infty \end{aligned} \tag{4.11}$$

The local Nusselt number Nu and coefficient of skin friction C_f are the relevant physical

parameters for this modeland are given by

$$\sqrt{Re}C_f = 8\sqrt{a}\left(1+\frac{1}{\beta}\right)f^{''}(a), \quad \frac{Nu}{\sqrt{Re}} = -2\sqrt{a}\theta^{'}(a) \tag{4.12}$$

4.3 Solution of the Problem

The combined Eqns. (4.7) to (4.9) and conditions on boundary (4.12) are linearized through the successive linearization method (SLM) [78]. The solution of resulting linearized equations is obtained by Chebyshev collocation method.

On applying the procedure explained in Chapter 2 to the equations Eqns. (4.7) and (4.9), we get the following linearized equations.

$$a_1 f_j^{'''} + a_2 f_j^{''} + a_3 f_j = r_1 \tag{4.13}$$

$$b_1 f_j + b_2 \theta_j^{''} + b_3 \theta_j{}' + b_4 \phi_j{}'' + b_5 \phi_j{}' = r_2 \tag{4.14}$$

$$c_1 f_j + c_2 \theta_j^{''} + c_3 \theta_j{}' + c_4 \phi_j{}'' + c_5 \phi_j{}' = r_3 \tag{4.15}$$

$$a_1 = 2\eta\left(1+\frac{1}{\beta}\right), a_2 = 2\left(1+\frac{1}{\beta}\right) + \sum f_m, \quad a_3 = \sum f_m''$$

$$r_1 = -2\eta\left(1+\frac{1}{\beta}\right)(\sum f_m''') - 2\left(1+\frac{1}{\beta}\right)(\sum f_m'') - (\sum F_m)(\sum f_m'')$$

$$b_1 = (\sum \theta_m'), \quad b_2 = \frac{2\eta}{Pr}, \quad b_1 = \frac{2}{Pr} + (\sum f_m), \quad b_4 = D_f\eta, \quad b_5 = D_f$$

$$r_2 = -(\sum f_m)(\sum \theta_m') - \frac{2}{Pr}(\sum \theta_m') - \frac{2\eta}{Pr}(\sum \theta_m'') - D_f\eta(\sum \phi_m'') - D_f(\sum \phi_m')$$

$$c_1 = (\sum \phi_m'), \quad c_2 = Sr2\eta, \quad c_3 = Sr, \quad c_4 = \frac{2\eta}{Sc}, \quad c_5 = (\sum f_m) + \frac{1}{Sc}$$

$$r_3 = -(\sum f_m)(\sum \phi_m') - \frac{1}{Sc}(\sum \phi_m') - \frac{2\eta}{Sc}(\sum \phi_m'') - Sr(\sum \theta_m') - Sr2\eta(\sum \theta_m')$$

As explained in Chapter - 2, using Chebyshev collocation method on the system of linearized equations. (4.13) to (4.15), we obtain the following equation in matrix form

$$A_{j-1}X_j = R_{j-1} \tag{4.16}$$

where A_{j-1} is a $3(N+1)\times 3(N+1)$ order matrix and X_j and R_{j-1} are $3(N+1)\times 1$ column

matrix given by

$$A_{j-1} = \begin{pmatrix} A_{11} & A_{12} & A_{13} \\ A_{21} & A_{22} & A_{23} \\ A_{31} & A_{32} & A_{33} \end{pmatrix}, X_j = \begin{pmatrix} F_j \\ \Theta_j \\ \Phi_j \end{pmatrix}, R_{j-1} = \begin{pmatrix} r_{1,j-1} \\ r_{2,j-2} \\ r_{3,j-3} \end{pmatrix} \tag{4.17}$$

where

$$F_j = [f_i(\xi_0), f_i(\xi_1), ..., f_i(\xi_{N-1}), f_i(\xi_N)]^T,$$

$$\Theta_j = [\theta_i(\xi_0), \theta_i(\xi_1), .., \theta_i(\xi_{N-1}), \theta_i(\xi_N)]^T,$$

$$\Phi_j = [\phi_i(\xi_0), \phi_i(\xi_1), .., \phi_i(\xi_{N-1}), \phi_i(\xi_N)]^T,$$

$$A_{11} = a_1 D^3 + a_2 D^2 + a_3 D + a_4 I, A_{12} = O, A_{13} = O$$

$$A_{21} = b_1 I, A_{22} = b_2 D^2 + b_3 D, A_{23} = b_4 D^2 + b_5 D$$

$$A_{31} = c_1 I, A_{32} = c_2 D^2 + c_3 D, A_{33} = c_4 D^2 + c_5 D$$

$$r_1 = [r_1(\xi_0), r_1(\xi_1), ..., r_1(\xi_{N-1}), r_1(\xi_N)]^T,$$

$$r_2 = [r_2(\xi_0), r_2(\xi_1), ..., r_2(\xi_{N-1}), r_2(\xi_N)]^T,$$

$$r_3 = [r_3(\xi_0), r_3(\xi_1), ..., r_3(\xi_{N-1}), r_3(\xi_N)]^T$$

The superscript T stands for transpose, I is the identity matrix, O is the zero matrix. Imposing the boundary conditions in terms of the collocation points, the solution is provided by

$$X_j = A_{j-1}^{-1} R_{j-1}$$

4.4 Results and Discussion

4.1 Effect of the wall of the needle, velocity ratio parameter, Casson fluid parameter, Soret, and Dufour numbers on velocity:

The impact of a, β, λ, Df, and Sr on the velocity is exhibited in Figures 4.1(a) to 4.1(e). From Figure 4.1(a), it is detected that the velocity reduces as 'a' increases. For increasing values of the Casson fluid parameter, the velocity is decreasing, as depicted in Figure 4.1(b). From Figure4.1(c), it is detected that for intensifying, the velocity ratio parameter decreases the velocity close to the needle, then increases the velocity further from the needle. The

velocity does not change with changing the values of Df and Sr, as illustrated in Figures 4.1(d) and 4.1(e).

4.2 Effect of Wall of the needle, Velocity ratio parameter, Casson fluid parameter, Soret and Dufour numbers on Temperature:

The impact of a, β, λ, Df, and Sr on the temperature is exhibited in Figures 4.2(a) to 4.2(e). From Figure 4.2(a), it is noticed that the temperature decreases as 'a' increases. It is clear from the figure 4.2(b) that there is no real impact of the Casson fluid parameter on temperature. The influence of the velocity ratio parameter on the temperature profile is negligible, as presented in Figure 4.2(c). The temperature is decreasing for enhancing values of Df, as depicted in figure 4.2(d). There is slight variation in the temperature for enhancing values of the Soret number, as presented in Figure 4.2(e).

4.3 Effect of Wall of the needle, Velocity ratio parameter, Casson fluid parameter, Soret and Dufour numbers on Concentration:

The impact of a, β, λ, Df, and Sr on the temperature is presented in Figures 4.3(a) to 4.3(e). From Figure 4.3(a), it is observed that concentration reduces as 'a' increases. It is clear from the figure 4.3(b) that there is no real impact of the Casson fluid parameter on concentration. As depicted in Figure 4.3(c), the impact of the velocity ratio parameter on the concentration is almost negligible. The concentration is decreasing for enhancing values of Df, as depicted in figure 4.3(d). There is a slight variation in concentration for increasing values of the Soret number, as presented in Figure 4.3(e).

4.4 Effect of the wall of the needle, velocity ratio parameter, Soret, and Dufour numbers on skin friction coefficient:

The influence of a, λ, D_f, and Sr on the skin friction coefficient is presented in Figures 4.4(a) to 4.4(d). From Figures 4.4(a) and 4.4(b), it is noticed that skin friction coefficient reduces as 'a' and velocity ratio parameter enhances. The skin friction does not change with changing the values of Df and Sr, as exhibited in Figures 4.4(c) and 4.4(d).

4.5 Effect of Wall of the needle, Velocity ratio parameter, Soret and Dufour numbers on Nusselt number:

The influence of a, λ, Df, and Sr on the Nusselt number is presented in Figures 4.5(a) to 4.5(d). From Figures 4.5(a), it is noticed that the Nusselt number decreases as 'a' increases. An increase in the velocity ratio parameter increases the local Nusselt number, as illustrated in Figure 4.5(b). As exhibited in Figure 4.5(c), the Nusselt number decreases as

'Df' increases. The Nusselt number increases as 'Sr' increases, which is illustrated in Figure 4.5(d).

4.6 Effect of the wall of the needle, velocity ratio parameter, Soret and Dufour numbers on the Sherwood number

The influence of a, λ, D_f, and Sr on the Nusselt number is presented in Figures 4.6(a) to 4.6(d). From Figures 4.6(a), it is noticed that the Sherwood number decreases as 'a' increases. A rise in the velocity ratio parameter enhances the Sherwood number, as portrayed in Figure 4.6(b). As exhibited in Figure 4.6(c), the Sherwood number increases as 'Df' increases. The Sherwood number decreases as 'Sr' increases, as portrayed in Figure 4.6(d).

4.5 Conclusion

In the presence of cross-diffusion effects, the steady flow over a horizontal, thin needle submerged in Casson fluid is investigated. The flow equations are initially converted into a set of ordinary differential equations employing suitable transformations, then linearized by means of successive linearization. With the use of the Chebyshev spectral collocation method, the linearized equations are solved.

- The velocity reduces and temperature, and concentration improve with the increasing size of the needle.
- A rise in Df leads to a rise in temperature and concentration profiles.
- An upsurge in Sr produces a rise in temperature and concentration distribution.
- Skin friction coefficient, local heat, and mass transfer coefficients reduce with enhancing needle size.
- The implications of Df and Sr on the Nusselt and Sherwood numbers are in reverse.

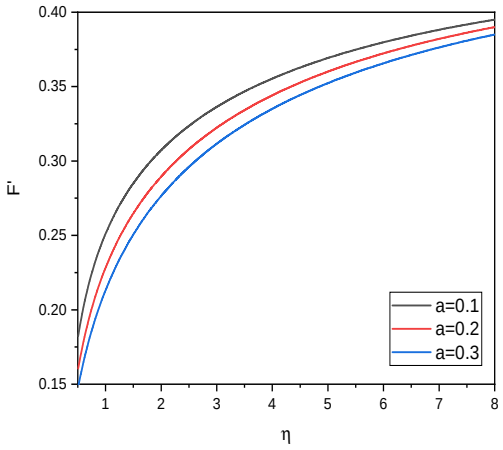

(a)

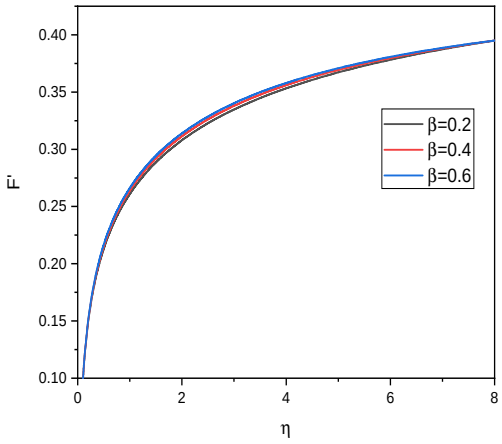

(b)

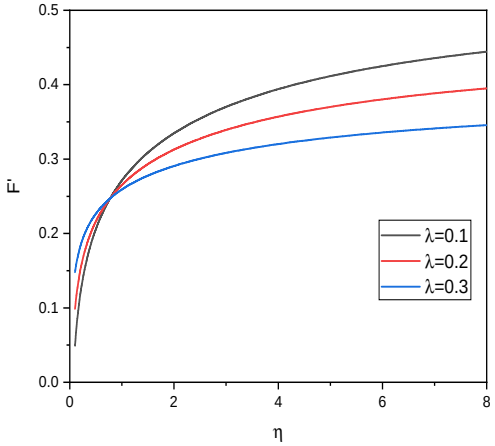

(c)

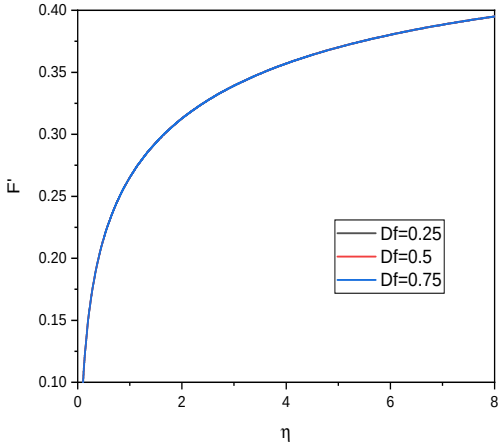

(d)

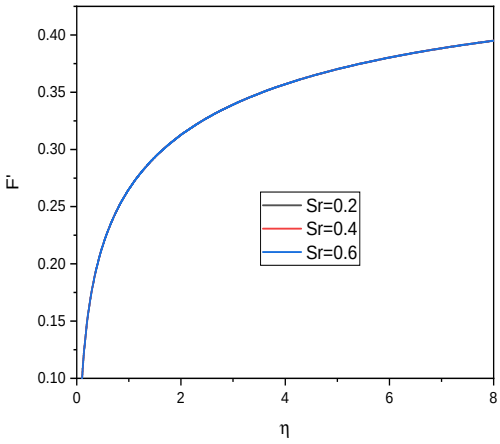

(e)

Figure 4.1: "Effect of (a) a (b) β (c) λ (d) Df (e) Sr on the velocity"

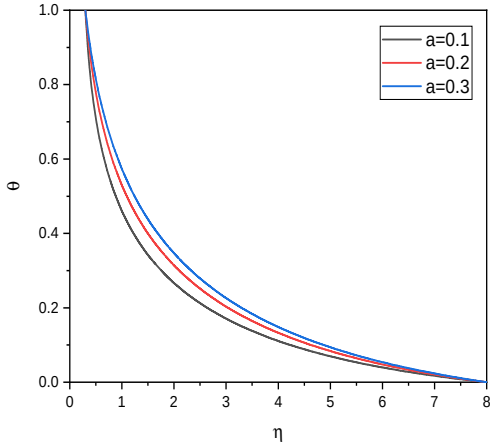

(a)

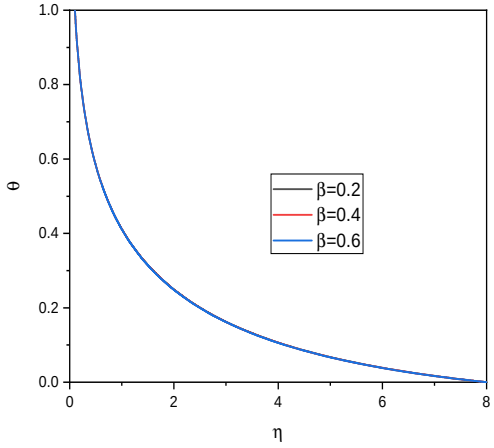

(b)

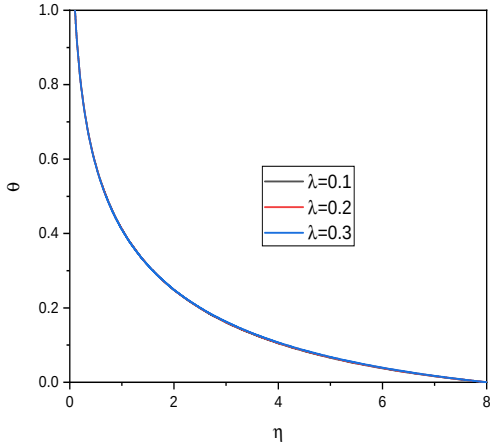

(c)

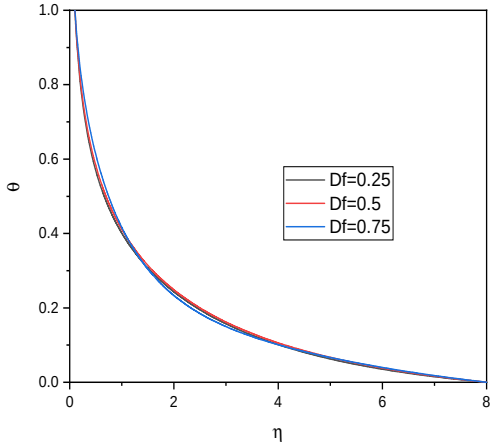

(d)

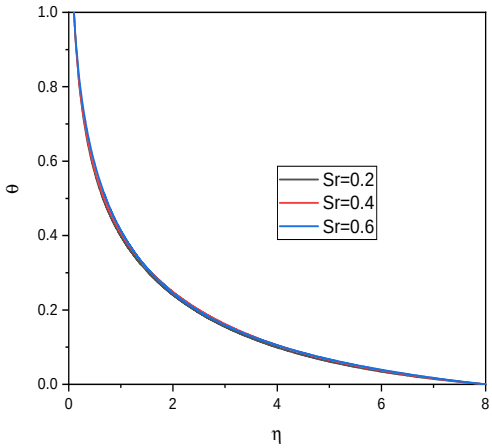

(e)

Figure 4.2: "Effect of (a) a (b) β (c) λ (d) Df (e) Sr on the temperature"

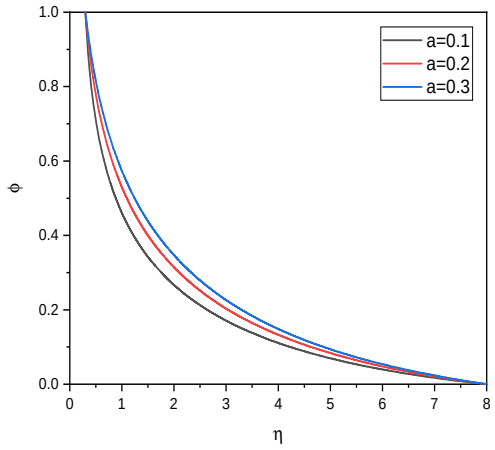

(a)

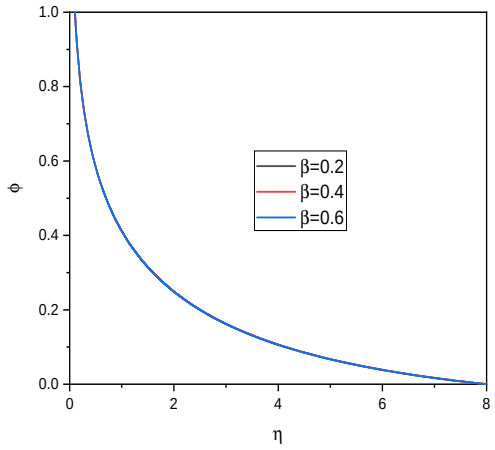

(b)

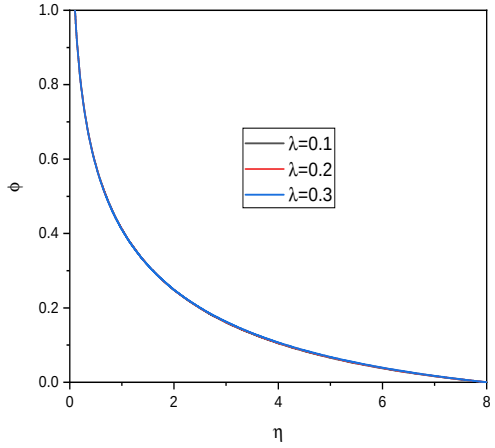

(c)

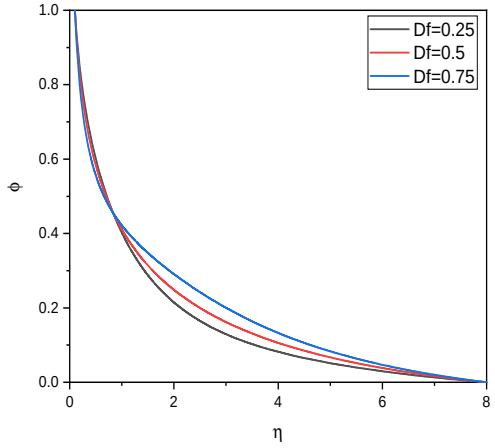

(d)

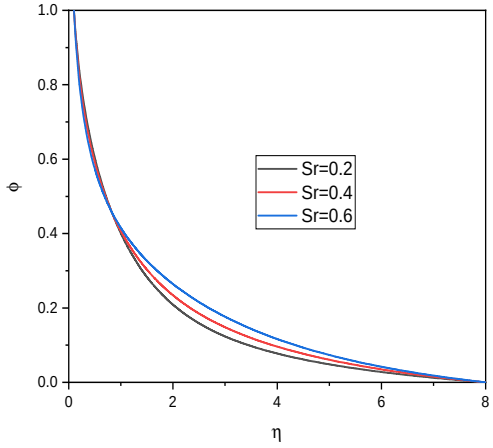

(e)

Figure 4.3: "Effect of (a) a (b) β (c) λ (d) Df (e) Sr on the Concentration"

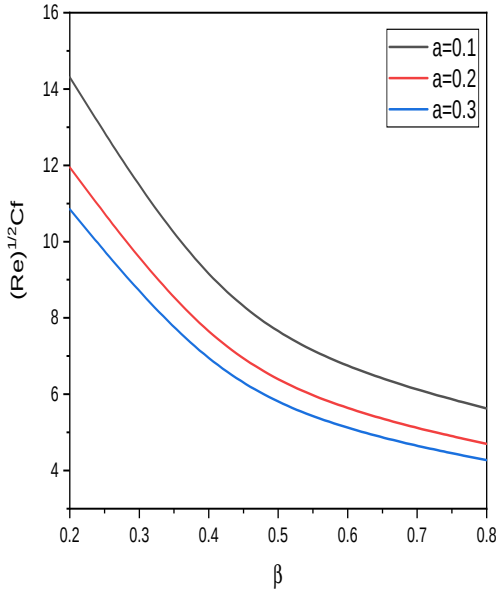

(a)

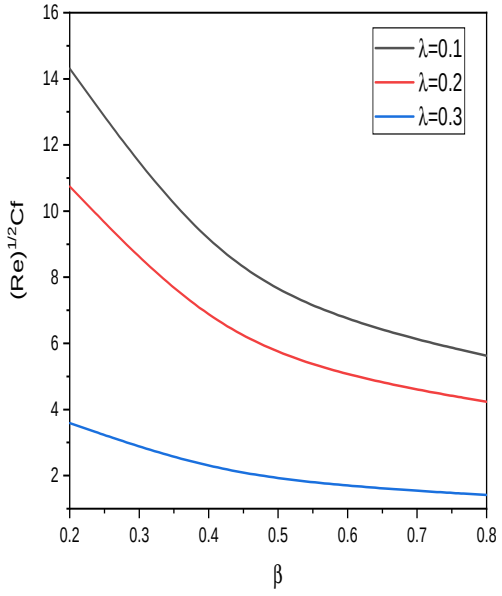

(b)

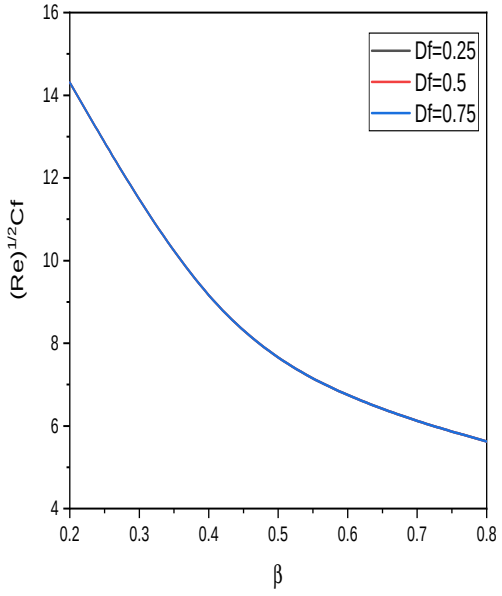

(c)

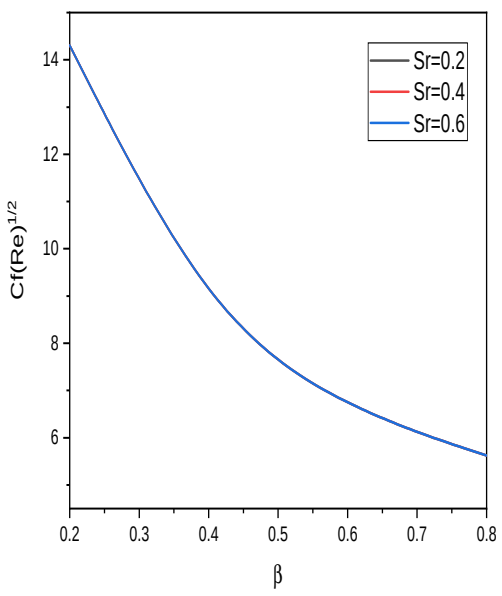

(d)

Figure 4.4: "Effect of (a) a (b) λ (c) Df (d) Sr on $C_f(Re)^{\frac{1}{2}}$"

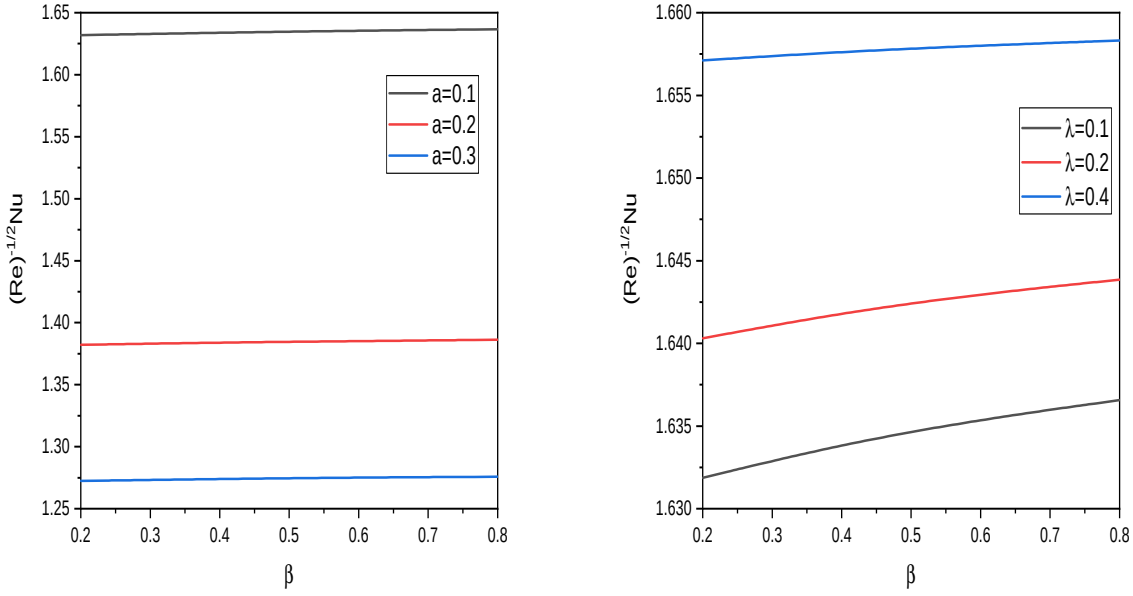

(a) (b)

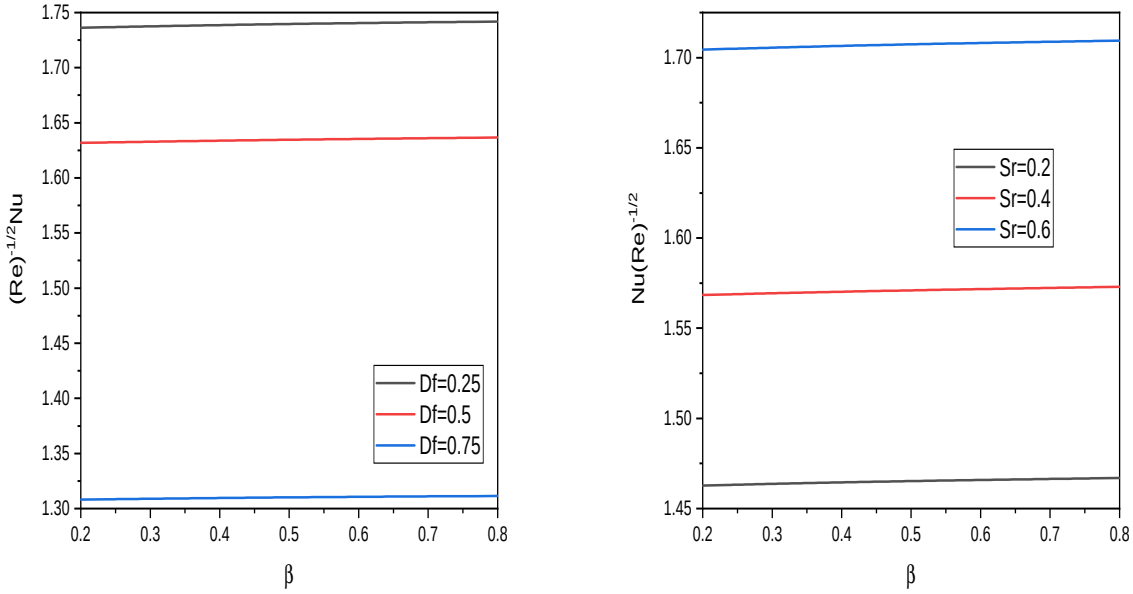

(c) (d)

Figure 4.5: "Effect of (a) a (b) λ (c) Df (d) Sr on $Nu(Re)^{\frac{-1}{2}}$"

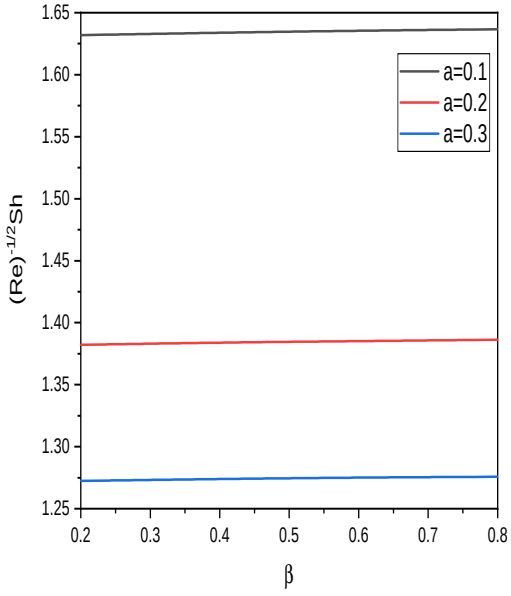

(a)

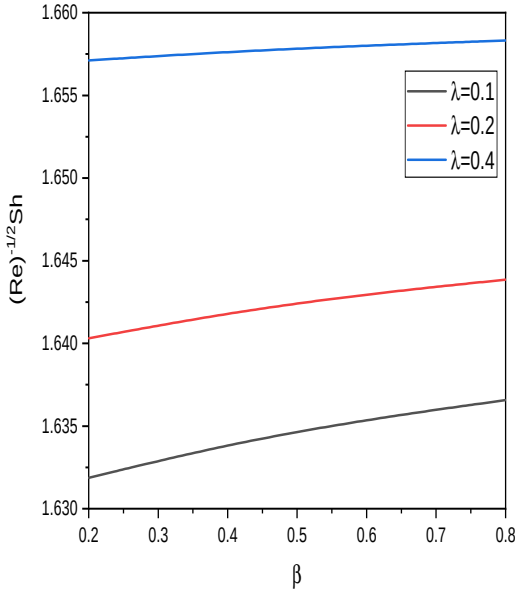

(b)

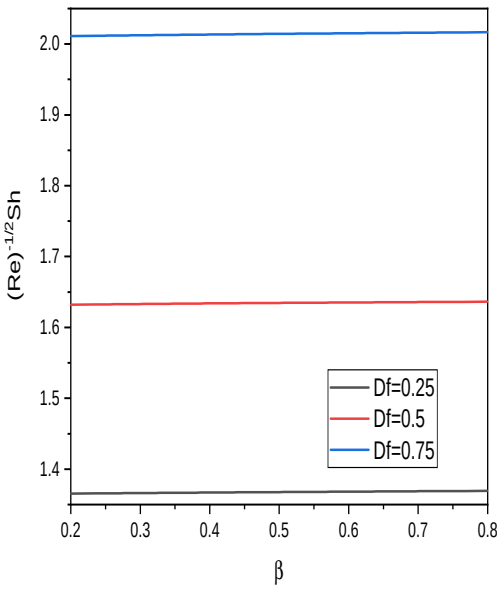

(c)

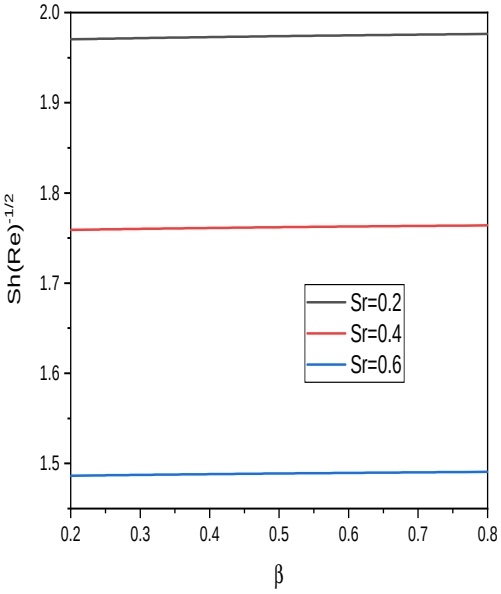

(d)

Figure 4.6: "Effect of (a) a (b) λ (c) Df (d) Sr on $Sh(Re)^{\frac{-1}{2}}$"

Chapter 5

Casson Fluid Flow Past a Thin Needle with Radiation, Viscous Dissipation and Chemical Reaction Effects [1]

5.1 Introduction

The increase in fluid temperature caused by flow-induced friction at the surface is referred to as viscous dissipation. It is required in viscous fluids such as polymers and oils. It has numerous uses in industry and technology. Viscous dissipation is commonly used in electrical equipment like light bulbs, electric heaters, electric stoves, and electric fuses. Furthermore, the influence of chemical reactions is a crucial aspect in analyzing heat and mass transport in many disciplines of engineering, industry, and science. Khan *et al.* [47] examined effects of chemical reaction on Casson fluid flowing on stretched sheet. Sulochana *et al.* [49] covered viscous dissipation and non-uniform heat source/sink in 2-D forced convective MHD ferrofluid stream upon a horizontally moving needle. Afridi *et al.* [48] examined the Rosseland radiation and entropy generation of moving tiny needle on self-similar surface in the existence of viscous dissipation. Raju *et al.* [50] studied effect of Darcy-Forchheimer flow on a tiny needle in viscoelastic fluid.

According to reviews of the literature, no research have yet been published that examine stream of Casson fluid across needle when radiation, viscous dissipation and chemical reaction are used. This study investigates how Casson fluid stream across tiny needle is affected by

[1] Publication in "**Journal of Xidian University**"

altering viscous dissipation, chemical reaction and thermal radiation.

5.2 Formulation of the Problem

Consider the stream of Casson fluid with uniform velocity U_∞ over a tiny needle moving horizontally with a velocity U_w . Assume that the flow is steady, laminar, and incompressible. The x-axis runs horizontally from main edge of needle, and the radial axis runs perpendicular to it as shown in Fig. 2.1. Apart from the assumption of Chapter - 2, here we assume that Radiation, Viscous dissipation and Chemical reaction effects are present in the medium. The governing equations of the flow are

$$\frac{\partial(rv)}{\partial r} + \frac{\partial(ru)}{\partial x} = 0 \tag{5.1}$$

$$v\frac{\partial u}{\partial r} + u\frac{\partial u}{\partial x} = \frac{1}{r}\left(1+\frac{1}{\beta}\right)\nu\frac{\partial}{\partial r}\left(r\frac{\partial u}{\partial r}\right) \tag{5.2}$$

$$v\frac{\partial T}{\partial r} + u\frac{\partial T}{\partial x} = \frac{1}{r}\alpha\frac{\partial}{\partial r}\left(r\frac{\partial T}{\partial r}\right) - \frac{1}{\rho c_\rho}\frac{1}{r}\frac{\partial}{\partial r}\left(rq_r\right) + \frac{\mu}{\rho c_\rho}\left(1+\frac{1}{\beta}\right)\left(\frac{\partial u}{\partial r}\right)^2 \tag{5.3}$$

$$v\frac{\partial C}{\partial r} + u\frac{\partial C}{\partial x} = D_m\frac{1}{r}\frac{\partial}{\partial r}\left(r\frac{\partial C}{\partial r}\right) - K^*(C - C_\infty) \tag{5.4}$$

where q_r is radiative heat flux, K^* is reaction rate of solute and the remaining quantities are already defined in Chapter - 2

The boundary conditions are:

$$\begin{aligned} v = 0, T = T_w, u = u_w, C = C_w \ \text{ at } r = R(x) \\ T \to \infty, u \to u_\infty, C \to \infty \ \text{ at } r \to \infty \end{aligned} \tag{5.5}$$

To non-dimensionlize the equations (5.1) to (5.4), we use the following similarity transformations:

$$\eta = \frac{Ur^2}{\nu x}, \quad \psi = \nu x f(\eta), \quad \theta(\eta) = \frac{T - T_\infty}{T_w - T_\infty}, \phi(\eta) = \frac{C - C_\infty}{C_w - C_\infty} \tag{5.6}$$

where ψ is the stream function

Surface $\eta = a$ refers to the needle's wall and relates to the revolution's surface. Substituting $\eta = a$ in Eq. (5.6) characterises both the shape and size the physical body's surface.

and is given by $R = \sqrt{\frac{\nu a x}{U}}$

Substituting the similarity variables given in (5.6) in Eqns. (5.1) to (5.4), we obtain

$$2\eta\left(1+\frac{1}{\beta}\right)f''' + 2\left(1+\frac{1}{\beta}\right)f'' + ff'' = 0 \tag{5.7}$$

$$8\eta Ec\left(1+\frac{1}{\beta}\right)(f'')^2 + \frac{2\eta}{Pr}\left(1+\frac{4R_1}{3}\right)\theta'' + \frac{2}{Pr}\left(1+\frac{4R_1}{3}\right)\theta' + f\theta' = 0 \tag{5.8}$$

$$\frac{1}{Sc}\left(2\eta\phi'' + 2\phi'\right) + f\phi' - \frac{k\phi}{2} = 0 \tag{5.9}$$

where R_1 is Radiation parameter, Ec is Eckert number, Sc is Schmidth number, and k is chemical reaction parameter.

The modified conditions on boundary becomes

$$\begin{aligned} f'(\eta) = \frac{\lambda}{2}, \quad f(\eta) = \frac{\lambda a}{2}, \quad \theta(\eta) = 1 \quad \phi(\eta) = 1 \quad \text{at} \quad \eta = a \\ f'(\eta) \to \frac{1-\lambda}{2}, \quad \theta(\eta) \to 0 \quad \phi(\eta) \to 0 \quad \text{at} \quad \eta \to \infty \end{aligned} \tag{5.10}$$

The non-dimensional form of skin friction coefficient, local Nusselt number and sherwood number are

$$\sqrt{Re}C_f = 8\sqrt{a}\left(1+\frac{1}{\beta}\right)f''(a), \quad \frac{Nu}{\sqrt{Re}} = -2\sqrt{a}\theta'(a), \quad \frac{Sh}{\sqrt{Re}} = -2\sqrt{a}\theta'(a) \tag{5.11}$$

5.3 Solution of the Problem

The combined Eqns. (5.7) to (5.9) and conditions on boundary (5.10) are linearized through the successive linearization method (SLM) [78]. The solution of resulting linearized equations is obtained by Chebyshev collocation method.

On applying the procedure explained in Chapter 2 to the equations Eqns. (5.7) to (5.9), we get the following linearized equations.

$$a_1 f_j''' + a_2 f_j'' + a_3 f_j + = r_1 \tag{5.12}$$

$$b_1 f_j'' + b_2 f_j + b_3 \theta_j'' + b_4 \theta_j' = r_2 \tag{5.13}$$

$$c_1 f_j + c_2 \phi_j^{''} + c_3 \phi_j^{'} + c_4 \phi_j = r_3 \tag{5.14}$$

where

$$a_1 = 2\eta \left(1 + \frac{1}{\beta}\right), \quad a_2 = 2\left(1 + \frac{1}{\beta}\right) + (\sum f_m), \quad a_3 = (\sum f_m'')$$

$$r_1 = -2\eta \left(1 + \frac{1}{\beta}\right)(\sum f_m''') - 2\left(1 + \frac{1}{\beta}\right)(\sum f_m'')) - (\sum f_m)(\sum f_m'')$$

$$b_1 = 16\eta Ec \left(1 + \frac{1}{\beta}\right)(\sum f_m''), \quad b_2 = (\sum \theta_m'), \quad b_3 = \frac{2\eta}{Pr}\left(1 + \frac{4R_1}{3}\right),$$

$$b_4 = (\sum f_m) + \frac{2}{Pr}\left(1 + \frac{4R_1}{3}\right)$$

$$r_2 = -(8\eta Ec)\left(1 + \frac{1}{\beta}\right)(\sum f_m'')^2 - (\sum f_m)(\sum \theta_m') - \frac{2\eta}{Pr}\left(1 + \frac{4R_1}{3}\right)(\sum \theta_m'') - \frac{2}{Pr}\left(1 + \frac{4R_1}{3}\right)(\sum \theta_m')$$

$$c_1 = (\sum \phi_m'), \quad c_2 = \frac{2\eta}{Sc}, \quad c_3 = (\sum f_m) + \frac{2}{Sc}, \quad c_4 = -\frac{k}{2}$$

$$r_3 = \frac{k}{2}(\sum \phi_m) - \frac{2\eta}{Sc}(\sum \phi_m'') - \frac{2}{Sc}(\sum \phi_m') - (\sum f_m)(\sum \phi_m')$$

As explained in Chapter - 2, using Chebyshev collocation method on the system of linearized equations. (5.12) to (5.14), we obtain the following equation in matrix form

$$A_{j-1} X_j = R_{j-1} \tag{5.15}$$

where A_{j-1} is a $3(N+1) \times 3(N+1)$ order matrix and X_j and R_{j-1} are $3(N+1) \times 1$ column matrix given by

$$A_{j-1} = \begin{pmatrix} A_{11} & A_{12} & A_{13} \\ A_{21} & A_{22} & A_{22} \\ A_{31} & A_{32} & A_{33} \end{pmatrix}, X_j = \begin{pmatrix} F_j \\ \Theta_j \\ \Phi_j \end{pmatrix}, R_{j-1} = \begin{pmatrix} r_{1,j-1} \\ r_{2,j-2} \\ r_{3,j-2} \end{pmatrix} \tag{5.16}$$

where

$$F_j = [f_j(\xi_0), f_j(\xi_1), ..., f_j(\xi_{N-1}), f_j(\xi_N)]^T,$$

$$\Theta_j = [\theta_j(\xi_0), \theta_j(\xi_1), .., \theta_j(\xi_{N-1}), \theta_j(\xi_N)]^T,$$

$$\Phi_j = [\phi_j(\xi_0), \phi_j(\xi_1), .., \phi_j(\xi_{N-1}), \phi_j(\xi_N)]^T,$$

$$A_{11} = a_1 D^3 + a_2 D^2 + a_3 I, A_{12} = O, A_{13} = O,$$

$$A_{21} = b_1 D^2 + b_2 I, A_{22} = b_3 D^2 + b_4 D, A_{23} = O,$$

$$A_{31} = c_1 I, A_{32} = O, A_{33} = c_2 D^2 + c_3 D + c_4 I,$$

$$r_1 = [r_1(\xi_1), r_1(\xi_2), r_1(\xi_3)...., r_1(\xi_{N+1})]^T,$$

$$r_2 = [r_2(\xi_1), r_2(\xi_2), r_2(\xi_3)...., r_2(\xi_N)]^T,$$

$$r_3 = [r_3(\xi_1), r_3(\xi_2), r_3(\xi_3)...., r_3(\xi_N)]^T,$$

The superscript T stands for transpose, I is the identity matrix, O is the zero matrix.

Imposing the boundary conditions in terms of the collocation points, the solution is provided by

$$X_j = A_{j-1}^{-1} R_{j-1}$$

5.4 Results and Discussion

The five dimensionless parameter effects are primarily the focus of the current model. They are size of the needle (a), velocity ratio parameter (λ), Eckert number (Ec), chemical reaction parameter (k), radiation parameter ($R1$) on velocity and temperature profiles together with local Nusselt number $\frac{Nu}{\sqrt{Re}}$ and coefficient of local skin friction $\sqrt{Re}C_f$. A detailed numerical parametric analysis is conducted to assure a greater comprehension of the technical issue, and the findings are presented graphically (Figs. 5.1-5.13). Numerous a, λ, k, Ec, and $R1$ values have been calculated numerically.

The effect of the size of the needle on velocity, temperature, and concentration profiles is depicted in Fig. 5.1. As shown in Fig.5.1, enlarging a elevates the velocity. As a rises, temperature and concentration are also increasing.

The variation of velocity, temperature, and concentration profiles with the Casson fluid parameter β is given in Fig.5.2. It is understood from Fig. 5.2(a) that velocity improves as the Casson fluid parameter decreases. The effect of the Casson fluid parameter on temperature and concentration profiles is almost negligible.

The fluctuation of Eckert number Ec on velocity, temperature, and concentration profiles is given in Fig. 5.3. It is represented in Fig. 5.3(b) that temperature improves slightly as the Eckert parameter rises. The effect of Eckert number on velocity and concentration profile is almost negligible, as shown in Figs. 5.3(a) and 5.3(c).

Figure 5.4 presents the effect of the chemical reaction parameter on velocity, temperature, and concentration profiles. Figs. 5.4(a) and 5.4(b) exhibit that velocity and temperature profile are independent of k. It is depicted in Fig. 5.4(c) that concentration rises as the chemical reaction parameter decreases.

The variation of velocity, temperature, and concentration profiles with the velocity ratio parameter λ is given in Fig. 5.5. As presented in Fig.5.5(a), intensifying λ decreases velocity near the needle and then increases velocity away from the needle. It is represented in Fig.5.5(b) that temperature improves slightly as the The velocity ratio parameter rises. The effect of the velocity ratio parameter on concentration is negligible, as presented in Fig. 5.5(c).

The impact of the radiation parameter ($R1$) on velocity, temperature, and concentration profiles is given in Fig. 5.6. It is detected from Fig. 5.6(b) that temperature enhances as the radiation parameter rises. As displayed in Figs. 5.6(a) and 5.6(c), velocity and concentration distribution relative to $R1$ are constant.

Figure 5.7 presents the impact of Schmidth number on velocity, temperature, and concentration profiles. Figs. 5.7(a) and 5.7(b) exhibit that velocity and temperature profile are independent of Sc. It is depicted in Fig. 5.7(c) that concentration rises as Sc decreases.

The impact of size of needle a on Nusselt number $\frac{Nu}{\sqrt{Re}}$, coefficient of local skin friction $\sqrt{Re}C_f$, and Sherwood number $\frac{Sh}{\sqrt{Re}}$ is depicted in Fig.5.8. As shown in Fig.5.8(a), $\sqrt{Re}C_f$ is improved by increasing a. As a enhances, $\frac{Nu}{\sqrt{Re}}$ and $\frac{Sh}{\sqrt{Re}}$ are also increasing, as seen in Fig. 5.8(b) and 5.8(c).

The impact of the thermal Eckert number Ec on the local Nusselt number $\frac{Nu}{\sqrt{Re}}$, the coefficient of local skin friction $\sqrt{Re}C_f$, and the Sherwood number $\frac{Sh}{\sqrt{Re}}$ is given in Fig. 5.9. It is understood from Figs. 5.9(a) and 5.9(c) that $\sqrt{Re}C_f$ and $\frac{Sh}{\sqrt{Re}}$ are independent of Ec. As shown in Fig.5.9(b), the $\frac{Nu}{\sqrt{Re}}$ is improved by decreasing Ec.

Figure 5.10. presents the influence of the chemical reaction parameter k on the $\frac{Nu}{\sqrt{Re}}$, $\sqrt{Re}C_f$, and $\frac{Sh}{\sqrt{Re}}$. The variation in the $\sqrt{Re}C_f$ and $\frac{Nu}{\sqrt{Re}}$ are independent of k, as depicted in Figs. 5.10(a) and 5.10(b). Fig. 5.10(c) exhibits that the $\frac{Sh}{\sqrt{Re}}$ rises as k rises.

The fluctuation of $\frac{Nu}{\sqrt{Re}}$, $\sqrt{Re}C_f$, and $\frac{Sh}{\sqrt{Re}}$ with velocity ratio parameter λ is given in Fig.5.11. As presented in Fig.5.11(a), dropping the value of λ increases the skin friction coefficient. An increase in the velocity ratio parameter decreases the Nusselt number, as shown in Fig. 5.11(b). An enhancement in the velocity ratio parameter enhances the Sherwood number, as depicted in Fig. 5.11(c).

The effect of the radiation parameter $R1$ on $\frac{Nu}{\sqrt{Re}}$, $\sqrt{Re}C_f$ and $\frac{Sh}{\sqrt{Re}}$ is given in Fig. 5.12. It is noticed from Fig. 5.12(b) that the $\frac{Nu}{\sqrt{Re}}$ enhances as the velocity ratio parameter decreases. Figs. 5.11(a) and 5.11(c) exhibit that the variation in the $\sqrt{Re}C_f$ and $\frac{Sh}{\sqrt{Re}}$ are independent of $R1$.

Figure 5.13. presents variations of Schmidth number Sc on the $\frac{Nu}{\sqrt{Re}}$, $\sqrt{Re}C_f$, and $\frac{Sh}{\sqrt{Re}}$. The variation in the $\sqrt{Re}C_f$ and $\frac{Nu}{\sqrt{Re}}$ are independent of k, as depicted in Figs. 5.13(a) and 5.13(b). Fig. 5.13(c) exhibits that the $\frac{Sh}{\sqrt{Re}}$ rises as Sc rises.

5.5 Conclusion

The assumption that radiation and chemical reactions change with temperature and concentration is used to explore the boundary layer stream across a tiny needle in casson fluid. The Chebyshev spectral technique is utilized to locate the solution of the resulting system after the non-dimensional equations are linearized using a successive linearized procedure.

- While concentration, temperature, and velocity of flow rise as needle size increases, skin friction coefficient, heat transfer coefficient, and Sherwood number decrease.
- With improved concentration distribution, the chemical reaction parameter decreases, and with an increased chemical reaction parameter, the Sherwood number rises.
- The temperature rises as the radiation parameter is improved, whereas the Nusselt number rises as the radiation parameter is reduced.

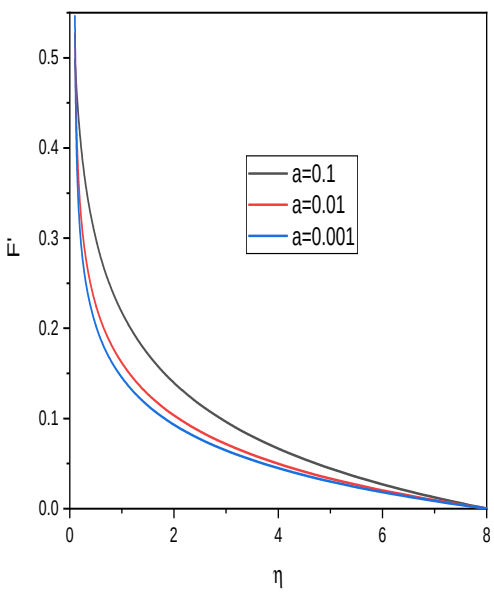

(a) velocity

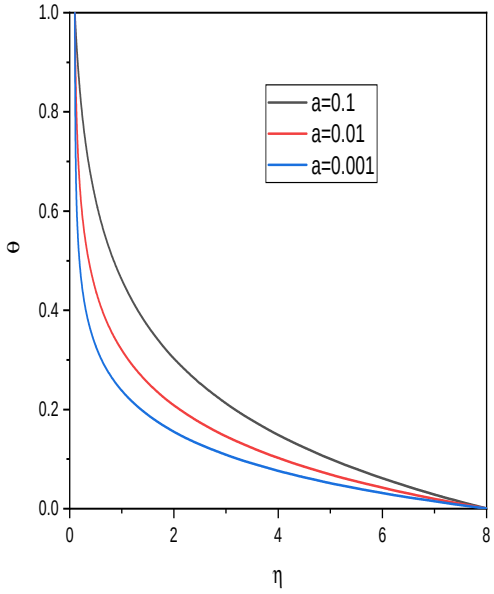

(b) Temperature

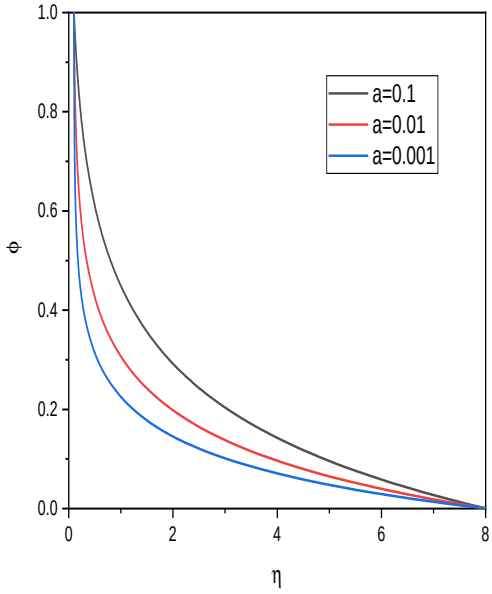

(c) Concentration

Figure 5.1: "Effect of a on the velocity,temperature and concentration profiles"

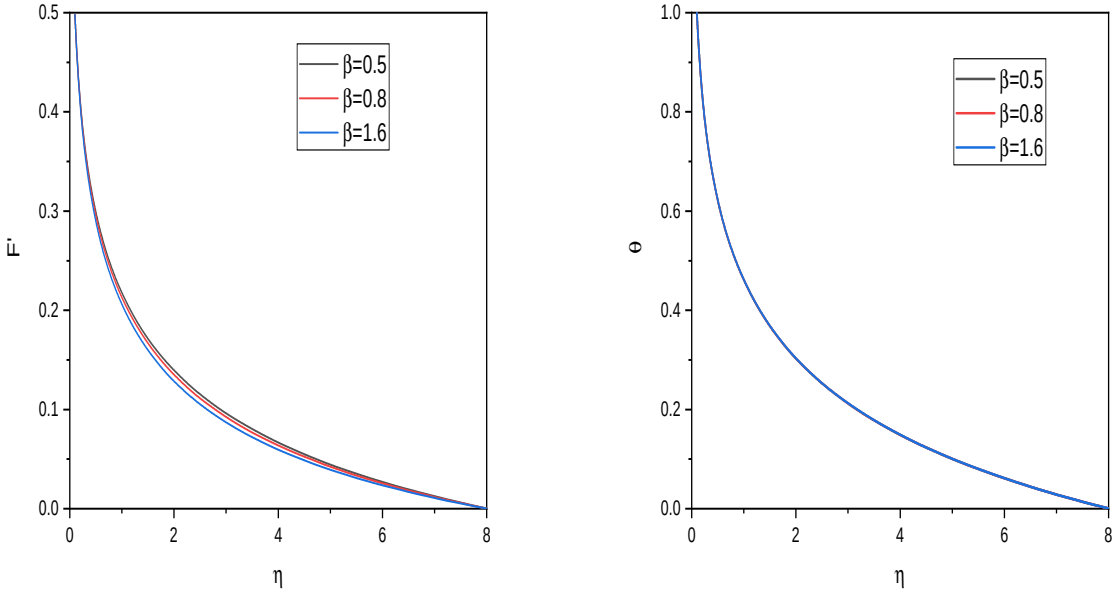

(a) velocity

(b) Temperature

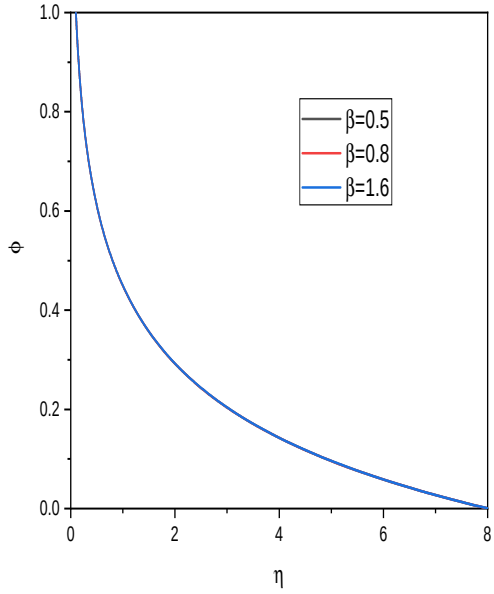

(c) Concentration

Figure 5.2: "Effect of β on the velocity,temperature and concentration profiles"

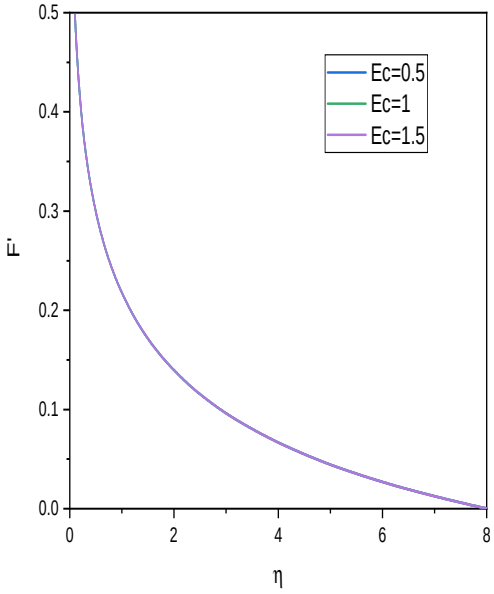

(a) velocity

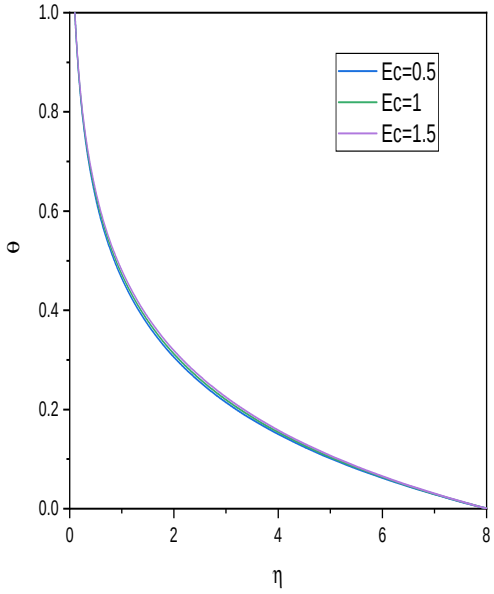

(b) Temperature

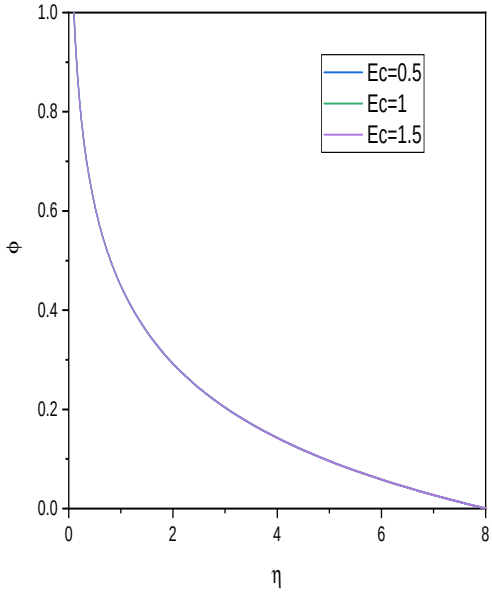

(c) Concentration

Figure 5.3: "Effect of Ec on the velocity,temperature and concentration profiles"

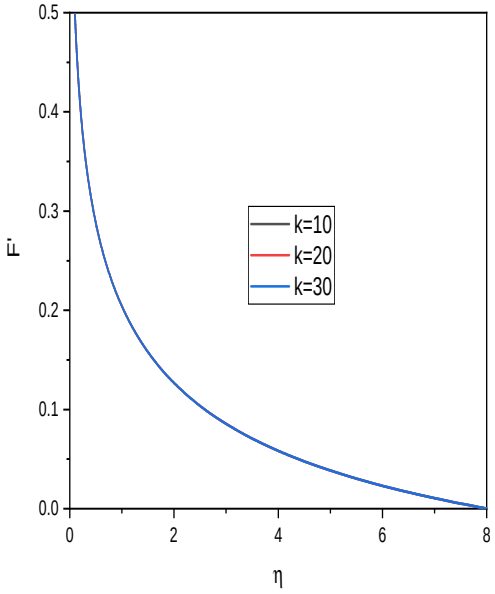

(a) velocity

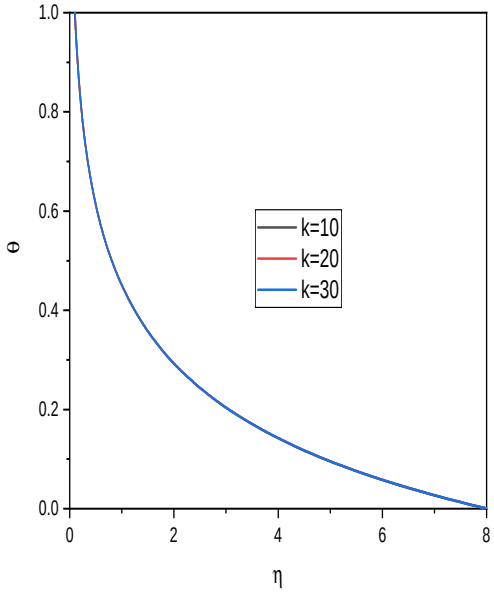

(b) Temperature

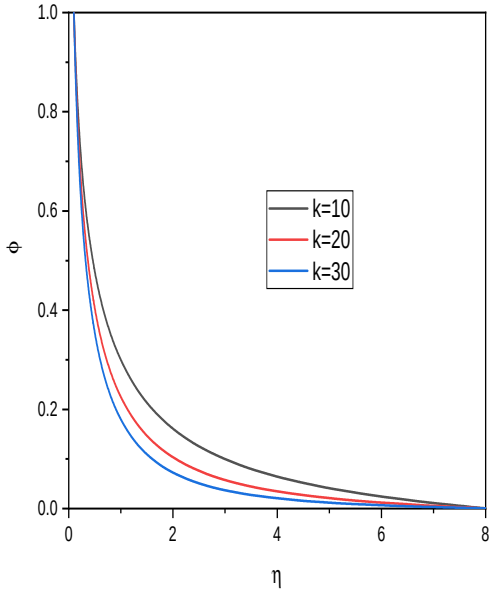

(c) Concentration

Figure 5.4: "Effect of k on the velocity,temperature and concentration profiles"

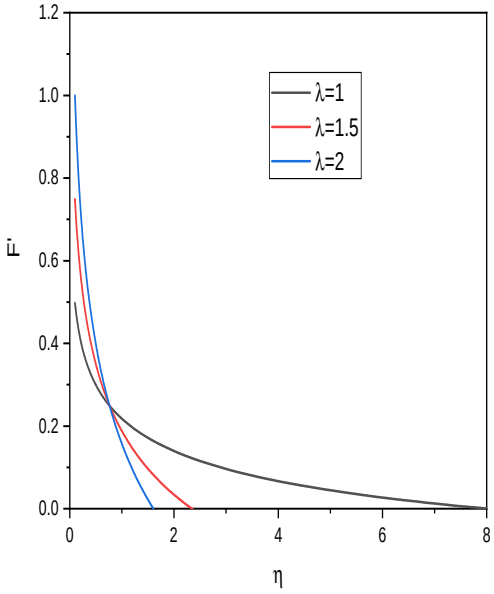

(a) velocity

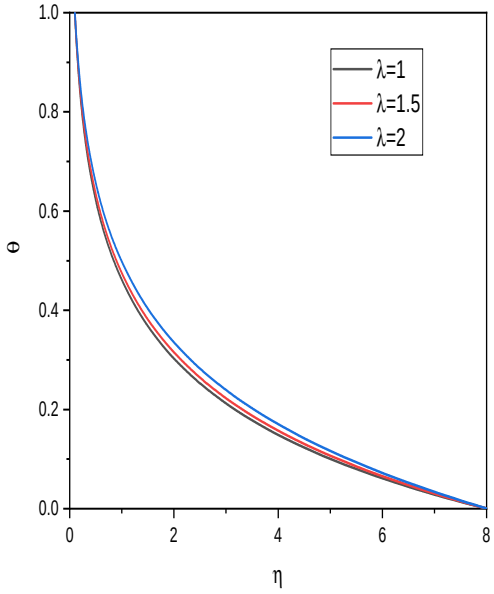

(b) Temperature

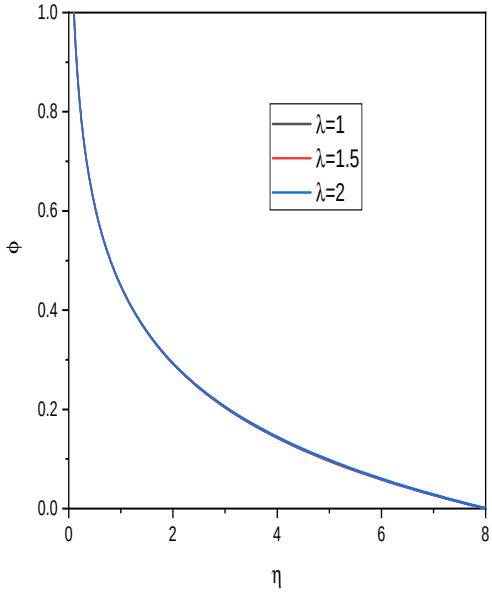

(c) Concentration

Figure 5.5: "Effect of λ on the velocity,temperature and concentration profiles"

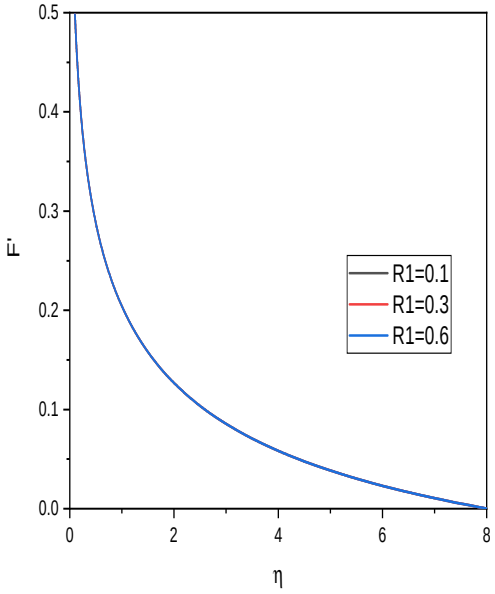

(a) velocity

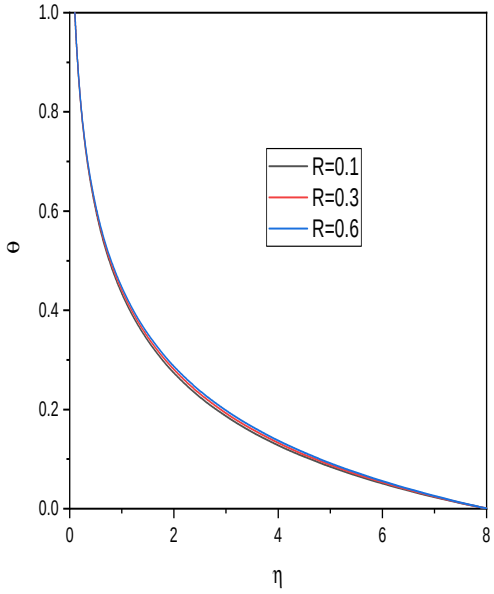

(b) Temperature

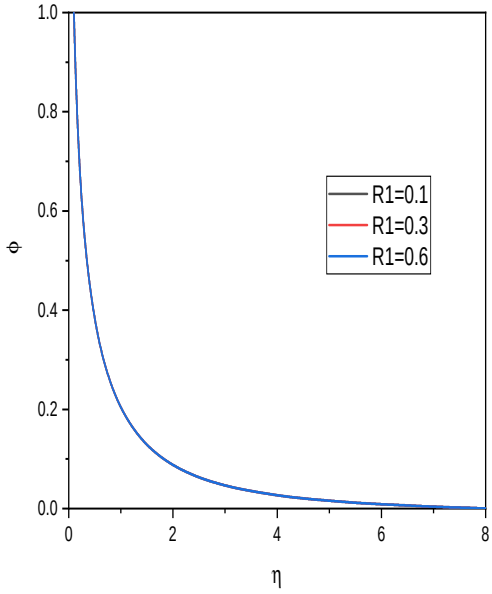

(c) Concentration

Figure 5.6: "Effect of $R1$ on the velocity,temperature and concentration profiles"

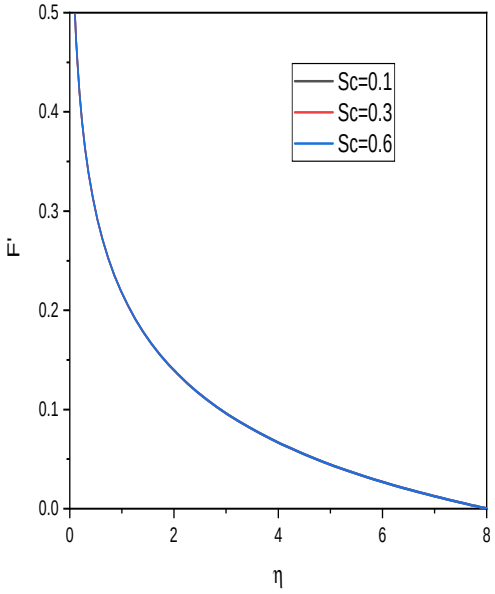

(a) velocity

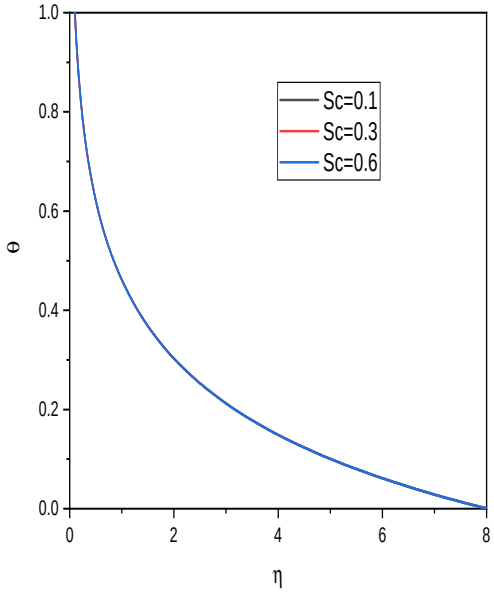

(b) Temperature

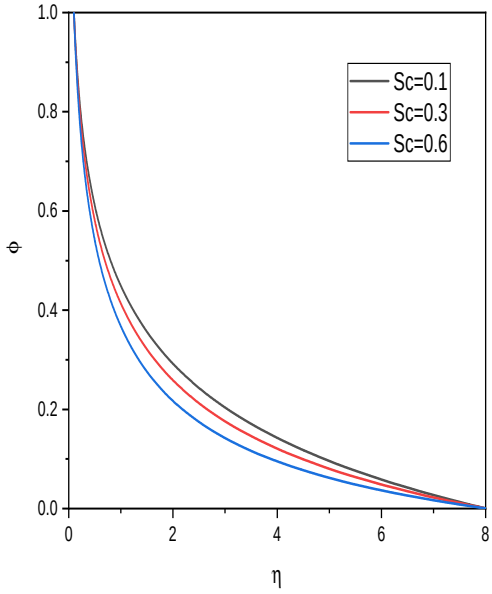

(c) Concentration

Figure 5.7: "Effect of Sc on the velocity, temperature and concentration profiles"

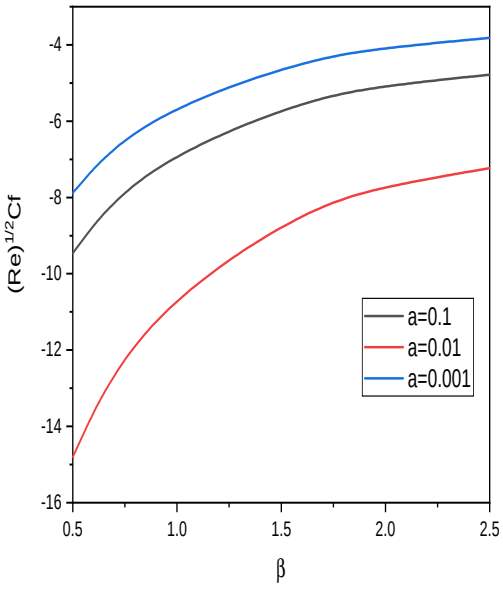

(a) Skin Friction coefficient profile

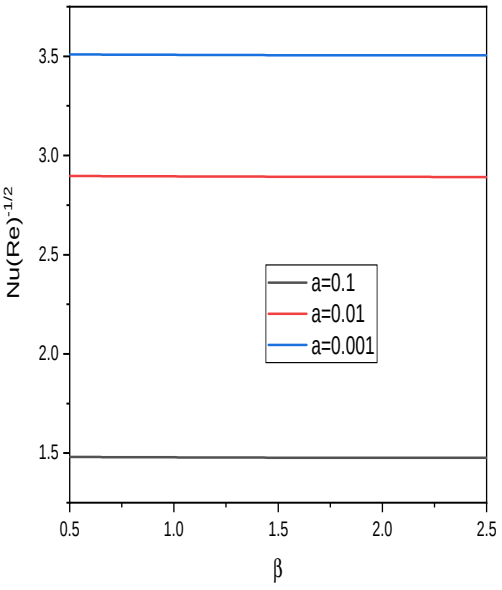

(b) Nusselt number

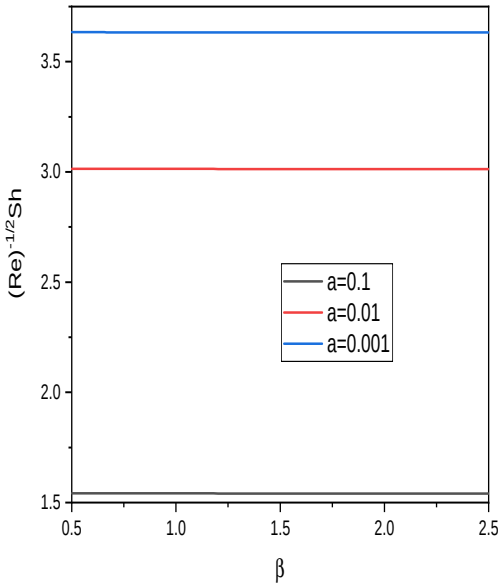

(c) Sherwood number

Figure 5.8: "Effect of a on the coefficient of skin friction, Nusselt number and Sherwood number"

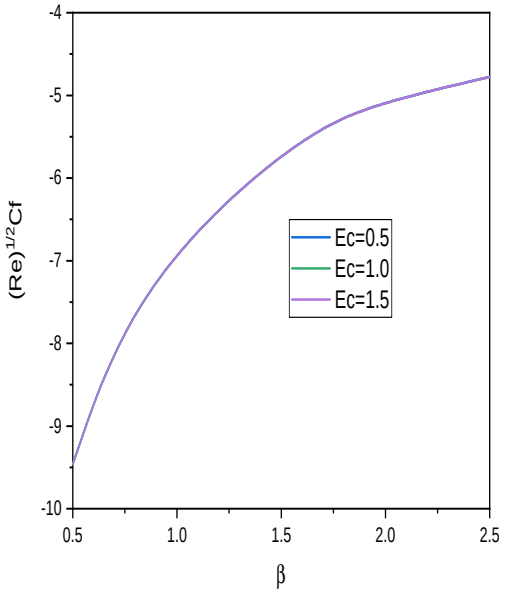

(a) Skin Friction coefficient profile

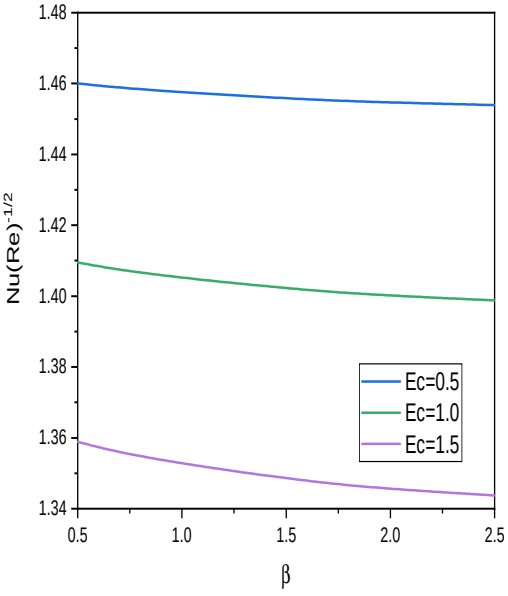

(b) Nusselt number

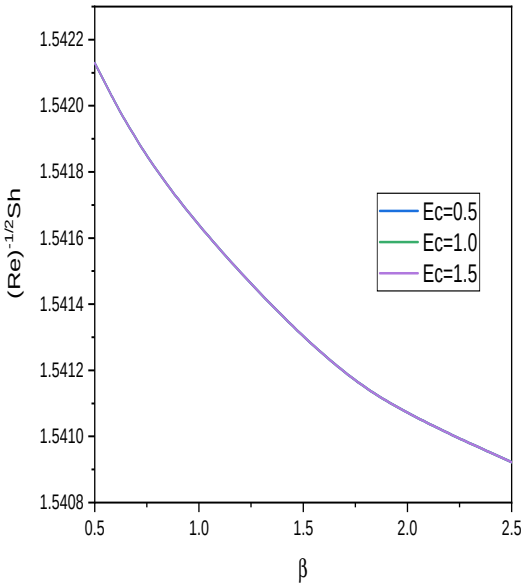

(c) Sherwood number

Figure 5.9: "Effect of Ec on the coefficient of skin friction, Nusselt number and Sherwood number"

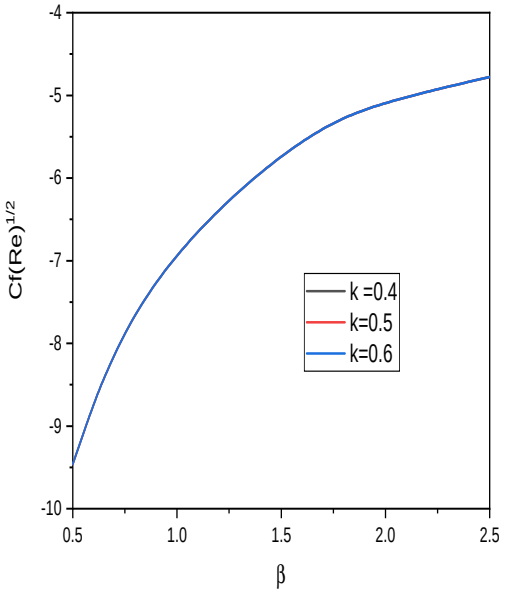

(a) Skin Friction coefficient profile

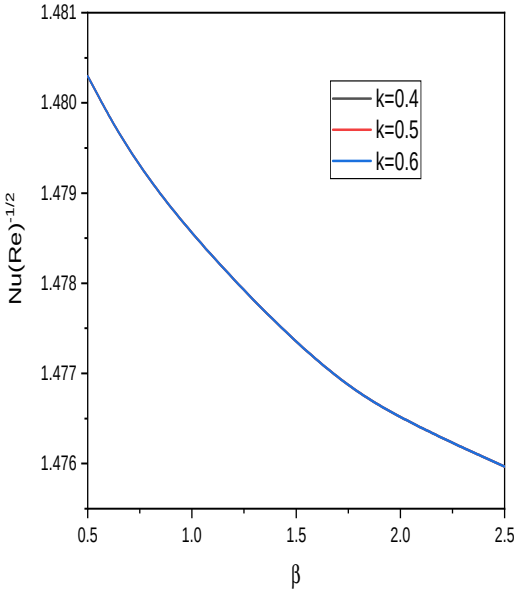

(b) Nusselt number

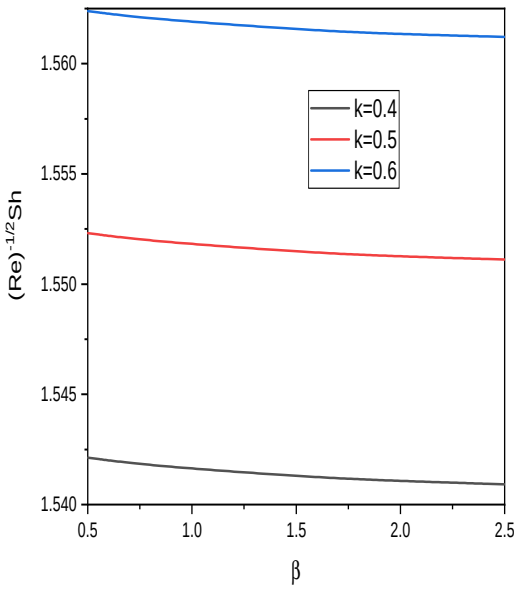

(c) Sherwood number

Figure 5.10: "Effect of k on the coefficient of skin friction, Nusselt number and Sherwood number"

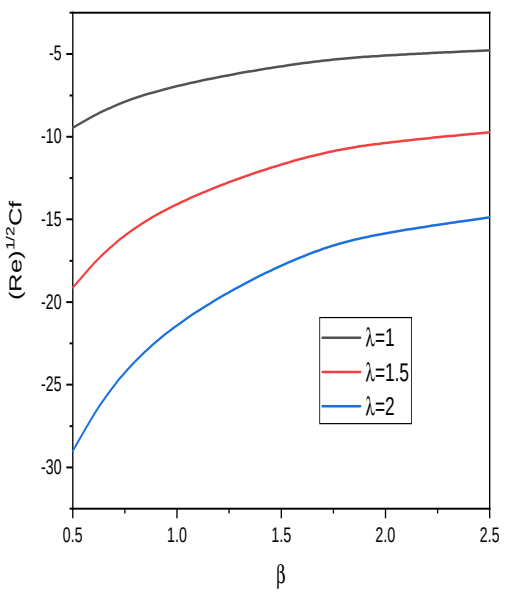

(a) Skin Friction coefficient profile

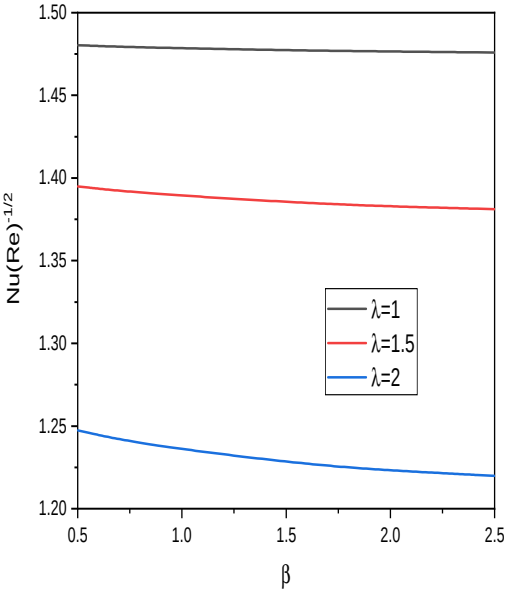

(b) Nusselt number

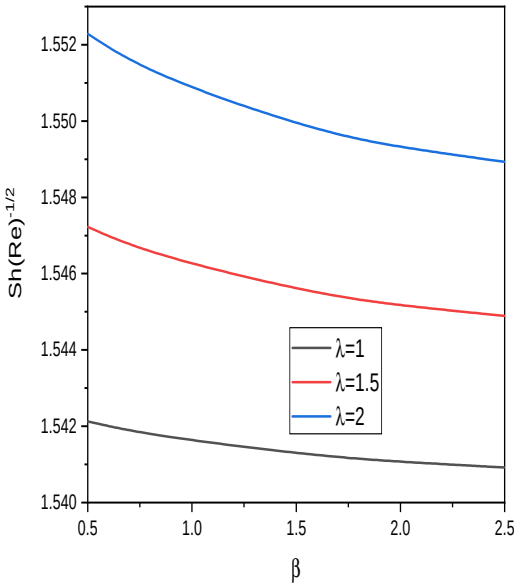

(c) Sherwood number

Figure 5.11: "Effect of λ on the coefficient of skin friction, Nusselt number and Sherwood number"

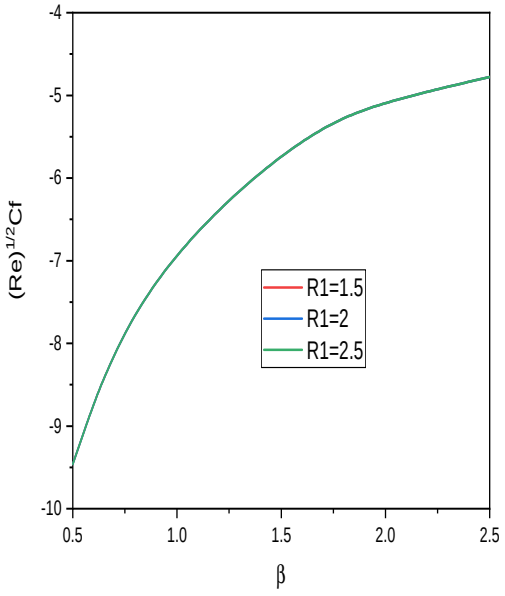

(a) Skin Friction coefficient profile

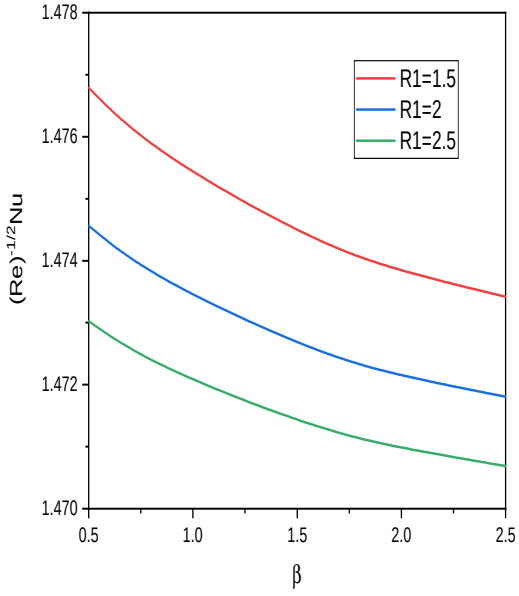

(b) Nusselt number

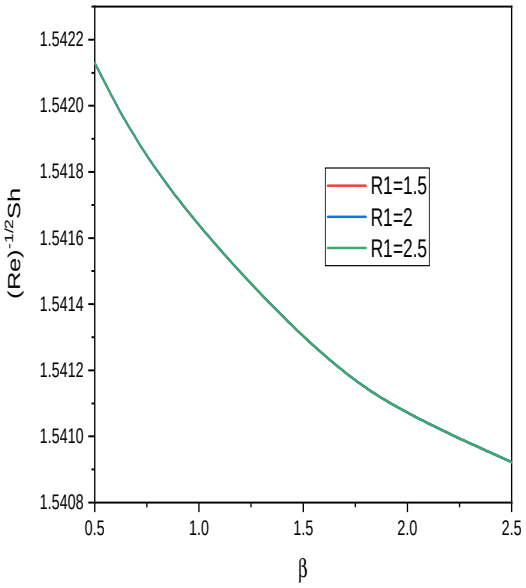

(c) Sherwood number

Figure 5.12: "Effect of $R1$ on the coefficient of skin friction, Nusselt number and Sherwood number"

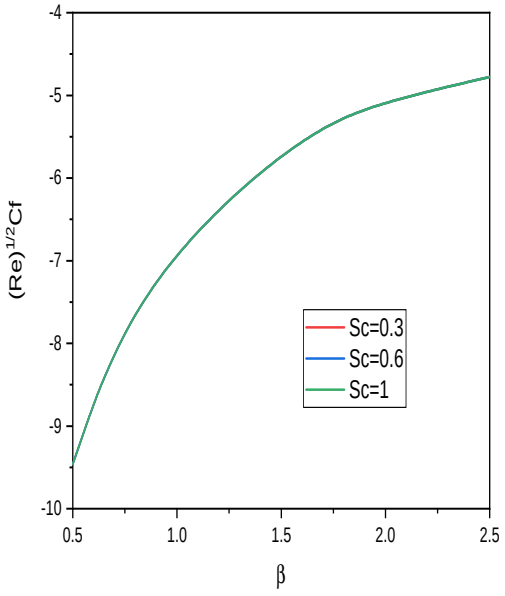

(a) Skin Friction coefficient profile

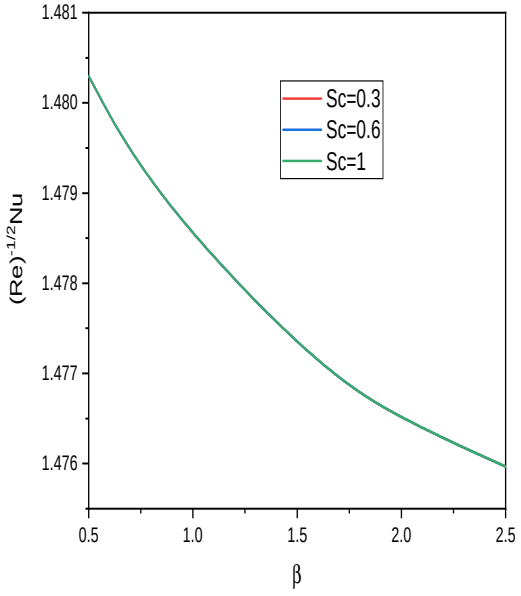

(b) Nusselt number

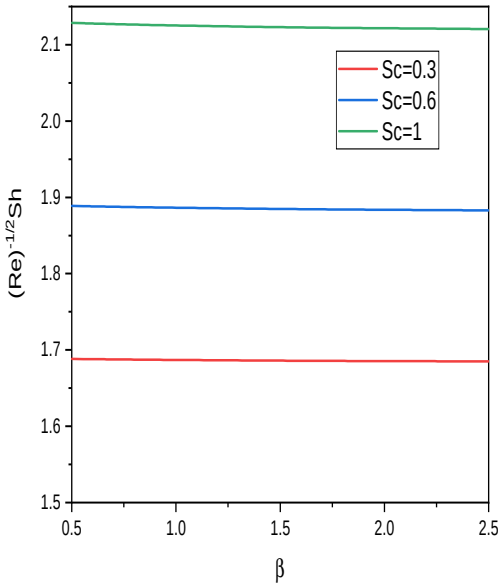

(c) Sherwood number

Figure 5.13: "Effect of Sc on the coefficient of skin friction, Nusselt number and Sherwood number"

Part III

MIXED CONVECTION IN BOUNDARY LAYER FLOW OF CASSON FLUID PAST A THIN NEEDLE

Chapter 6

Mixed Convection Flow Past a Thin Needle in a Casson fluid [1]

6.1 Introduction

Modern industries and technologies are mostly involved in processes that use convection in mixed which is outcome of forced and free convection occurring simultaneously. Examples include heat-exchangers maintained in a reduced velocity environment to cool nuclear reactors during emergency shutdowns and fans-driven electrical equipment cooling techniques. Wang [56] calculated the numerical solutions for mixed convective boundary layer stream over vertical needle and found that while result for opposing flows may be single, dual, or nonexistent, solutions for aiding flows are unique. In both supporting and opposing flow scenarios, Ahmed *et al.* [57] correlated the problem, boundary layer stream of constant laminar mixed convection of a viscous incompressible liquid moving along vertical tiny needles. Ahmed *et al.* [58]investigated both aiding and opposing stream situations boundary layer stream of continuous laminar mixed convection of a viscous incompressible liquid across vertical moving tiny needles with changing heat flux. Trimbitas *et al.* [59] combined heat transmission through vertical needle with a changeable wall temperature and convective boundary layer flow by using nanofluids. Salleh *et al.* [60] discusses both assisting and opposing situations of mixed convection stream of nanofluid caused by motion of tiny vertical needle. Qasim and Afridi [61] looked at how different thermal conductivities and energy dissipation affected the rate at which entropy developed in mixed convection flow. Rehman *et al.* [62] examines the

[1] Accepted to "**Journal of Advanced Research in Fluid Mechanics and Thermal Sciences**"

Cross fluid's magnetohydrodynamic mixed convection stream. A moving, tiny needle with the Soret and Dufour effect is the cause of stream. The energy equation makes use of both nonlinear heat radiation and heat generation/absorption.

This chapter deals with a steady mixed convection flow past a horizontal tiny needle submerged in Casson fluid is inspected. The flow-governing equations are changed into a set of non-linear ordinary differential equations utilising proper transforms. Utilising successive linearization, the resulting equations are linearized, and then the Chebyshev spectral collocation technique is implemented. The affect of needle size and mixed convection parameter on stream on velocity and temperature, together with graphical representations of the coefficient of skin friction and local heat transfer rate, are provided.

6.2 Formulation of the Problem

Consider boundary layer stream of mixed convection in Casson fluid with uniform velocity $U\bar{}_{\infty}(\bar{x})$ over a tiny needle moving horizontally with a velocity $U\bar{}_{w}(\bar{x})$. Assume that the stream is steady, laminar, and incompressible. The $\bar{(}x)$-axis runs horizontally from main edge of needle, and the radial axis runs perpendicular to it as shown in Fig. 6.1. The equation for radius of the needle $\bar{r} = R(\bar{x})$. It is believed that needle is thin while the needle's thickness is less than that of boundary layer surrounding it. Temperature of the needle is $\bar{T}_w(\bar{x})$, whereas temperature of surrounding fluid is T_∞, where $\bar{T}_w > T_\infty$.

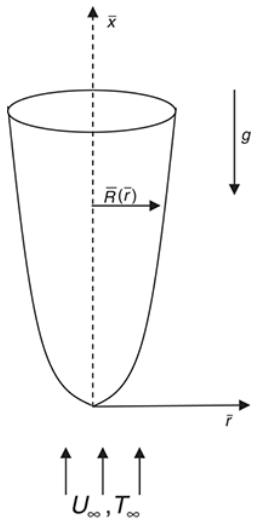

Figure 6.1: "Coordinate system and physical flow model".

With the above premises, the governing equations becomes

$$\frac{\partial(\bar{r}\bar{u})}{\partial\bar{x}} + \frac{\partial(\bar{r}\bar{v})}{\partial\bar{r}} = 0 \tag{6.1}$$

$$\bar{v}\frac{\partial\bar{u}}{\partial\bar{r}} + \bar{u}\frac{\partial\bar{u}}{\partial\bar{x}} = \bar{U}\frac{d\bar{U}}{d\bar{x}} + \nu\left(1+\frac{1}{\beta}\right)\frac{1}{\bar{r}}\frac{\partial}{\partial\bar{r}}\left(\bar{r}\frac{\partial\bar{u}}{\partial\bar{r}}\right) + g\beta(\bar{T}-T_\infty) \tag{6.2}$$

$$\bar{v}\frac{\partial\bar{T}}{\partial\bar{r}} + \bar{u}\frac{\partial\bar{T}}{\partial\bar{x}} = \alpha\left(\frac{1}{\bar{r}}\frac{\partial}{\partial\bar{r}}\left(\bar{r}\frac{\partial\bar{T}}{\partial\bar{r}}\right)\right) \tag{6.3}$$

where $\bar{u}$ and $\bar{v}$ represents the velocity components in the axial and radial directions repectively. T represents the fluid temperature, ν represent the kinematic viscosity,β represents Casson parameter,α represents the thermal conductivity, g represents extent of gravity's acceleration.

The conditions on the surface of the needle are

$$\begin{aligned} \bar{v}=0, \bar{u}=0, \bar{T}=\bar{T_w}(\bar{x}) \ \ at\ \bar{r}=\bar{R}(\bar{x}) \\ \bar{T}\to T_\infty, \bar{u}\to\bar{U}(\bar{x}) \ \ at\ \bar{r}\to\infty \end{aligned} \tag{6.4}$$

The non-dimensional variables listed below

$$\begin{aligned} r = Re^{1/2}\frac{\bar{r}}{L}, x=\frac{\bar{x}}{L}, R(x)=Re^{1/2}\frac{\bar{R}(\bar{x})}{L}, u=\frac{\bar{u}}{U_\infty}, \\ U(x)=\frac{\bar{U}(\bar{x})}{U_\infty}, v=Re^{1/2}\frac{\bar{v}}{U_\infty}, T=\frac{\bar{T}-T_\infty}{\Delta T}, \end{aligned} \tag{6.5}$$

Substituting Eq.(6.5) into Eq.(6.1)-(6.3), we get

$$\frac{\partial(ru)}{\partial x} + \frac{\partial(rv)}{\partial r} = 0 \tag{6.6}$$

$$u\frac{\partial u}{\partial x} + v\frac{\partial u}{\partial r} = U\frac{dU}{dx} + \left(1+\frac{1}{\beta}\right)\frac{1}{r}\frac{\partial}{\partial r}\left(r\frac{\partial u}{\partial r}\right) + \lambda T \tag{6.7}$$

$$u\frac{\partial T}{\partial x} + v\frac{\partial T}{\partial r} = \frac{1}{Pr}\left(\frac{1}{r}\frac{\partial}{\partial r}\left(r\frac{\partial T}{\partial r}\right)\right) \tag{6.8}$$

where $\lambda = \frac{Gr}{Re^2}$ is mixed convection parameter, Pr is Prandtl number.

Conditions on boundary Eq. (6.4) become

$$\begin{aligned} u = 0, v = 0, T = T_w(x) \ \ at\, r = R(x) \\ u \to U(x), T \to \infty \ \ as\, r \to \infty \end{aligned} \tag{6.9}$$

Similarity Transformations are described as:

$$\psi = xf(\eta), T(x) = x^{2m-1}\theta(\eta), \eta = x^{m-1}r^2 \tag{6.10}$$

where ψ is stream function detailed as :

$$u = \frac{1}{r}\frac{\partial \psi}{\partial r} and v = \frac{-1}{r}\frac{\partial \psi}{\partial x} \tag{6.11}$$

Using Eq. (6.10) in the equation to the surface of the wall $\eta = a$, it can be written as $R = a^{1/2}x^{(1-m)/2}$ which characterizes shape and size of the needle.

$$8\eta[1 + \frac{1}{\beta}]f''' + 8[1 + \frac{1}{\beta}]f'' + m[1 - 4(f')^2] + 4ff'' + \lambda\theta = 0 \tag{6.12}$$

$$\frac{2\eta}{Pr}\theta'' + \frac{2}{Pr}\theta' + f\theta' - (2m-1)f'\theta = 0 \tag{6.13}$$

The modified conditions on boundary becomes

$$\begin{aligned} f(\eta) = 0, \theta(a) = 1, f'(\eta) = 0 \quad at \quad \eta = a \\ f'(\eta) \to \frac{1}{2}, \quad \theta(\eta) \to 0 \quad as \quad \eta \to \infty \end{aligned} \tag{6.14}$$

where λ is the mixed convection parameter,$Pr = \frac{\mu}{\alpha_0}$ denotes the Prandtl number.

The non-dimensional form of skin friction coefficient (C_f) and the heat transfer rate (Nusselt number (Nu)) are

$$Re^{\frac{1}{2}}C_f = 8a^{\frac{1}{2}}(1 + \frac{1}{\beta})f''(a), \quad Re^{\frac{-1}{2}}Nu = -2a^{\frac{1}{2}}\theta'(a) \tag{6.15}$$

6.3 Solution of the Problem

The combined Eqns. (6.12) and (6.13) and conditions on boundary (6.14) are linearized through the successive linearization method (SLM) [78]. The solution of resulting linearized

equations is obtained by Chebyshev collocation method.

On applying the procedure explained in Chapter 2 to the equations Eqns. (6.12) and (6.13), we get the following linearized equations.

$$a_1 f_j^{'''} + a_2 f_j^{''} + a_3 f_j^{'} + a_4 f_j + a_5 \theta_j = r_1 \tag{6.16}$$

$$b_1 f_j^{'} + b_2 f_j + b_3 \theta_j^{''} + b_4 \theta_j{}' + b_5 \theta_j = r_2 \tag{6.17}$$

where

$$a_1 = 8\eta\left(1+\frac{1}{\beta}\right), \quad a_2 = 8\left(1+\frac{1}{\beta}\right) + 4\sum f_m,$$
$$a_3 = -8m\sum f'_m, \quad a_4 = 4\sum f''_m, \quad a_5 = \lambda,$$

$$r_1 = -8\eta\left(1+\frac{1}{\beta}\right)(\sum f'''_m) - 8\left(1+\frac{1}{\beta}\right)(\sum f''_m) + 4m(\sum f'_m)^2$$
$$-4(\sum F_m)(\sum f''_m) - \lambda(\sum \theta_m) - m$$

$$b_1 = \sum \theta_m - 2m(\sum \theta_m), \quad b_2 = \sum \theta'_m, \quad b_3 = \frac{2\eta}{Pr},$$
$$b_4 = \frac{2}{Pr} + (\sum f_m), \quad b_5 = \sum f'_m - 2m(\sum f'_m),$$
$$r_2 = -\frac{2\eta}{Pr}(\sum \theta''_m) - \frac{2}{Pr}(\sum \theta'_m) - (\sum f_m)(\sum \theta'_m) + 2m(\sum f'_m)(\sum \theta_m) - (\sum f'_m)(\sum \theta_m)$$

As explained in Chapter - 2, using Chebyshev collocation method on the system of linearized equations. (6.16) and (6.17), we obtain the following equation in matrix form

$$A_{j-1} X_j = R_{j-1} \tag{6.18}$$

where A_{j-1} is a $2(N+1)\times 2(N+1)$ order matrix and X_j and R_{j-1} are $2(N+1)\times 1$ column matrix given by

$$A_{j-1} = \begin{pmatrix} A_{11} & A_{12} \\ A_{21} & A_{22} \end{pmatrix}, X_j = \begin{pmatrix} F_j \\ \Theta_j \end{pmatrix}, R_{j-1} = \begin{pmatrix} r_{1,j-1} \\ r_{2,j-2} \end{pmatrix} \tag{6.19}$$

where

$$F_j = [f_j(\xi_0), f_j(\xi_1), ..., f_j(\xi_{N-1}), f_j(\xi_N)]^T,$$

$$\Theta_j = [\theta_j(\xi_0), \theta_j(\xi_1), .., \theta_j(\xi_{N-1}), \theta_j(\xi_N)]^T,$$

$$A_{11} = a_1 D^3 + a_2 D^2 + a_3 D + a_4 I, A_{12} = a_5 I,$$

$$A_{21} = b_1 D + b_2 I, A_{22} = b_3 D^2 + b_4 D + b_5 I,$$

$$r_1 = [r_1(\xi_1), r_1(\xi_2), r_1(\xi_3)...., r_1(\xi_{N+1})]^T,$$

$$r_2 = [r_2(\xi_1), r_2(\xi_2), r_2(\xi_3)...., r_2(\xi_N)]^T,$$

The superscript T stands for transpose, I is the identity matrix, O is the zero matrix.

Imposing the boundary conditions in terms of the collocation points, the solution is provided by

$$X_j = A_{j-1}^{-1} R_{j-1}$$

6.4 Results and Discussion

The effects of dimensionless parameters on velocity and temperature, together with the local heat transfer rate (Nusselt number) $\frac{Nu}{\sqrt{Re}}$ and the coefficient of local skin friction $\sqrt{Re}C_f$, are the primary focus of the current model. The dimensionless parameters are: size of the needle (a), mixed convection parameter (λ), and power index (m). A detailed numerical calculation for numerous values of a, λ, and m to assure a greater comprehension of the technical issue, and the findings are presented graphically in Figs. 6.2– 6.7.

The effect of the size of the needle on velocity and temperature for both aiding and opposing cases is represented in Fig. 6.2. It is understood from Figs. 6.2(a) and 6.2(b) show that as a reduces, the velocity improves for both cases. Similarity: as a reduces, the temperature decreases in both cases, as presented in Figs. 6.2(c) and 6.2(d).

The fluctuation of velocity and temperature profiles with the Casson fluid parameter β is given in Fig.6.3. It is understood from Fig. 6.3(a) that velocity improves as the Casson fluid parameter rises for assisting flow. But the velocity reduces as the Casson fluid parameter rises in the opposite case, as depicted in Fig. 6.3(b). Figs. 6.3(c) and 6.3(d) reveal that the effect of the Casson fluid parameter on temperature is almost negligible in both cases.

The variation of velocity and temperature with mixed convection parameter λ is given

in Fig.6.4. As presented in Fig. 6.4(a), intensifying λ increases the velocity in the assisting case. The velocity is decreasing in the opposing case, as given in Fig. 6.4(b). The effect of the mixed convection parameter on temperature is negligible in both cases, as presented in Figs. 6.4(c) and 6.4(d).

Figure 6.5 presents the effect of power index on velocity and temperature. Figs. 6.5(a) and 6.5(b) exhibit that the velocity rises as the power index rises for both aiding and opposing cases. The temperature decreases as m rises for both aiding and opposing cases, as depicted in Figs. 6.5(c) and 6.5(d).

The impact of the size of the needle on the coefficient of skin friction $\sqrt{Re}C_f$ and the nusselt number $\frac{Nu}{\sqrt{Re}}$ is depicted in Fig. 6.6. As depicted in Figs. 6.6(a) and 6.6(b), the skin friction coefficient is improved by decreasing a for both aiding and opposing cases. As a decreasing, local Nusselt number is also enhancing in both cases, as presented in Figs. 6.6(c) and 6.6(d).

The effect of power index on the coefficient of skin friction $\sqrt{Re}C_f$ and the Nusselt number $\frac{Nu}{\sqrt{Re}}$ is given in Fig. 6.7. It is understood from Figs.6.7(a) and 6.7(b) that the $\sqrt{Re}C_f$ enhances as the power index rises in both the assisting and opposing cases of the flow. As exhibited in Fig.6.7(c) and 6.7(d), $\frac{Nu}{\sqrt{Re}}$ is also enhanced with an enhancement in m in both aiding and opposing cases.

6.5 Conclusion

A mixed convection flow past a horizontal needle in Casson fluid is analyzed. The flow equations are changed into a set of non-linear ordinary differential equations utilizing appropriate transforms and then linearized using successive linearization. The Chebyshev spectral collocation technique is implemented to find the resulting equations.

- As the size of the needle reduces, velocity, coefficient of skin friction, and Nusselt number are improved in both cases, whereas temperature decreases in both cases.
- Intensifying λ increases the velocity in the assisting case and decreases in the opposing case, where the effect of the mixed convection parameter on temperature is negligible.
- The velocity rises and the temperature decreases as the power index rises for both aiding and opposing cases.

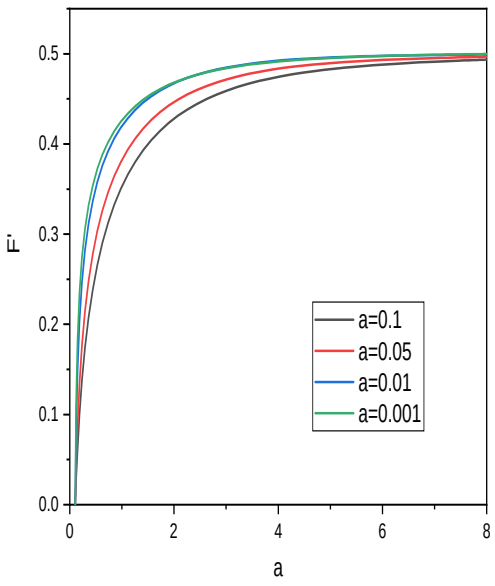

(a) Velocity profile (aiding flow)

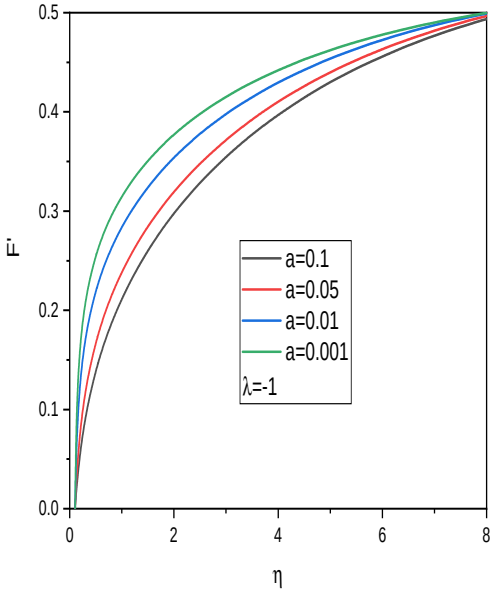

(b) Velocity profile (Opposing flow)

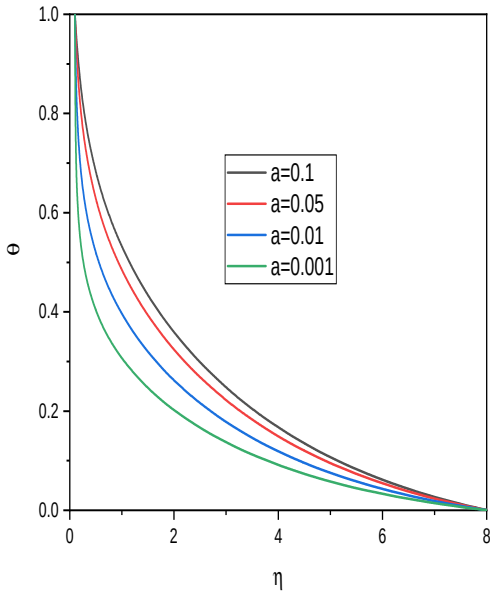

(c) Temperature profile (aiding flow)

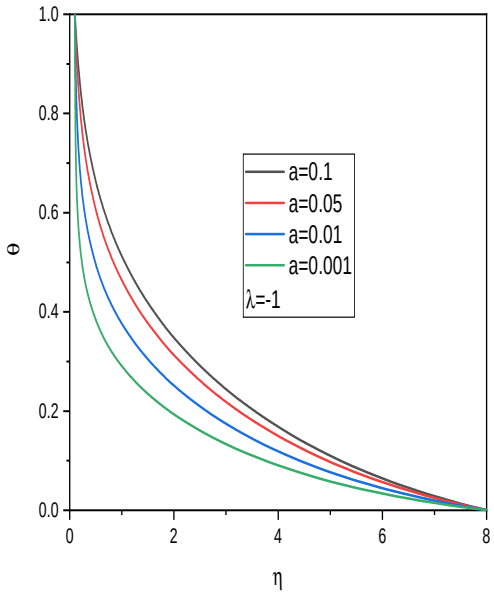

(d) Temperature profile (Opposing flow)

Figure 6.2: "Effect of size of the needle on the velocity and temperature"

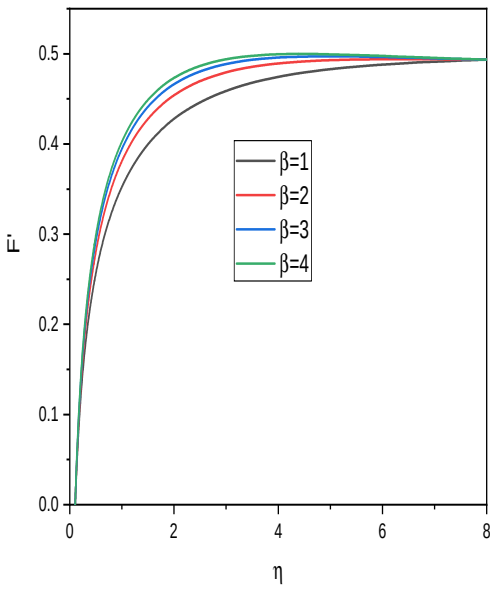

(a) Velocity profile (aiding flow)

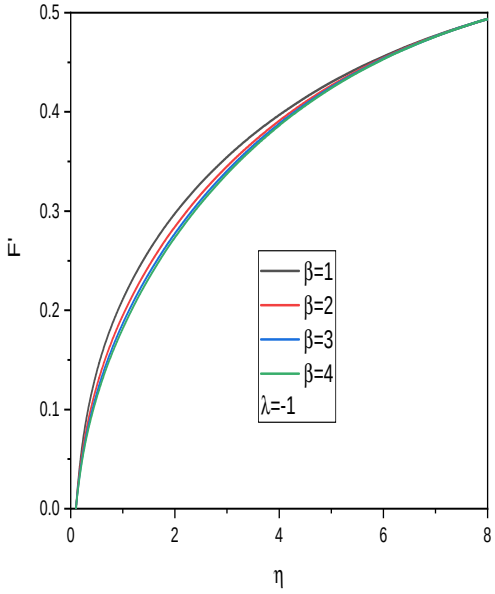

(b) Velocity profile (Opposing flow)

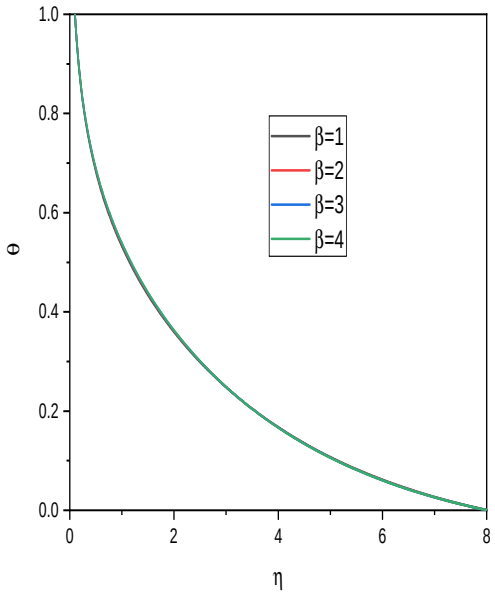

(c) Temperature profile (aiding flow)

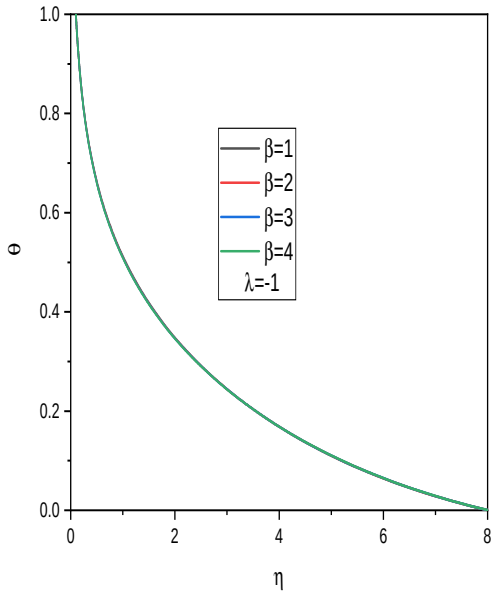

(d) Temperature profile (Opposing flow)

Figure 6.3: "Effect of β on the Velocity and Temperature"

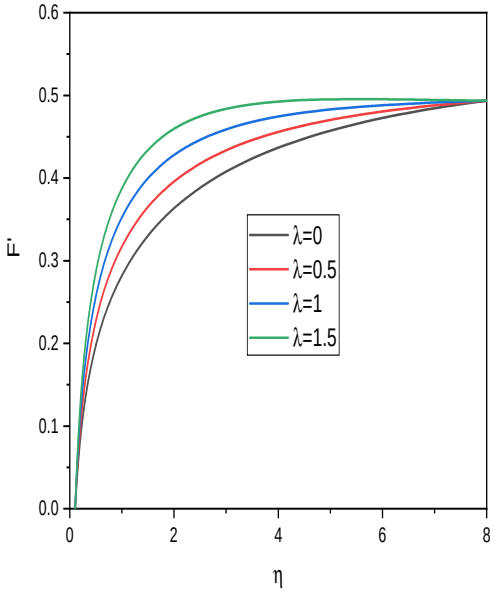

(a) Velocity profile (aiding flow)

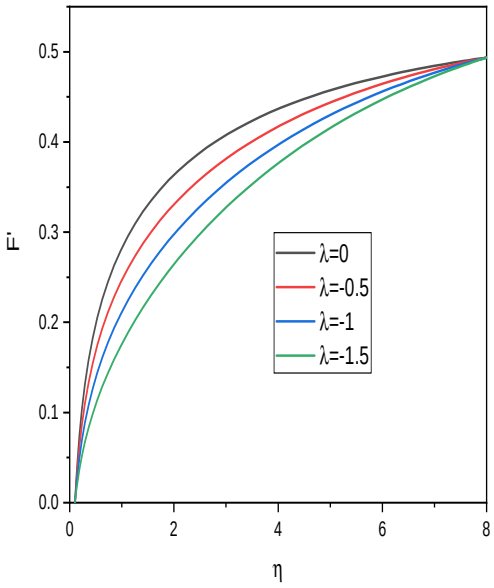

(b) Velocity profile (Opposing flow)

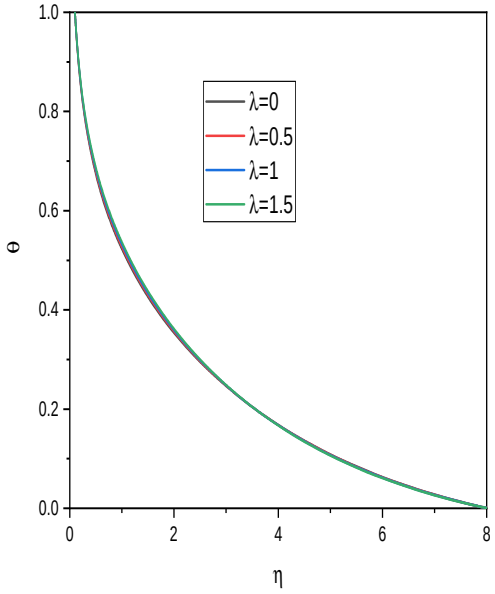

(c) Temperature profile (aiding flow)

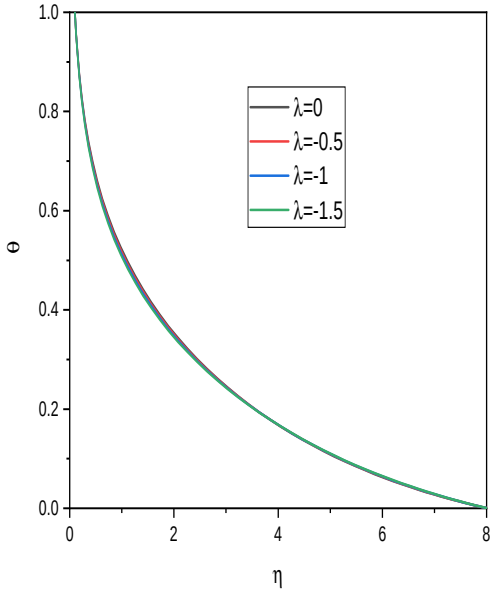

(d) Temperature profile (Opposing flow)

Figure 6.4: "Effect of λ on the Velocity and Temperature"

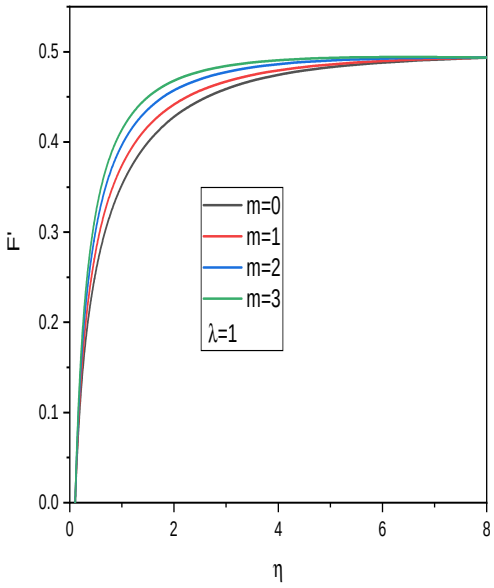

(a) Velocity profile (aiding flow)

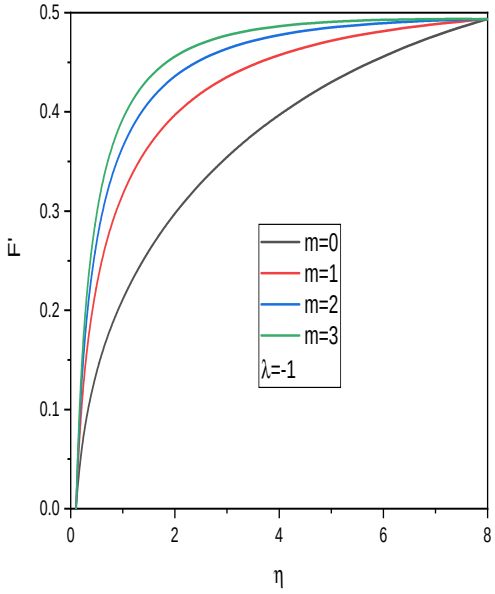

(b) Velocity profile (Opposing flow)

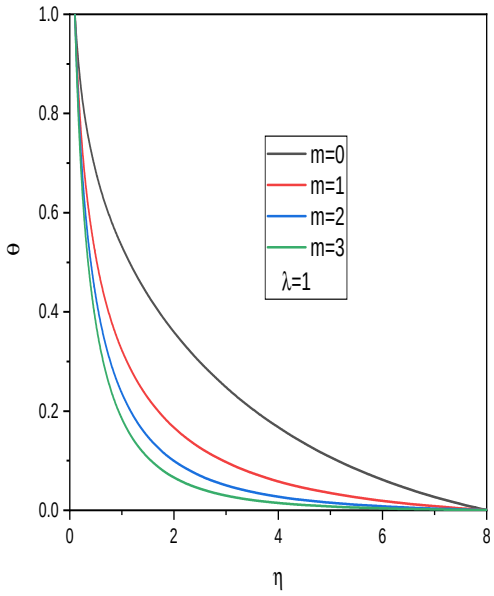

(c) Temperature profile (aiding flow)

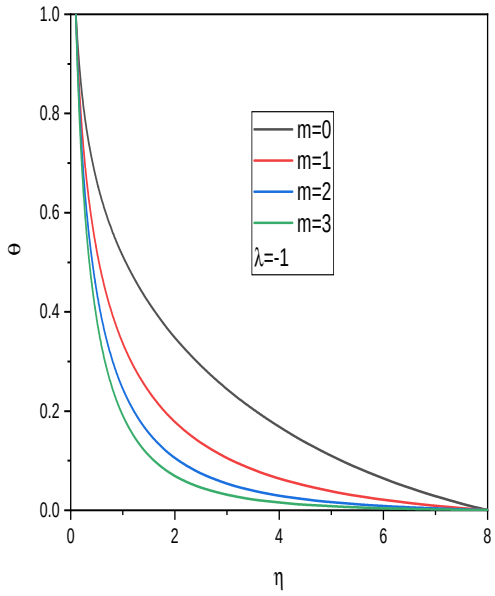

(d) Temperature profile (Opposing flow)

Figure 6.5: "Effect of m on the Velocity and Temperature"

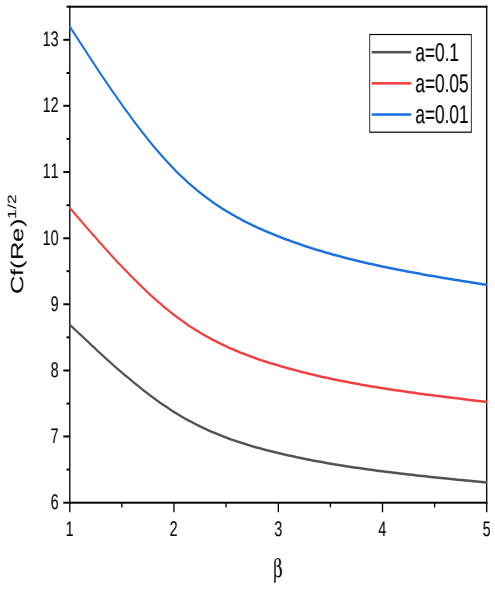

(a) Skin friction Coefficient (aiding flow)

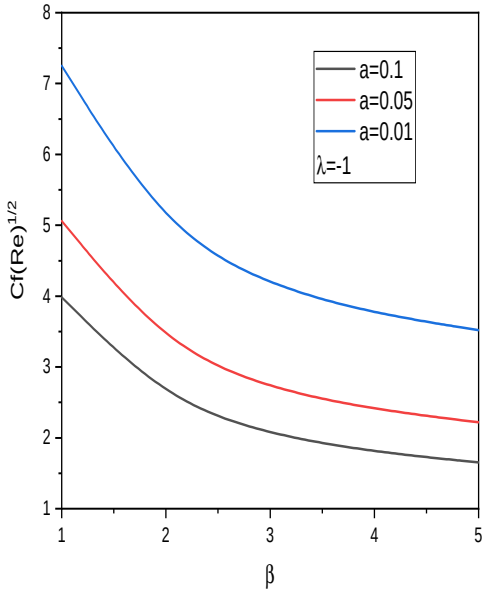

(b) Skin friction Coefficient (Opposing flow)

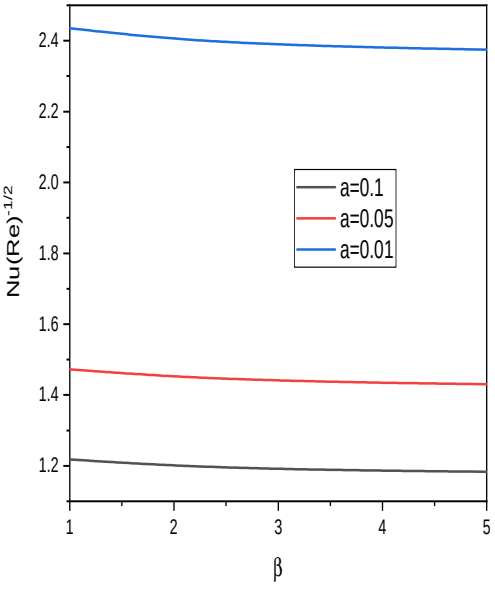

(c) Nusselt Number (aiding flow)

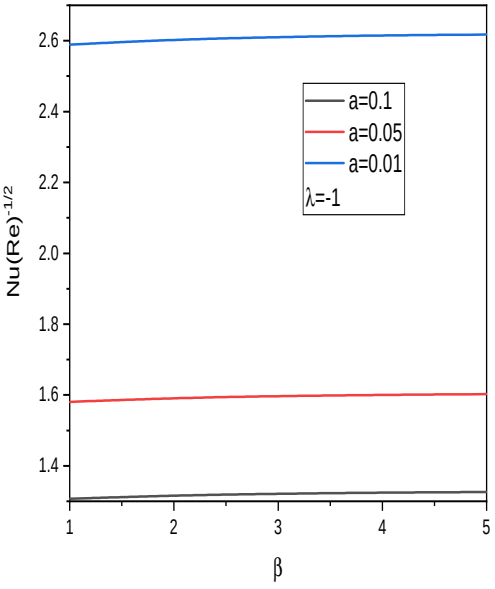

(d) Nusselt Number(Opposing flow)

Figure 6.6: "Effect of a on $\sqrt{Re}C_f$ and $\frac{Nu}{\sqrt{Re}}$"

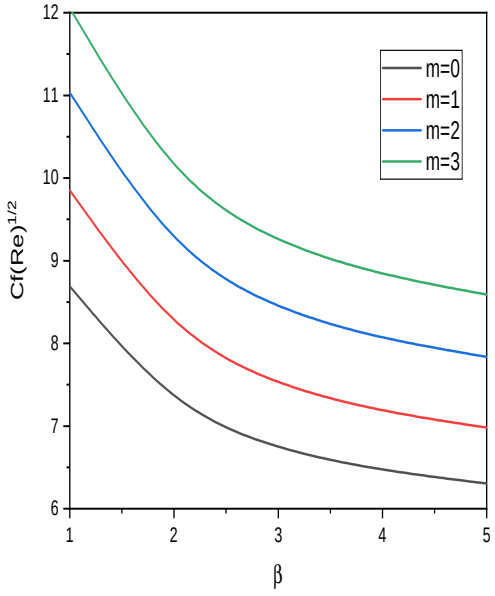

(a) Skin friction Coefficient (aiding flow)

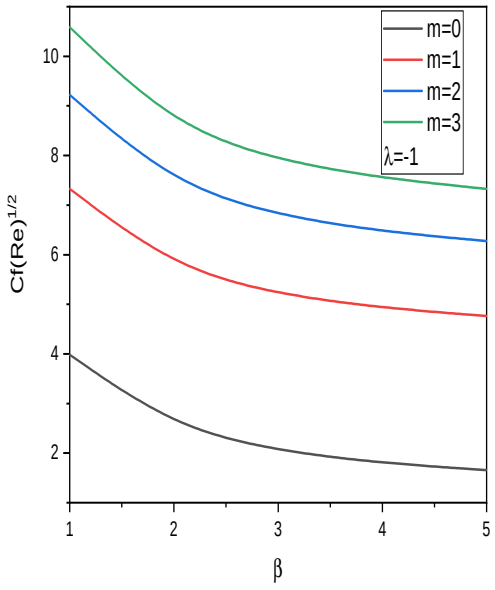

(b) Skin friction Coefficient (Opposing flow)

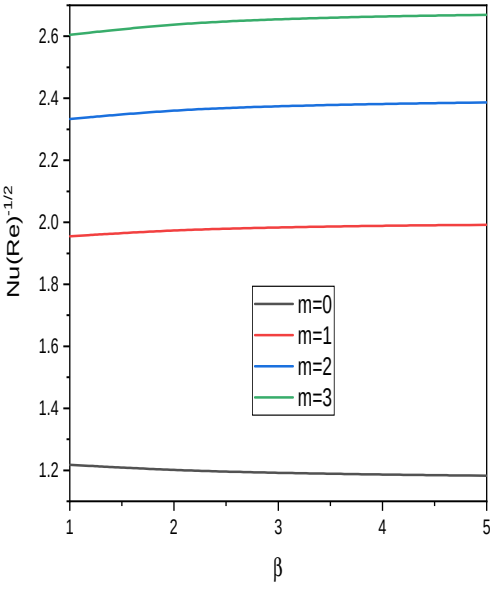

(c) Nusselt Number (aiding flow)

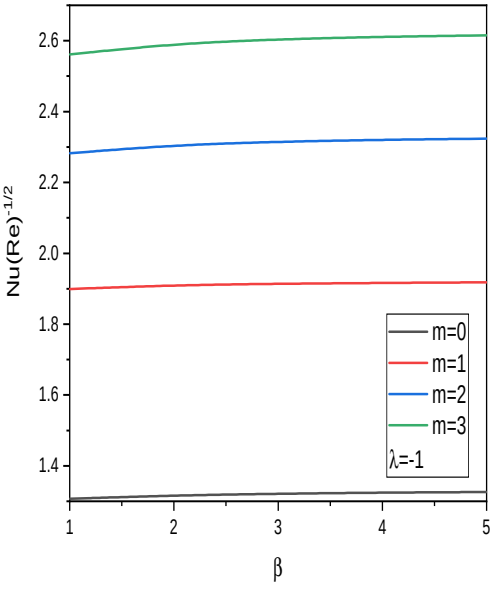

(d) Nusselt Number(Opposing flow)

Figure 6.7: "Effect of m on $\sqrt{Re}C_f$ and $\frac{Nu}{\sqrt{Re}}$"

Chapter 7

Heat source and Chemical reaction effects on a MHD mixed convection of a Casson fluid flow over a thin needle [1]

7.1 Introduction

Numerous researchers have examined how magnetic fields affect fluid stream and heat transfer properties with applications to a wide range of engineering issues, including plasma studies, MHD power generators, nuclear reactor cooling, crystal growth, the petroleum industry, and boundary layer control in aerodynamics.Many investigators have explored affect of an applied magnetic field on both Newtonian and non-Newtonian streams across different geometries in the instance of an electrically conducting fluid. Raza [63] investigated the various responses of mixed convection stream of Casson fluid in a porous channel beneath the force of magnetic field. The impacts of a consistent transverse magnetic field, heat radiation, and chemical reaction on the erratic Casson fluid stream flowing past upright plate that oscillates and is utilized in a porous medium were estimated by Kataria and Patel [64]. Ahmed [65] analyzed the MHD narrowing stream of a Casson fluid is presented among parallel plates. According to reviews of the literature, no research has yet been published on the examination of magnetic fields on heat transfer characteristics in a mixed convection stream through a

[1] Communicated to "**Journal of Applied and Computational Mathematics"**

horizontal tiny needle in Casson fluid.

This study investigates how the dimensionless parameters, namely size of needle and mixed convection parameter influence the heat transfer attributes in a mixed convective Casson fluid flow over a thin needle. The velocity component, temperature, and heat transfer rate are thoroughly examined.

7.2 Formulation of the Problem

Consider boundary layer stream of mixed convection in Casson fluid with uniform velocity $\bar{U_\infty}(\bar{x})$ across tiny needle moving horizontally with a velocity $\bar{U_w}(\bar{x})$. Assume that the stream is steady, laminar, and incompressible. The $\bar{(}x)$-axis runs horizontally from main edge of needle, and radial axis runs perpendicular to it as shown in Fig.6.1.Apart from the assumption of Chapter - 6, In addition, we assume Heat Source and Chemical reaction effects are present in the medium.

With the above premises,governing equations becomes

$$\frac{\partial(\bar{r}\bar{v})}{\partial\bar{r}} + \frac{\partial(\bar{r}\bar{u})}{\partial\bar{x}} = 0 \tag{7.1}$$

$$\bar{u}\frac{\partial\bar{u}}{\partial\bar{x}} + \bar{v}\frac{\partial\bar{u}}{\partial\bar{r}} = \bar{U}\frac{d\bar{U}}{d\bar{x}} + \nu\left(1+\frac{1}{\beta}\right)\frac{1}{\bar{r}}\frac{\partial}{\partial\bar{r}}\left(\bar{r}\frac{\partial\bar{u}}{\partial\bar{r}}\right) + g\beta(\bar{T}-T_\infty) - \sigma\frac{B^2\bar{u}}{\rho} \tag{7.2}$$

$$\bar{u}\frac{\partial\bar{T}}{\partial\bar{x}} + \bar{v}\frac{\partial\bar{T}}{\partial\bar{r}} = \alpha\left(\frac{1}{\bar{r}}\frac{\partial}{\partial\bar{r}}\left(\bar{r}\frac{\partial\bar{T}}{\partial\bar{r}}\right)\right) + Q(\bar{T}-T_\infty) \tag{7.3}$$

$$\bar{u}\frac{\partial\bar{C}}{\partial\bar{x}} + \bar{v}\frac{\partial\bar{C}}{\partial\bar{r}} = D_m\left(\frac{1}{\bar{r}}\frac{\partial}{\partial\bar{r}}\left(\bar{r}\frac{\partial\bar{C}}{\partial\bar{r}}\right)\right) - K^*(\bar{C}-C_\infty) \tag{7.4}$$

where the quantities used in the above equations are already defined in Chapter - 6.

The conditions on the surface of the needle are

$$\begin{aligned} \bar{u}=0, \bar{v}=0, \bar{T}=\bar{T_w}(\bar{x}), \bar{C}=\bar{C_w} \ \ at\ \bar{r}=\bar{R}(\bar{x}) \\ \bar{u}\to\bar{U}(\bar{x}), \bar{T}\to T_\infty, \bar{C}\to C_\infty \ \ at\ \bar{r}\to\infty \end{aligned} \tag{7.5}$$

The following are the non-dimensional variables:

$$\begin{aligned} x = \frac{\bar{x}}{L}, r = Re^{1/2}\frac{\bar{r}}{L}, R(x) = Re^{1/2}\frac{\bar{R}(\bar{x})}{L}, u = \frac{\bar{u}}{U_\infty}, \\ v = Re^{1/2}\frac{\bar{v}}{U_\infty}, U(x) = \frac{\bar{U}(\bar{x})}{U_\infty}, T = \frac{\bar{T}-T_\infty}{\Delta T}, C = \frac{\bar{C}-C_\infty}{\Delta C} \end{aligned} \tag{7.6}$$

Substituting Eq.(7.5) into Eq.(7.1) to (7.4) , we get

$$\frac{\partial(rv)}{\partial r} + \frac{\partial(ru)}{\partial x} = 0 \tag{7.7}$$

$$v\frac{\partial u}{\partial r} + u\frac{\partial u}{\partial x} = U\frac{dU}{dx} + \left(1+\frac{1}{\beta}\right)\frac{1}{r}\frac{\partial}{\partial r}\left(r\frac{\partial u}{\partial r}\right) + \lambda T - Mu \tag{7.8}$$

$$v\frac{\partial T}{\partial r} + u\frac{\partial T}{\partial x} = \frac{1}{Pr}\frac{1}{r}\frac{\partial}{\partial r}\left(r\frac{\partial T}{\partial r}\right) + Q_1 T \tag{7.9}$$

$$v\frac{\partial C}{\partial r} + u\frac{\partial C}{\partial x} = \frac{1}{Sc}\frac{1}{r}\frac{\partial}{\partial r}\left(r\frac{\partial C}{\partial r}\right) - K_1 C \tag{7.10}$$

Conditions on boundary Eq.7.5 become

$$\begin{aligned} v = 0, u = 0, T = T_w(x), C = C_w(x) \ \ at\ r = R(x) \\ u \to U(x), T \to 0, C \to 0 \ \ as\ r \to \infty \end{aligned} \tag{7.11}$$

Similarity Transformations are specified as:

$$\psi = xf(\eta), T(x) = x^{2m-1}\theta(\eta), \eta = x^{m-1}r^2 \tag{7.12}$$

where ψ is the stream function

Using Eq. (7.12) in the equation to the surface of the wall $\eta = a$, it can be written as $R = a^{1/2}x^{(1-m)/2}$ which characterizes shape and size of the needle.

Making use of above similarity variables in Eq.(7.8) to (7.10), we obtain

$$8\eta[1+\frac{1}{\beta}]f''' + 8[1+\frac{1}{\beta}]f'' + m[1-4(f')^2] + 4ff'' + \lambda\theta - 2Mf' = 0 \tag{7.13}$$

$$\frac{2\eta}{Pr}\theta'' + \frac{2}{Pr}\theta' + f\theta' - (2m-1)f'\theta + \frac{Q\theta}{2} = 0 \tag{7.14}$$

$$\frac{2\eta}{Sc}\phi^{''} + \frac{2}{Sc}\phi^{'} + f\phi' - (2m-1)f^{'}\phi - \frac{K\phi}{2} = 0 \tag{7.15}$$

The modified conditions on boundary becomes

$$\begin{aligned} f^{'}(\eta) = 0, f(\eta) = 0, \theta(\eta) = 1, \phi(\eta) = 1 \quad at \quad \eta = a \\ f^{'}(\eta) \to \frac{1}{2}, \quad \theta(\eta) \to 0, \phi(\eta) \to 0 \quad as \quad \eta \to \infty \end{aligned} \tag{7.16}$$

In additions to desired allotment for this model is Skin Friction C_f and the local Nusselt number Nu, Sherwood number Sh which are represented as:

$$Re^{\frac{1}{2}}C_f = 8a^{\frac{1}{2}}(1+\frac{1}{\beta})f^{''}(a), \quad Re^{\frac{-1}{2}}Nu = -2a^{\frac{1}{2}}\theta^{'}(a), \quad Re^{\frac{-1}{2}}Sh = -2a^{\frac{1}{2}}\theta^{'}(a) \tag{7.17}$$

7.3 Solution of the Problem

The combined Eqns. (7.13) to (7.15) and conditions on boundary (7.16) are linearized through the successive linearization method (SLM) [78]. The solution of resulting linearized equations is obtained by Chebyshev collocation method.

On applying the procedure explained in Chapter 2 to the equations Eqns. (7.13) to (7.15), we get the following linearized equations.

$$a_1 f_i^{'''} + a_2 f_i^{''} + a_3 f_i^{'} + a_4 f_i + a_5 \theta_i = r_1 \tag{7.18}$$

$$b_1 f_i^{'} + b_2 f_i + b_3 \theta_i^{''} + b_4 \theta_i{}' + b_5 \theta_i = r_2 \tag{7.19}$$

$$c_1 f_i^{'} + c_2 f_i + c_3 \phi_i^{''} + c_4 \phi_i{}' + c_5 \phi_i = r_3 \tag{7.20}$$

where

$$a_1 = 8\eta\left(1+\frac{1}{\beta}\right), \quad a_2 = 8\left(1+\frac{1}{\beta}\right) + 4\sum f_m$$

$$a_3 = -8m\sum f_m' - 2M, \quad a_4 = 4\sum f_m'', \quad a_5 = \lambda$$

$$\begin{aligned} r_1 = -8\eta\left(1+\frac{1}{\beta}\right)(\sum f_m''') - 8\left(1+\frac{1}{\beta}\right)(\sum f_m'') + 4m(\sum f_m')^2 \\ -4(\sum F_m)(\sum f_m'') + 2M(\sum f_m') - \lambda(\sum \theta_m) - m \end{aligned}$$

$$b_1 = \sum \theta_m - 2m(\sum \theta_m), \quad b_2 = \sum \theta'_m, \quad b_3 = \frac{2\eta}{Pr}$$
$$b_4 = \frac{2}{Pr} + (\sum f_m), \quad b_5 = \sum f'_m - (2m-1)(\sum f'_m)$$

$$r_2 = -\frac{2\eta}{Pr}(\sum \theta''_m) - \frac{2}{Pr}(\sum \theta'_m) - (\sum f_m)(\sum \theta'_m) + (2m-1)(\sum f'_m)(\sum \theta_m) - \frac{Q}{2}(\sum \theta_m)$$

$$c_1 = -(2m-1)(\sum \phi_m), \quad c_2 = (\sum \phi'_m), \quad c_3 = \frac{2\eta}{Sc}$$
$$c_4 = \frac{2}{Sc} + (\sum f_m), \quad b_5 = -(2m-1)(\sum f'_m) - \frac{K}{2}$$

$$r_3 = -\frac{2\eta}{Sc}(\sum \phi''_m) - \frac{2}{Sc}(\sum \phi'_m) - (\sum f_m)(\sum \phi'_m) + (2m-1)(\sum f'_m)(\sum \phi_m) + \frac{K}{2}(\sum \phi_m)$$

As explained in Chapter - 2, using Chebyshev collocation method on the system of linearized equations. (7.18) t0 (7.20), we obtain the following equation in matrix form

$$A_{j-1}X_j = R_{j-1} \tag{7.21}$$

where A_{j-1} is a $3(N+1) \times 3(N+1)$ order matrix and X_j and R_{j-1} are $3(N+1) \times 1$ column matrix given by

$$A_{j-1} = \begin{pmatrix} A_{11} & A_{12} & A_{13} \\ A_{21} & A_{22} & A_{23} \\ A_{31} & A_{32} & A_{33} \end{pmatrix}, X_j = \begin{pmatrix} F_j \\ \Theta_j \\ \phi_j \end{pmatrix}, R_{j-1} = \begin{pmatrix} r_{1,j-1} \\ r_{2,j-2} \\ r_{3,j-3} \end{pmatrix} \tag{7.22}$$

Where

$$F_j = [f_i(\xi_0), f_i(\xi_1), ..., f_i(\xi_{N-1}), f_i(\xi_N)]^T,$$
$$\Theta_j = [\theta_i(\xi_0), \theta_i(\xi_1), .., \theta_i(\xi_{N-1}), \theta_i(\xi_N)]^T,$$
$$\Phi_j = [\phi_i(\xi_0), \phi_i(\xi_1), .., \phi_i(\xi_{N-1}), \phi_i(\xi_N)]^T,$$

$$A_{11} = a_1D^3 + a_2D^2 + a_3D + a_4I, A_{12} = a_5I, A_{13} = O$$

$$A_{21} = b_1D + b_2I, A_{22} = b_3D^2 + b_4D + b_5I, A_{23} = O$$

$$A_{31} = c_1D + c_2I, A_{32} = O, A_{33} = c_3D^2 + c_4D + c_5I$$

$$r_1 = [r_1(\xi_0), r_1(\xi_1), ..., r_1(\xi_{N-1}), r_1(\xi_N)]^T,$$

$$r_2 = [r_2(\xi_0), r_2(\xi_1), ..., r_2(\xi_{N-1}), r_2(\xi_N)]^T,$$

$$r_3 = [r_3(\xi_0), r_3(\xi_1), ..., r_3(\xi_{N-1}), r_3(\xi_N)]^T$$

the superscript T stands for transpose, I is the identity matrix, O is the zero matrix. Imposing the boundary conditions in terms of the collocation points, the solution is provided by

$$X_j = A_{j-1}^{-1} R_{j-1}$$

7.4 Results and Discussion

The effects of dimensionless parameters on velocity and temperature, together with the local heat transfer rate (Nusselt number) $\frac{Nu}{\sqrt{Re}}$, the sherwood number $\frac{Sh}{\sqrt{Re}}$, and the coefficient of local skin friction $\sqrt{Re}C_f$, are the primary focus of the current model. The dimensionless parameters are: size of the needle (a), mixed convection parameter (λ), magnetic parameter (M), chemical reaction parameter (K), heat source parameter (Q), casson fluid parameter (β). A detailed numerical calculation for numerous values of a, M, K, Q, and β is performed to assure a greater comprehension of the problem, and the findings are presented graphically in Figs. 7.1 – 7.11.

The effect of the size of the needle on velocity, temperature, and concentration distribution is represented in Fig. 7.1. It is understood from Fig. 7.1(a) that as the size of the needle reduces, velocity improves. Similarly, as a reduces, temperature and concentration decrease, as presented in Figs. 7.1(b) and 7.1(c).

The fluctuation of velocity, temperature, and concentration profiles with the Casson fluid parameter β is given in Fig.7.2. It is understood from Fig. 7.2(a) that velocity improves as the Casson fluid parameter rises. Figs. 7.2(b) and 7.2(c) reveal that the effect of *beta* on temperature and concentration is almost negligible.

The variation of velocity, temperature, and concentration profiles on the chemical reaction

parameter (K) is given in Fig. 7.3. Figs. 7.3(a), 7.3(b), and 7.3(c) reveal that the effect of K on velocity, temperature, and concentration is almost negligible.

Figure 7.4 presents the effect of the magnetic parameter (M) on velocity, temperature, and concentration. Fig. 7.4(a) exhibits that the velocity reduces as M rises. Figs. 7.4(b) and 7.4(c) reveal that the effect of M on temperature and concentration is almost negligible.

The fluctuation of velocity, temperature, and concentration profiles with the heat source parameter (Q) is given in Fig. 7.5. It is understood from Fig. 7.5(a) that The effect of Q on velocity is almost negligible. Figs. 7.5(b) and 7.5(c) reveal that as the heat source rises, the temperature and concentration increase.

Figure 7.6 presents the effect of λ on velocity, temperature, and concentration. Fig. 7.6(a) exhibits that the velocity increases as λ rises. Figs. **??** and 7.6(c) reveal that as λ reduces, the temperature and concentration increase.

The impact of the size of the needle (a) on $\sqrt{Re}C_f$, $\frac{Nu}{\sqrt{Re}}$, and $\frac{Sh}{\sqrt{Re}}$ is presented in Fig. 7.7. As depicted in Fig.7.7(a), skin friction coefficient is improved by lowering a. As a decreases, $\frac{Nu}{\sqrt{Re}}$ and $\frac{Sh}{\sqrt{Re}}$ are also enhanced, as presented in Figs. 7.7(b) and 7.7(c).

Figure 7.8 presents the effects of K on $\sqrt{Re}C_f$, $\frac{Nu}{\sqrt{Re}}$, and $\frac{Sh}{\sqrt{Re}}$. Figs. 7.8(a),7.8(b), and 7.8(c) reveal that the effect of the chemical reaction parameter on $\sqrt{Re}C_f$, $\frac{Nu}{\sqrt{Re}}$, and $\frac{Sh}{\sqrt{Re}}$ is almost negligible.

The effect of magnetic parameters on $\sqrt{Re}C_f$, $\frac{Nu}{\sqrt{Re}}$, and $\frac{Sh}{\sqrt{Re}}$ is presented in Fig. 7.9. Fig.7.9(a) clarifies that when the magnetic parameter decreases, the $\sqrt{Re}C_f$ rises. The values of $\frac{Nu}{\sqrt{Re}}$ and $\frac{Sh}{\sqrt{Re}}$ also increase as the magnetic parameter decreases, as represented in Figs. 7.9(b) and 7.9(c).

The effect of heat source on $\sqrt{Re}C_f$, $\frac{Nu}{\sqrt{Re}}$, and $\frac{Sh}{\sqrt{Re}}$ is presented in Fig. 7.10. As the heat source parameter decreases, it is evident from Fig.7.10(a) that $\sqrt{Re}C_f$ rises. $\frac{Nu}{\sqrt{Re}}$ and $\frac{Sh}{\sqrt{Re}}$ are also increasing with a decrease in heat source parameter, as illustrated in Figs.7.10(b) and 7.10(c).

The effect of λ on $\frac{Sh}{\sqrt{Re}}$, $\frac{Nu}{\sqrt{Re}}$, and $\sqrt{Re}C_f$ is illustrated in Fig. 7.11. Lowering λ improves $\sqrt{Re}C_f$, as illustrated in Fig.7.11(a). According to Figs. 7.11(b) and 7.11(c), $\frac{Nu}{\sqrt{Re}}$ and $\frac{Sh}{\sqrt{Re}}$ increase with λ .

7.5 Conclusion

A constant mixed convection stream past a horizontal needle in Casson fluid is analyzed. The flow equations are changed into a scheme of non-linear ordinary differential equations utilizing appropriate transforms and then linearized using successive linearization. The Chebyshev spectral collocation technique is implemented to find the resulting equations.

- As the size of the needle reduces, velocity and the coefficient of skin friction improve, whereas temperature, the Nusselt number, and the Sherwood number decrease.
- While skin friction coefficient, Nusselt number, and Sherwood number increase with a decline in the magnetic parameter, velocity decreases when the magnetic parameter intensifies.
- When the heat source is enhanced, temperature and concentration increase while Sherwood and Nusselt numbers decrease.
- With a gain in the mixed convection parameter, the Nusselt number and Sherwood number increase.

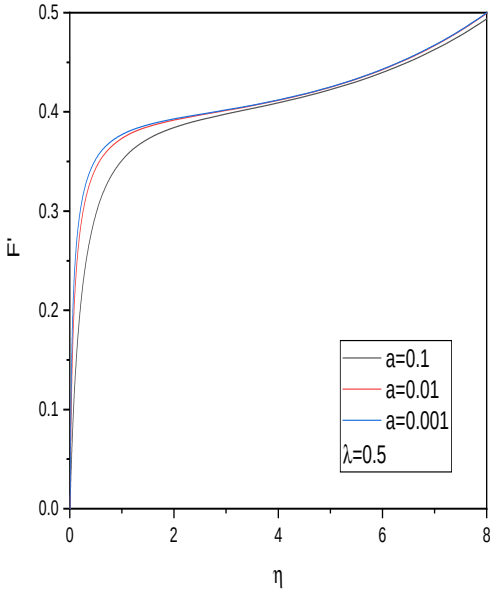

(a)

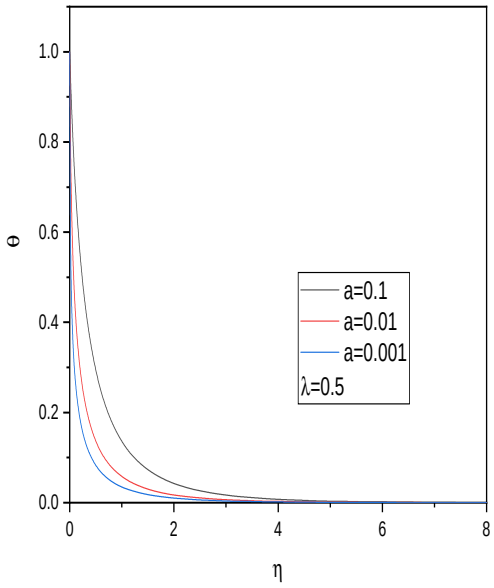

(b)

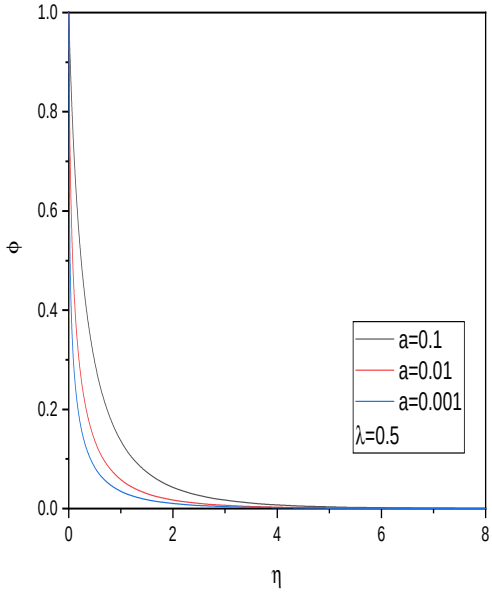

(c)

Figure 7.1: "Effect of a on the velocity, temperature and concentratrion"

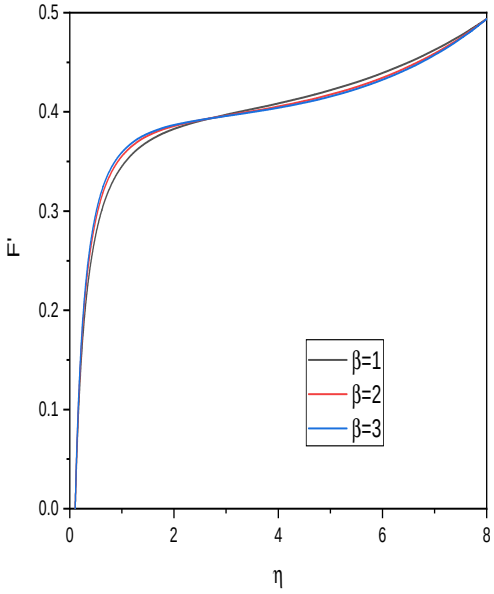

(a)

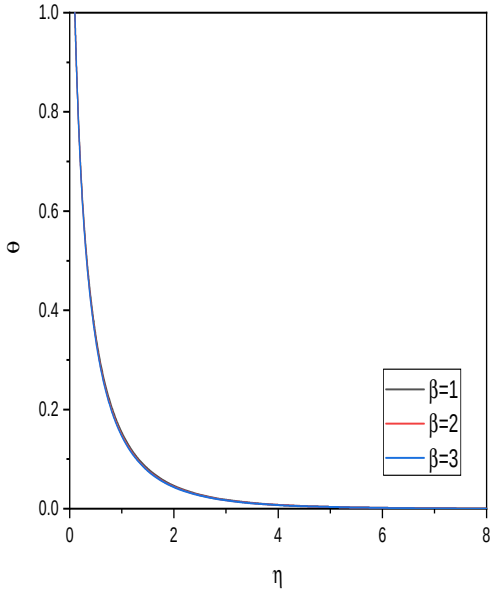

(b)

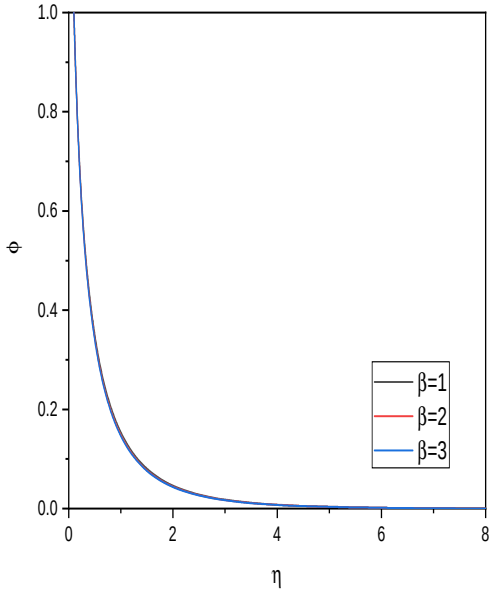

(c)

Figure 7.2: "Effect of β on the velocity, temperature and concentratrion"

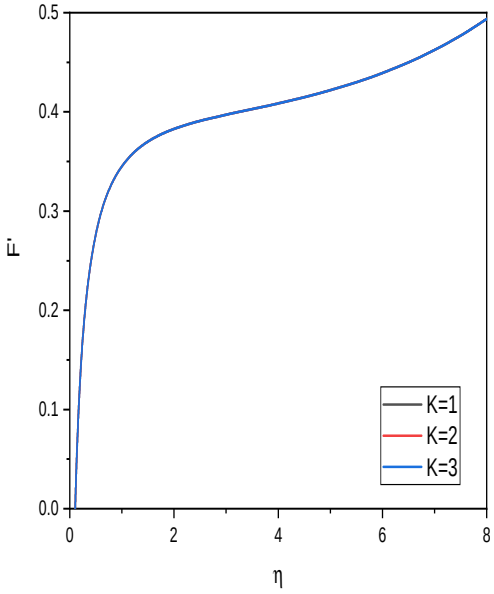

(a)

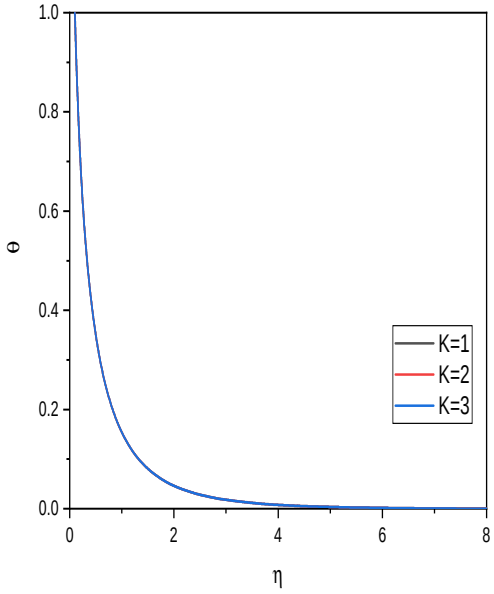

(b)

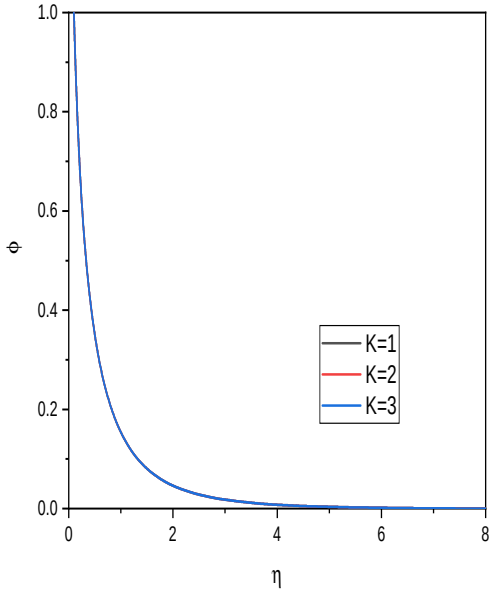

(c)

Figure 7.3: "Effect of K on the velocity, temperature and concentratrion"

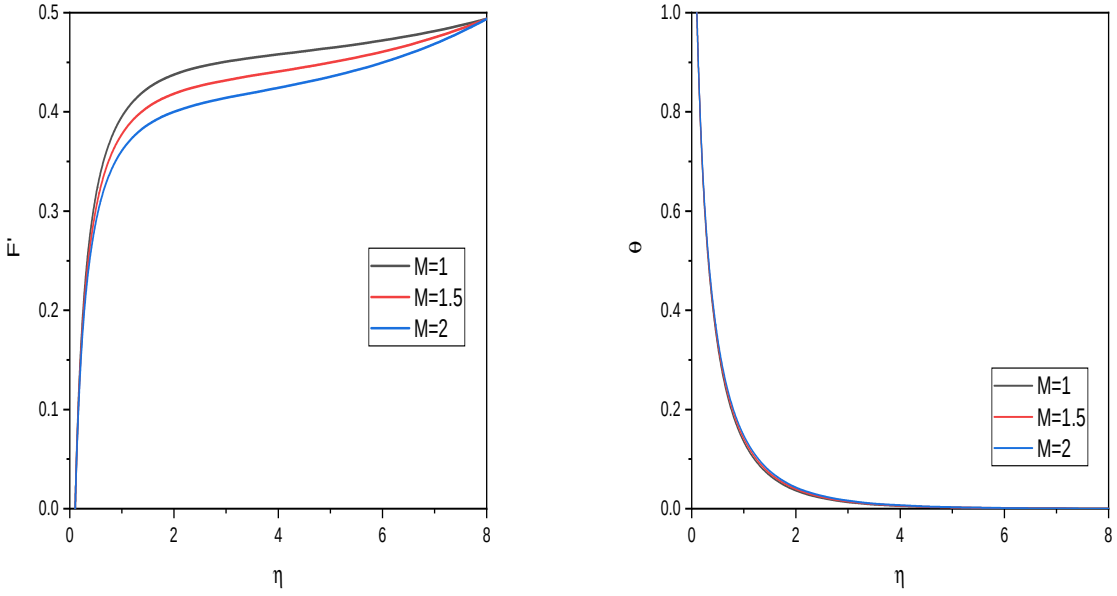

(a) (b)

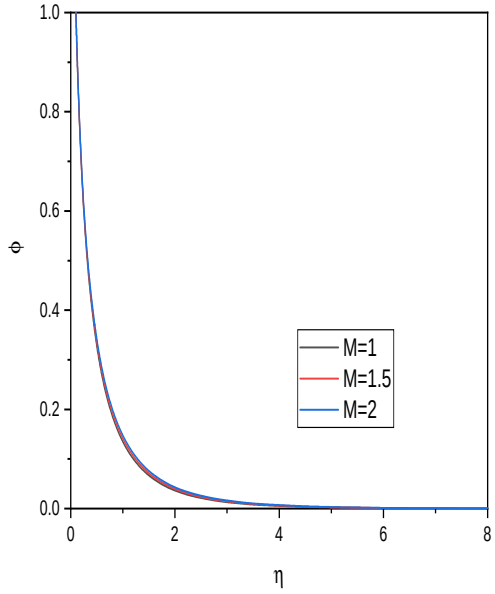

(c)

Figure 7.4: "Effect of M on the velocity, temperature and concentratrion"

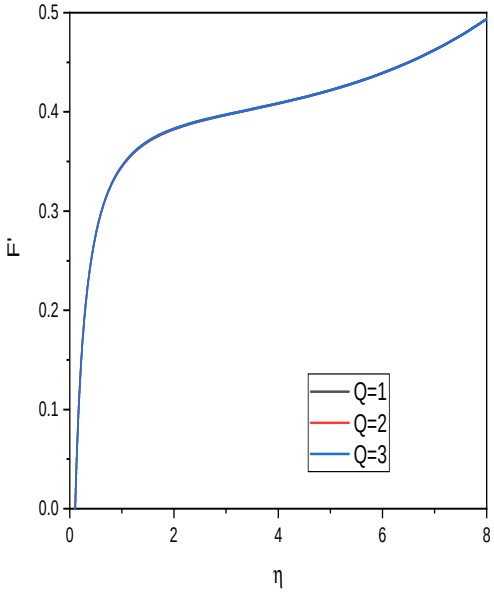

(a)

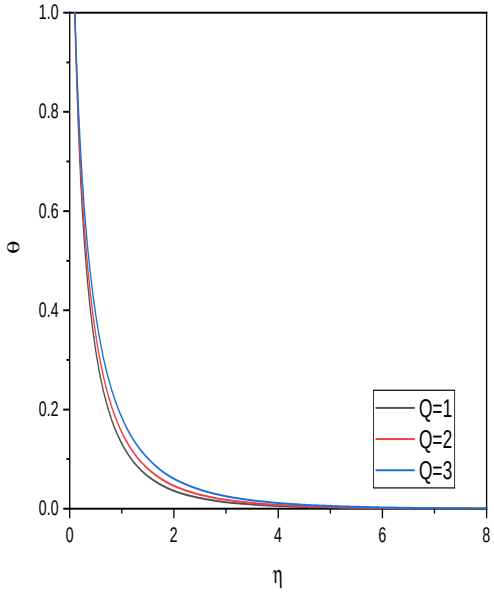

(b)

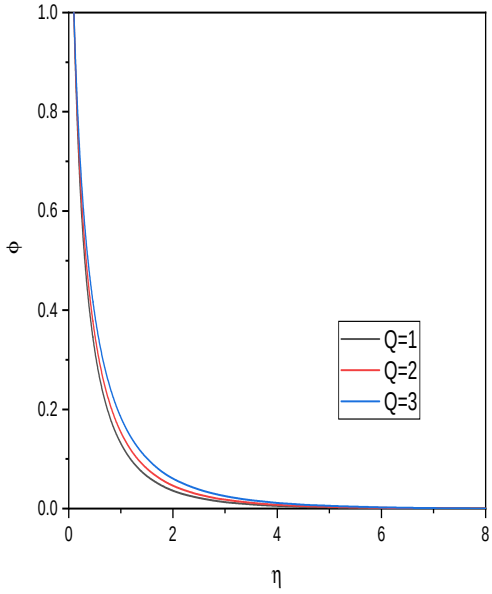

(c)

Figure 7.5: "Effect of Q on the velocity, temperature and concentratrion"

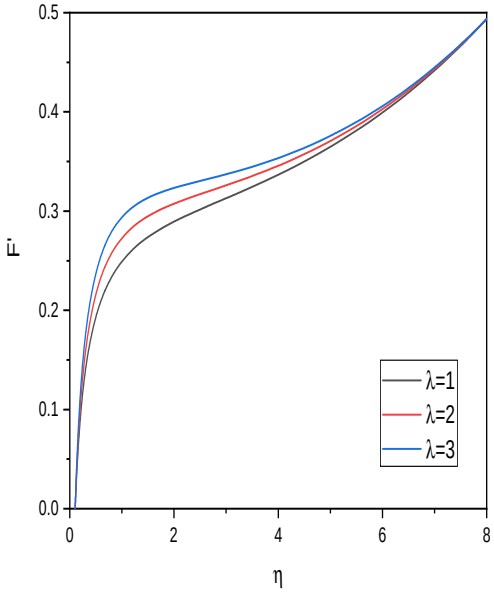

(a)

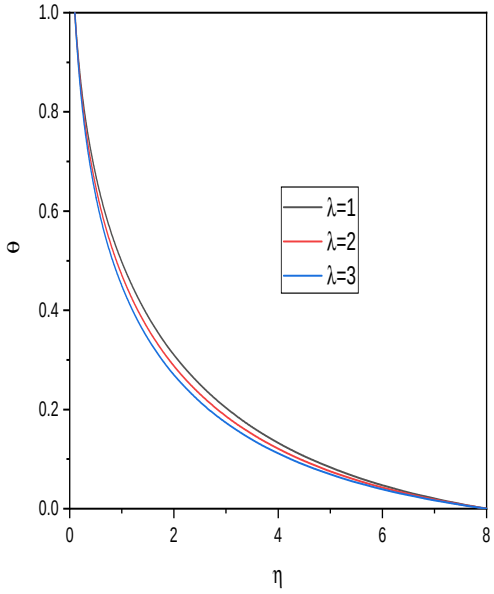

(b)

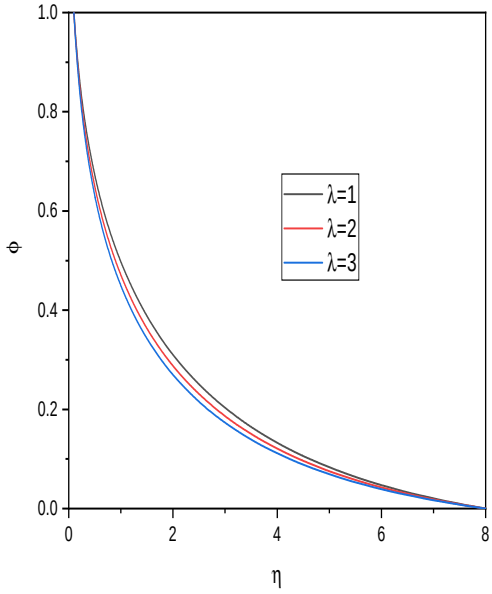

(c)

Figure 7.6: "Effect of λ on the velocity, temperature and concentratrion"

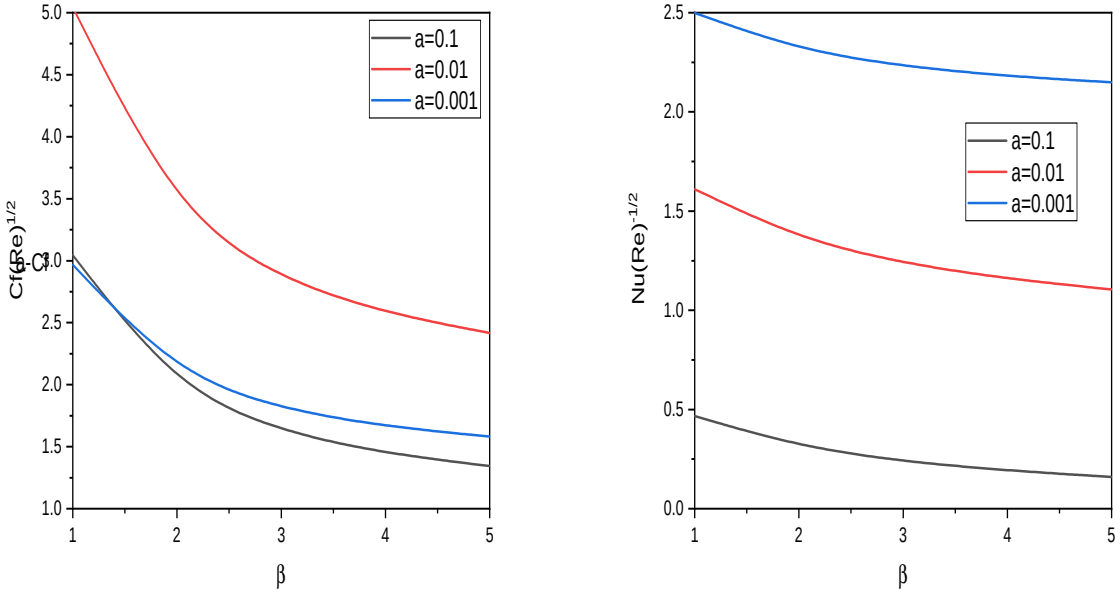

(a)

(b)

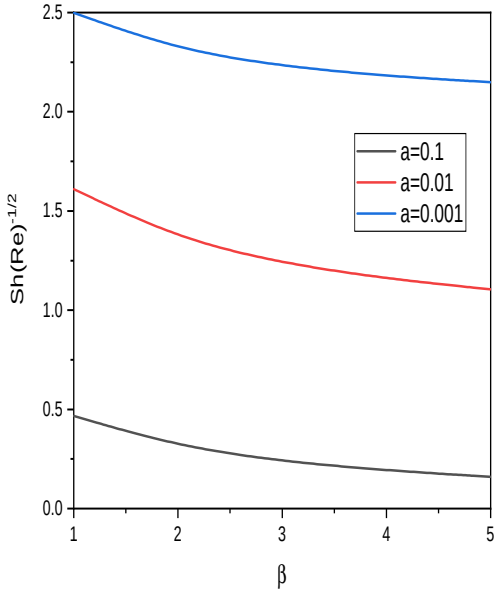

(c)

Figure 7.7: "Effect of a on $C_f(Re)^{\frac{1}{2}}$, $Nu(Re)^{\frac{-1}{2}}$ and $Sh(Re)^{\frac{-1}{2}}$"

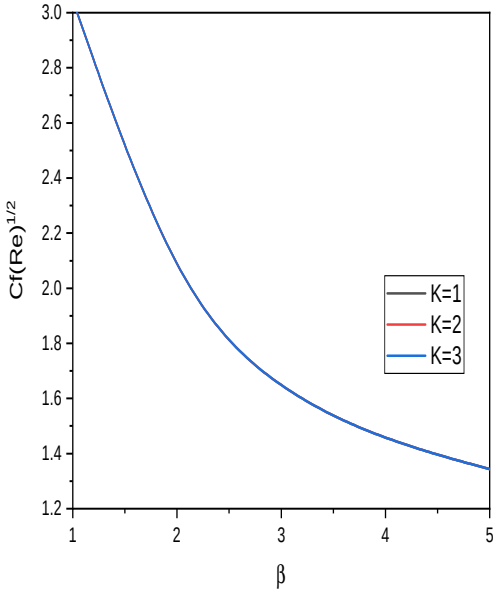

(a)

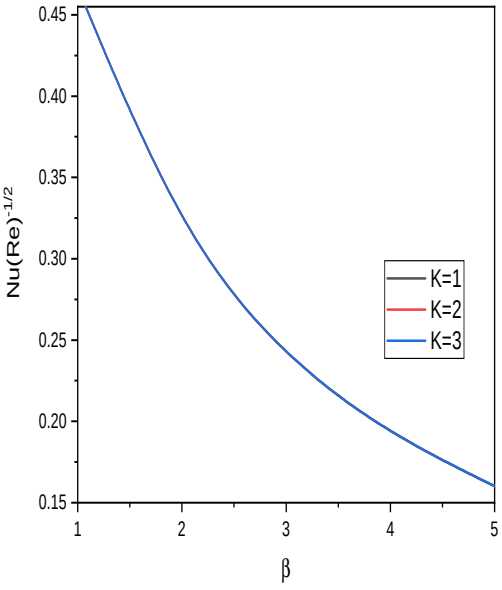

(b)

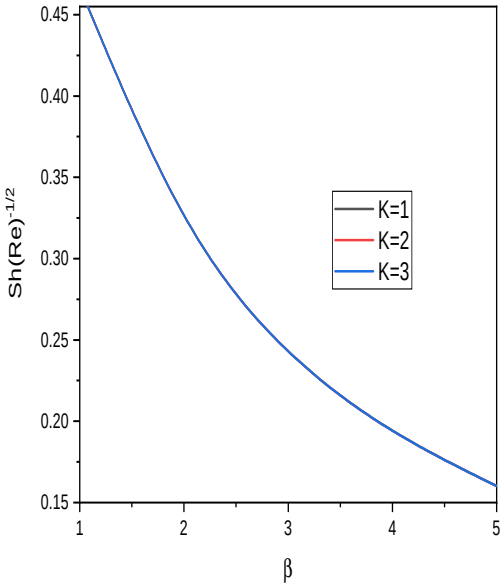

(c)

Figure 7.8: "Effect of K on $C_f(Re)^{\frac{1}{2}}$, $Nu(Re)^{\frac{-1}{2}}$ and $Sh(Re)^{\frac{-1}{2}}$"

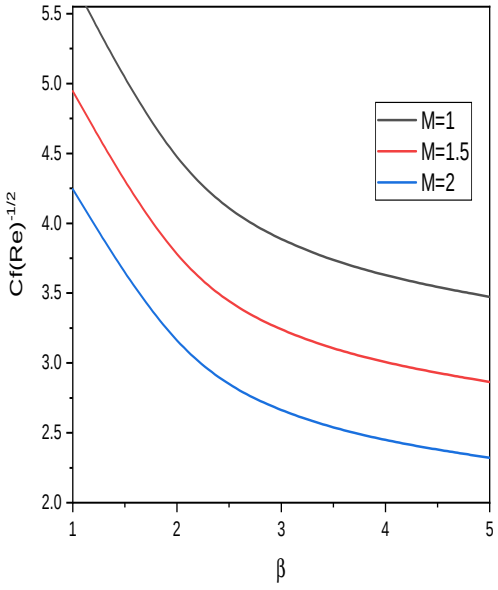

(a)

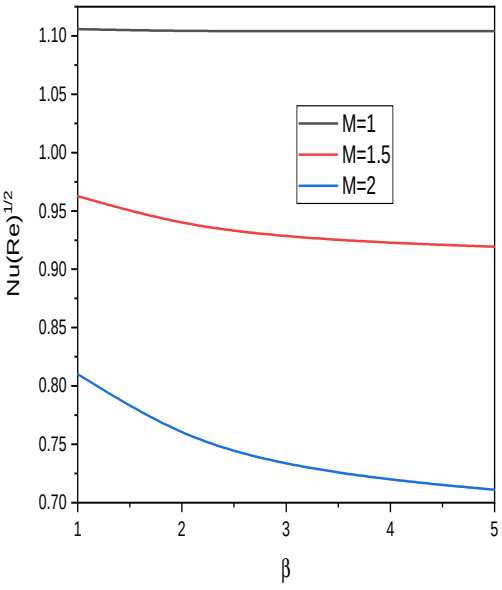

(b)

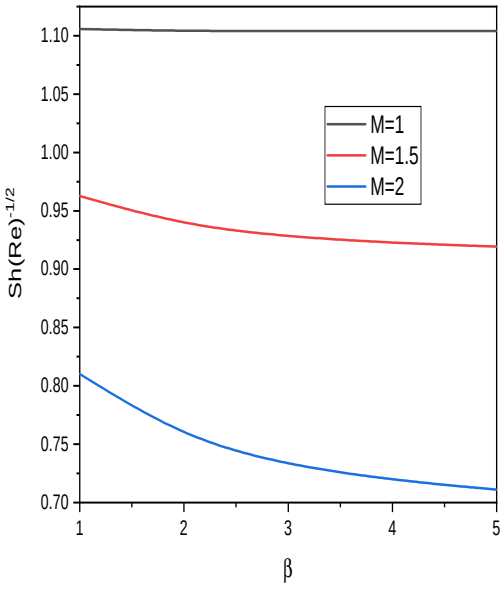

(c)

Figure 7.9: "Effect of M on $C_f(Re)^{\frac{1}{2}}$, $Nu(Re)^{\frac{-1}{2}}$ and $Sh(Re)^{\frac{-1}{2}}$"

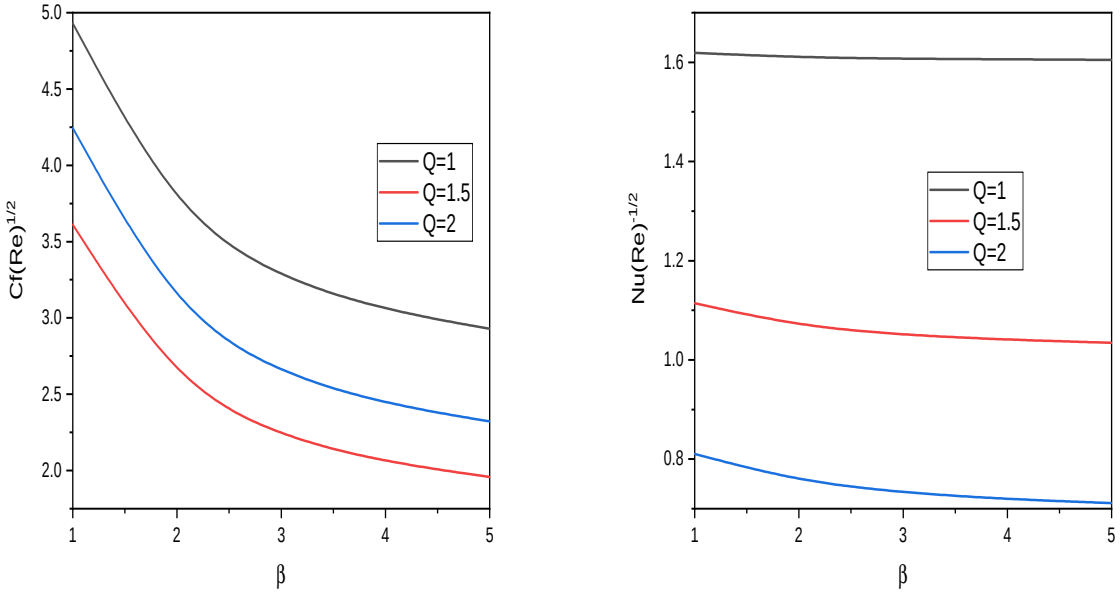

(a) (b)

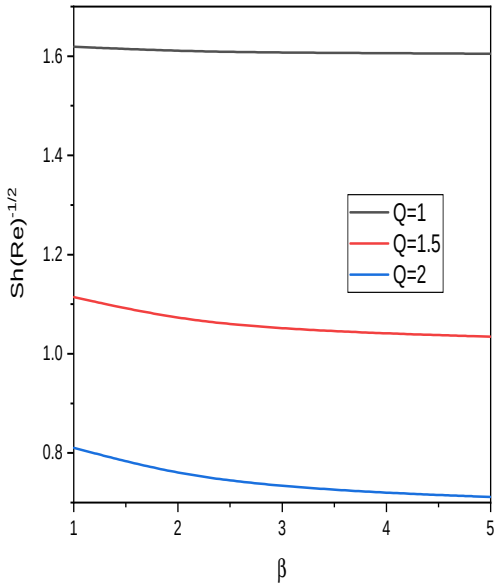

(c)

Figure 7.10: "Effect of Q on $C_f(Re)^{\frac{1}{2}}$, $Nu(Re)^{\frac{-1}{2}}$ and $Sh(Re)^{\frac{-1}{2}}$"

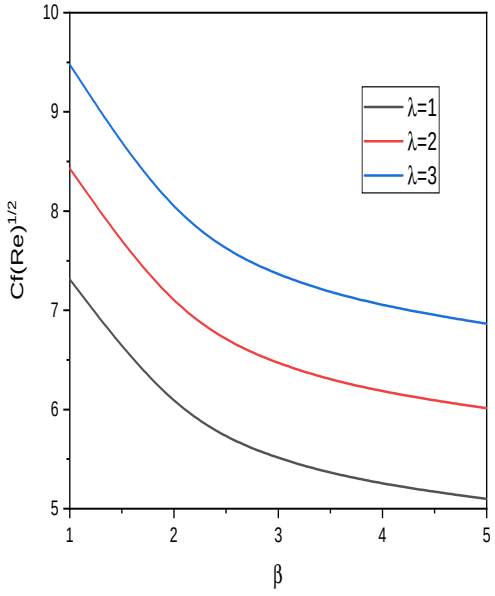

(a)

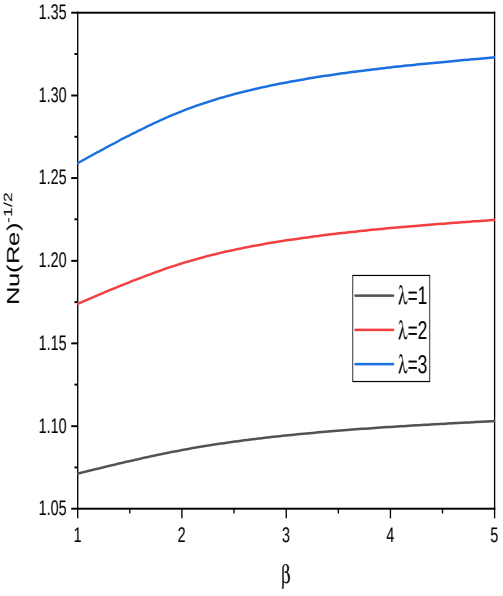

(b)

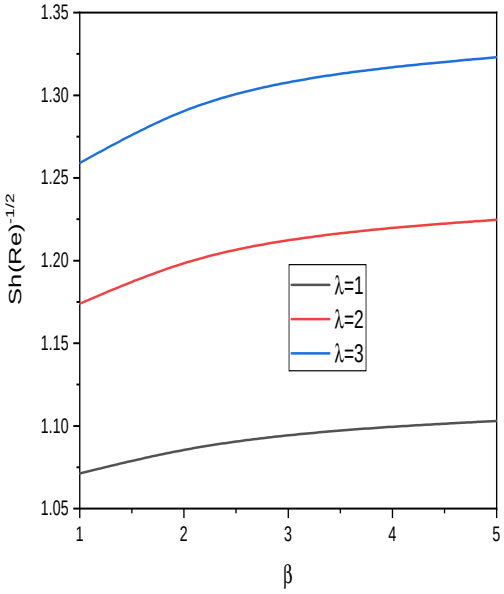

(c)

Figure 7.11: "Effect of λ on $C_f(Re)^{\frac{1}{2}}$, $Nu(Re)^{\frac{-1}{2}}$ and $Sh(Re)^{\frac{-1}{2}}$"

Chapter 8

Effects of Variable Properties on Mixed Convection of a Casson Fluid Flow Over a Thin Needle [1]

8.1 Introduction

The boundary layer flow and heat transfer along tiny needle have wide range of application including biomedicine, lubrication and power generation, microstructure electronic devices, hot wire anemometers, aerodynamics, microscale cooling devices, blood flow, cancer therapy, wire coating, and many more. In the past, Lee[19] introduced a boundary layer stream across a thin moving needle in a parallel free stream and described asymptotic behaviour of approximation solution. Thereafter, Narain and Uberoi [20, 21, 22] presented similarity solutions for convective flow over an isothermal needle.

This chapter studies the effect of variable properties on the mixed convective Casson fluid flow over a thin needle. The effect of dimensionless parameters, namely size of needle and mixed convection parameter on the The velocity component, temperature, and heat transfer rate are explained through graphs.

[1] Communicated to "**Heat Source**"

8.2 Formulation of the Problem

Consider the steady, laminar and mixed convection flow of Casson fluid over a horizontally moving thin needle. Assume that the uniform velocity of the fluid be $\bar{U_\infty}(\bar{x})$ and the moving velocity of the needle be $\bar{U_w}(\bar{x})$. Figure 6.1 shows the schematic of the problem along with coordinate system. The radius of the needle is given by $r = R(\bar{x})$. Apart from the assumption of Chapter - 6, In addition, we assume the viscosity and thermal conductivity depends on the temperature.

With the above premises, the governing equations becomes

$$\frac{\partial(\bar{r}\bar{u})}{\partial\bar{x}} + \frac{\partial(\bar{r}\bar{v})}{\partial\bar{r}} = 0 \tag{8.1}$$

$$\bar{u}\frac{\partial\bar{u}}{\partial\bar{x}} + \bar{v}\frac{\partial\bar{u}}{\partial\bar{r}} = \bar{U}\frac{d\bar{U}}{d\bar{x}} + \left(1+\frac{1}{\beta}\right)\frac{1}{\bar{r}}\frac{\partial}{\partial\bar{r}}\left(\mu(\bar{T})\bar{r}\frac{\partial\bar{u}}{\partial\bar{r}}\right) + g\beta_T(\bar{T}-T_\infty) \tag{8.2}$$

$$\bar{u}\frac{\partial\bar{T}}{\partial\bar{x}} + \bar{v}\frac{\partial\bar{T}}{\partial\bar{r}} = \left(\alpha(\bar{T})\frac{1}{\bar{r}}\frac{\partial}{\partial\bar{r}}\left(\bar{r}\frac{\partial\bar{T}}{\partial\bar{r}}\right)\right) \tag{8.3}$$

where the quantities used in the above equations are already defined in Chapter - 6.

The conditions on the surface of the needle are

$$\begin{aligned} \bar{u} = 0, \bar{v} = 0, \bar{T} = \bar{T_w}(\bar{x}) \;\; at\; \bar{r} = \bar{R}(\bar{x}) \\ \bar{u} \to \bar{U}(\bar{x}), \bar{T} \to T_\infty \;\; at\; \bar{r} \to \infty \end{aligned} \tag{8.4}$$

The following non-dimensional variables:

$$\begin{aligned} x = \frac{\bar{x}}{L}, r = Re^{1/2}\frac{\bar{r}}{L}, R(x) = Re^{1/2}\frac{\bar{R}(\bar{x})}{L}, u = \frac{\bar{u}}{U_\infty}, \\ v = Re^{1/2}\frac{\bar{v}}{U_\infty}, U(x) = \frac{\bar{U}(\bar{x})}{U_\infty}, T = \frac{\bar{T}-T_\infty}{\Delta T} \end{aligned} \tag{8.5}$$

Substituting Eq.(8.4) into Eq.(8.1) to (8.3) , we get

$$\frac{\partial(ru)}{\partial x} + \frac{\partial(rv)}{\partial r} = 0 \tag{8.6}$$

$$u\frac{\partial u}{\partial x} + v\frac{\partial u}{\partial r} = U\frac{dU}{dx} + \left(1+\frac{1}{\beta}\right)\frac{1}{r}\frac{\partial}{\partial r}\left((1+A(1-\theta)r\frac{\partial u}{\partial r}\right) + \lambda T \tag{8.7}$$

$$u\frac{\partial T}{\partial x}+v\frac{\partial T}{\partial r}=\frac{1}{Pr}\frac{1}{r}\frac{\partial}{\partial r}\left((1+\epsilon\theta)r\frac{\partial T}{\partial r}\right) \tag{8.8}$$

It is presumed that thermal conductivity and viscosity are linearly dependent on the temperature as

$$\alpha(T)=\alpha_0[1+E(T-T_\infty)] \quad \text{and} \quad \mu(T)=\mu_\infty[1+b(T_w-T)] \tag{8.9}$$

where α_0 and μ_∞ are the absolute thermal conductivity and viscosity, b and E are constants.

Conditions on boundary Eq.(8.4) become

$$\begin{aligned} u=0, v=0, T=T_w(x) \;\; at\; r=R(x) \\ u\to U(x), T\to 0 \;\; as\; r\to\infty \end{aligned} \tag{8.10}$$

Similarity Transformations are defined as:

$$\psi=xf(\eta), T(x)=x^{2m-1}\theta(\eta), \eta=x^{m-1}r^2 \tag{8.11}$$

Using Eq. (8.11) in the equation to the surface of the wall $\eta=a$, it can be written as $R=a^{1/2}x^{(1-m)/2}$ which characterizes shape and size of the needle.

Making use of above similarity variables in Eq.(8.6) to (8.8), we obtain

$$8\eta[1+\frac{1}{\beta}][1-A(1+\theta)]f'''+8[1+\frac{1}{\beta}][1-A(1-\theta)]f''-8\eta[1+\frac{1}{\beta}]A\theta' f''+4ff''-4m(f')^2+m+\lambda\theta=0 \tag{8.12}$$

$$\frac{2\eta}{Pr}(1+\epsilon\theta)\theta''+\frac{2\eta\epsilon}{Pr}(\theta')^2+\frac{2}{Pr}(1+\epsilon\theta)\theta'+f\theta'-(2m-1)f'\theta=0 \tag{8.13}$$

where A is viscosity parameter, $Pr=\frac{\nu}{\alpha}$, is Prandtl number, $\lambda=\frac{Gr}{Re}$ is mixed convection parameter and ϵ is thermal conductivity parameter.

The modified conditions on boundary becomes

$$\begin{aligned} f'(\eta)=0, f(\eta)=0, \theta(\eta)=1 \quad at \quad \eta=a \\ f'(\eta)\to\frac{1}{2}, \quad \theta(\eta)\to 0, \quad as \quad \eta\to\infty \end{aligned} \tag{8.14}$$

In additions to desired allotment for this model is Skin Friction C_f and the local Nusselt

number Nu which are represented as:

$$\sqrt{Re}C_f = 8\sqrt{a}\left(1+\frac{1}{\beta}\right)f^{''}(a), \frac{Nu}{\sqrt{Re}} = -2\sqrt{a}\theta^{'}(a) \tag{8.15}$$

8.3 Solution of the Problem

The combined Eqns. (8.12) and (8.13) and conditions on boundary (8.14) are linearized through the successive linearization method (SLM) [78]. The solution of resulting linearized equations is obtained by Chebyshev collocation method.

On applying the procedure explained in Chapter 2 to the equations Eqns. (8.12) and (8.13), we get the following linearized equations.

$$a_1 f_i^{'''} + a_2 f_i^{''} + a_3 f_i^{'} + a_4 f_i + a_5 \theta_i^{'} + a_6 \theta_i = r_1 \tag{8.16}$$

$$b_1 f_i^{'} + b_2 f_i + b_3 \theta_i^{''} + b_4 \theta_i{}' + b_5 \theta_i = r_2 \tag{8.17}$$

Where

$$a_1 = 8\eta\left(1+\frac{1}{\beta}\right)\left[1-A-A(\sum\theta_m)\right],$$

$$a_2 = 8\left(1+\frac{1}{\beta}\right)\left[1+A-A\eta(\sum\theta'_m)-A(\sum\theta_m)\right]+4\sum f_m,$$

$$a_3 = -8m\sum f'_m, \quad a_4 = 4\sum f''_m,$$

$$a_5 = 8A\eta\left(1+\frac{1}{\beta}\right)\sum f''_m, \qquad a_6 = \lambda - 8A\left(1+\frac{1}{\beta}\right)\sum f''_m - 8A\eta\left(1+\frac{1}{\beta}\right)\sum f'''_m$$

$$r_1 = -a_1(\sum f'''_m) - a_2(\sum f''_m) - m - 4m(\sum f'_m)^2 - \lambda(\theta_m)$$

$$b_1 = -(2m-1)(\sum\theta_m), \quad b_2 = \sum\theta'_m, \quad b_3 = \frac{2\eta\epsilon}{Pr}(\sum\theta_m)+\frac{2\eta}{Pr},$$

$$b_4 = \frac{4\eta\epsilon}{Pr}(\sum\theta'_m)+\frac{2}{Pr}+\frac{2\epsilon}{Pr}(\sum\theta_m)+(\sum f_m)$$

$$b_5 = \frac{2\eta\epsilon}{Pr}(\sum\theta''_m)-\frac{2\epsilon}{Pr}(\sum\theta'_m)-(2m-1)(\sum f'_m)$$

$$r_2 = -b_3(\sum \theta''_m) - \frac{2\eta\epsilon}{Pr}(\sum \theta'_m)^2 - \frac{2}{Pr}(\sum \theta'_m) - \frac{2\epsilon}{Pr}(\sum \theta_m)(\sum \theta'_m)$$
$$-(\sum f_m)(\sum \theta'_m) + (2m-1)(\sum f'_m)(\sum \theta_m)$$

As explained in Chapter - 2, using Chebyshev collocation method on the system of linearized equations. (8.16) t0 (8.17), we obtain the following equation in matrix form

$$A_{j-1}X_j = R_{j-1} \tag{8.18}$$

where A_{j-1} is a $2(N+1) \times 2(N+1)$ order matrix and X_j and R_{j-1} are $2(N+1) \times 1$ column matrix given by

$$A_{j-1} = \begin{pmatrix} A_{11} & A_{12} \\ A_{21} & A_{22} \end{pmatrix}, X_j = \begin{pmatrix} F_j \\ \Theta_j \end{pmatrix}, R_{j-1} = \begin{pmatrix} r_{1,j-1} \\ r_{2,j-2} \end{pmatrix} \tag{8.19}$$

where

$$F_j = [f_j(\xi_0), f_j(\xi_1), ..., f_j(\xi_{N-1}), f_j(\xi_N)]^T,$$
$$\Theta_j = [\theta_j(\xi_0), \theta_j(\xi_1), .., \theta_j(\xi_{N-1}), \theta_j(\xi_N)]^T,$$
$$A_{11} = a_1D^3 + a_2D^2 + a_3D + a_4I, A_{12} = a_5D + a_6I,$$
$$A_{21} = b_1D + b_2I, A_{22} = b_3D^2 + b_4D + b_5I,$$
$$r_1 = [r_1(\xi_1), r_1(\xi_2), r_1(\xi_3)...., r_1(\xi_{N+1})]^T,$$
$$r_2 = [r_2(\xi_1), r_2(\xi_2), r_2(\xi_3)...., r_2(\xi_N)]^T,$$

The superscript T stands for transpose, I is the identity matrix, O is the zero matrix.

Imposing the boundary conditions in terms of the collocation points, the solution is provided by

$$X_j = A_{j-1}^{-1}R_{j-1}$$

8.4 Results and Discussion

The effect of six dimensionless parameters—size of the needle (a), mixed convection parameter (λ), casson fluid parameter (β), thermal conductivity parameter (ϵ), variable viscosity parameter (A), power index (m)—on the relevant physical quantities is the primary focus of the current model. To ensure a deeper understanding of the technical problem, a comprehensive numerical parametric analysis is carried out, and the results are displayed graphically (Figs. 8.1-8.11).

Figure8.1 illustrates how the needle's size affects the velocity and temperature profiles. As shown in Fig.8.1(a), enlarging a elevates the velocity. As a rises, the temperature is increasing, as presented in Fig. 8.1(b).

The variation of velocity and temperature with β is shown in Fig.8.2. As the Casson fluid parameter decreases, velocity increases, as illustrated in Fig. 8.2(a). As depicted in Fig. 8.2(b), the influence of β on the temperature profile is insignificant.

The consequence of the thermal conductivity parameter ϵ on velocity and temperature is given in Fig. 8.3. It is represented in Fig. 8.3(a) that the velocity improves slightly as the variable thermal conductivity parameter reduces. The temperature profile is also enhanced with an enhancement in ϵ, as depicted in Fig. 8.3(b).

The variation of velocity and temperature with λ is presented in Fig.8.4. As shown in Fig.8.4(a), increasing λ improves the velocity. The effect of the velocity ratio parameter on temperature is negligible, as depicted in Fig. 8.4(b).

Figure 8.5 explains the effect of power index on velocity and temperature. Fig. **??** exhibits that the velocity rises as the power index rises. The temperature decreases as m rises, as depicted in Fig. 8.5(b).

The impact of the variable viscosity parameter (A) on velocity and temperature is given in Fig. 8.6. It is detected from Fig. 8.6(a) that the velocity enhances as the variable viscosity parameter rises. As displayed in Fig. 8.6(b), the temperature profile relative to A is constant.

The influence of size of needle a on the coefficient of skin friction $\sqrt{Re}C_f$ and Nusselt number $\frac{Nu}{\sqrt{Re}}$ is presented in Fig. 8.7. As depicted in Fig.8.7(a), the skin friction coefficient is improved by lowering a. As a decreases, $\frac{Nu}{\sqrt{Re}}$ is also enhanced, as presented in Fig. 8.7(b).

The impact of ϵ on the local rate of heat transfer $\frac{Nu}{\sqrt{Re}}$ and the coefficient of local skin

friction $\sqrt{Re}C_f$ is given in Fig. 8.8. It is understood from Fig. 8.8(a) that the $\sqrt{Re}C_f$ enhances as the variable thermal conductivity parameter reduces. As exhibited in Fig. 8.8(b), $\frac{Nu}{\sqrt{Re}}$ is also enhanced with diminution in ϵ.

The fluctuation of $\frac{Nu}{\sqrt{Re}}$ and $\sqrt{Re}C_f$ with velocity ratio parameter λ is given in Fig.8.11. As presented in Fig.8.9(a), intensifying λ increases the skin friction coefficient. A decrease in the velocity ratio parameter increases the local Nusselt number, as depicted in Fig. 8.9(b).

The effect of power index on $\frac{Nu}{\sqrt{Re}}$ and $\sqrt{Re}C_f$ is given in Fig. 8.10. It is understood from Fig.8.10(a) that $\sqrt{Re}C_f$ enhances as the power index rises. As exhibited in Fig.**??**, $\frac{Nu}{\sqrt{Re}}$ is also enhanced with an enhancement in m.

The impact of the variable viscosity parameter A on $\frac{Nu}{\sqrt{Re}}$ and $\sqrt{Re}C_f$ is given in Fig. 8.11. It is noticed from Fig. 8.11(a) that the $\sqrt{Re}C_f$ enhances as the variable viscosity parameter rises. Fig. 8.11(b) exhibits that the local Nusselt number is decreasing with an increase in A.

8.5 Conclusion

A steady mixed convection flow past a horizontal needle in Casson fluid is investigated by considering the variable thermal conductivity and variable viscosity. Using suitable transforms, the flow-equations are transformed into a set of non-linear ordinary differential equations, which are then linearized through successive linearization. The approach of Chebyshev spectral collocation is used to solve the resulting equations.

- Temperature and velocity both improve as needle size grows, while Nusselt number and the coefficient of skin friction both drop.
- Temperature rises and skin friction coefficient, Nusselt number, and velocity decrease with increasing thermal conductivity parameter.
- Temperature reduces and skin friction coefficient, Nusselt number, and velocity increase with increasing power index.
- Increasing the variable viscosity parameter and decreasing the Nusselt number leads to improvements in velocity and the coefficient of skin friction.

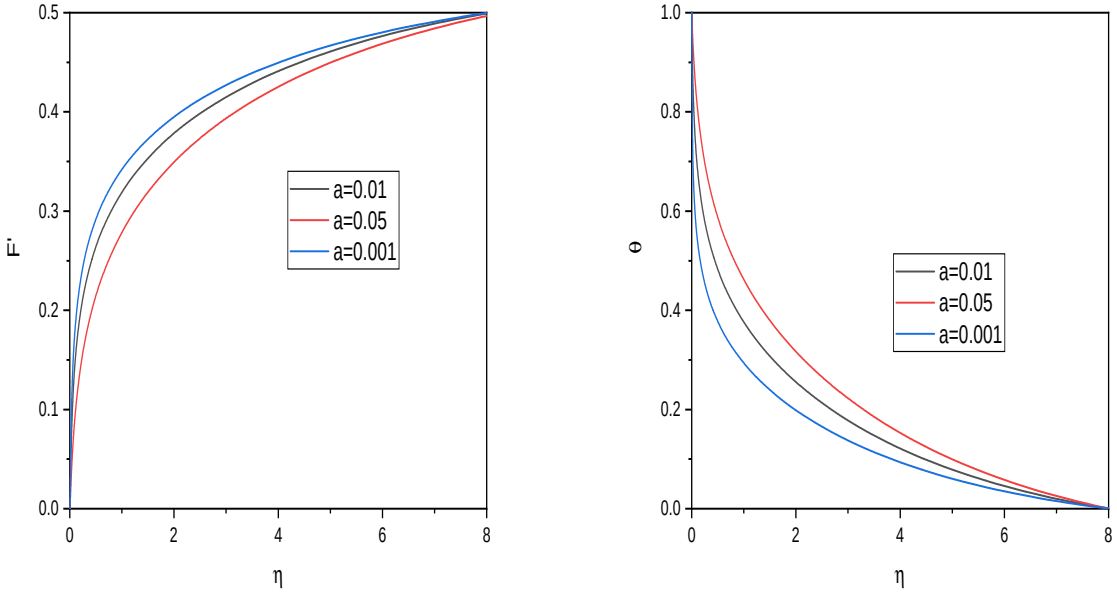

(a) (b)

Figure 8.1: "Effect of a on the velocity, temperature "

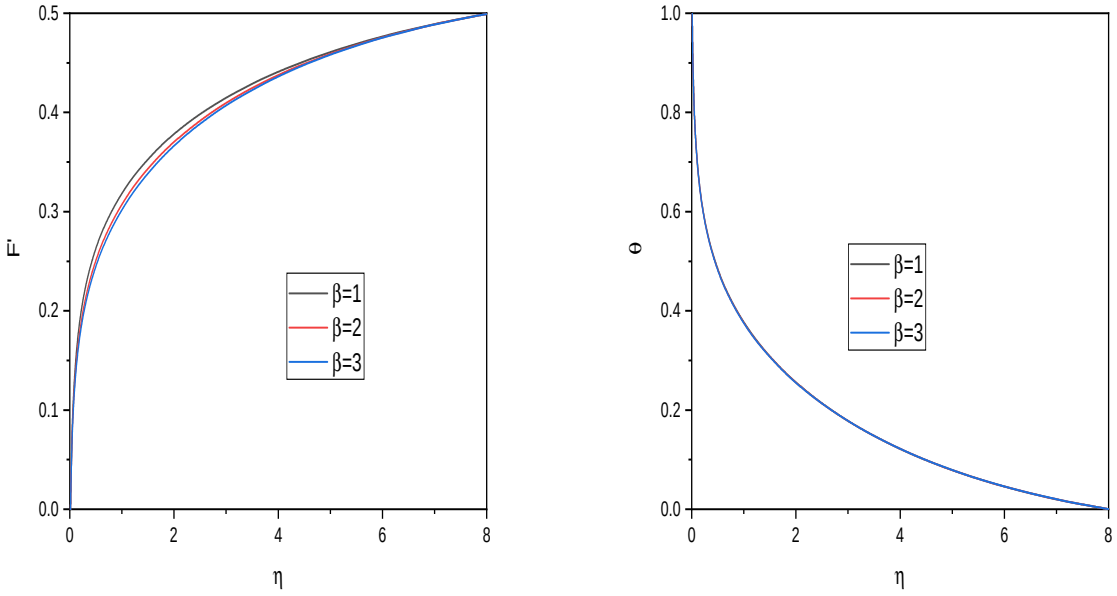

(a) (b)

Figure 8.2: "Effect of β on the velocity and temperature "

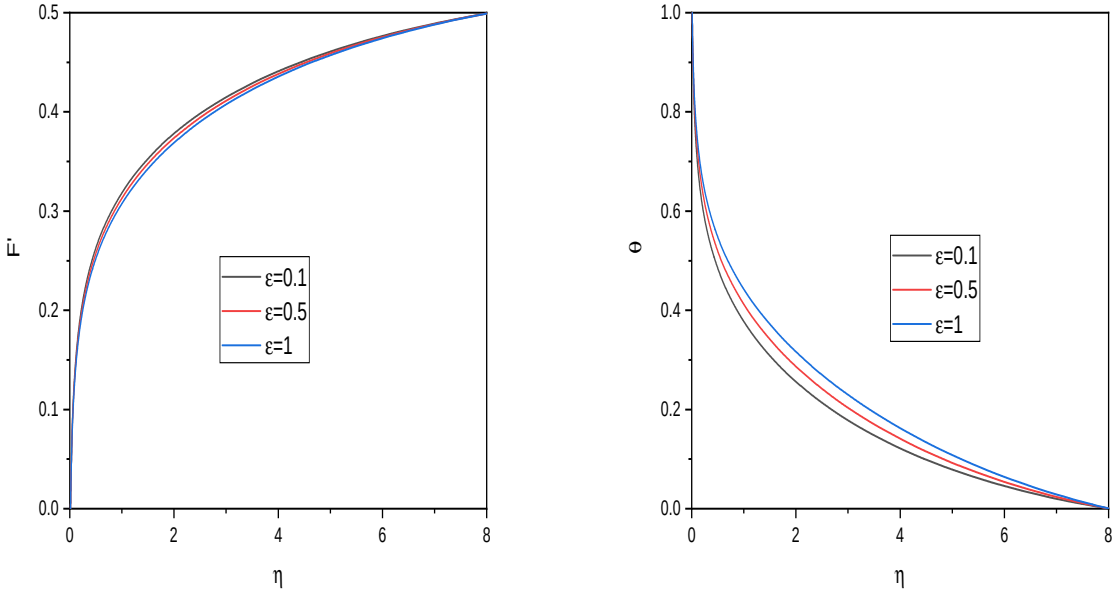

(a) (b)

Figure 8.3: "Effect of ϵ on the velocity and temperature"

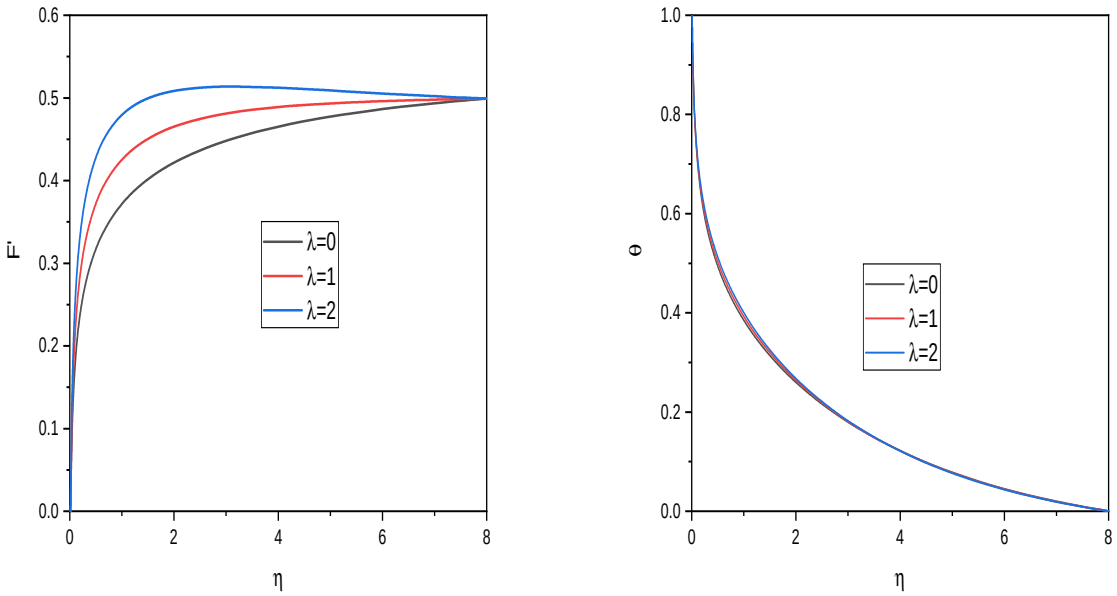

(a) (b)

Figure 8.4: "Effect of λ on the velocity and temperature "

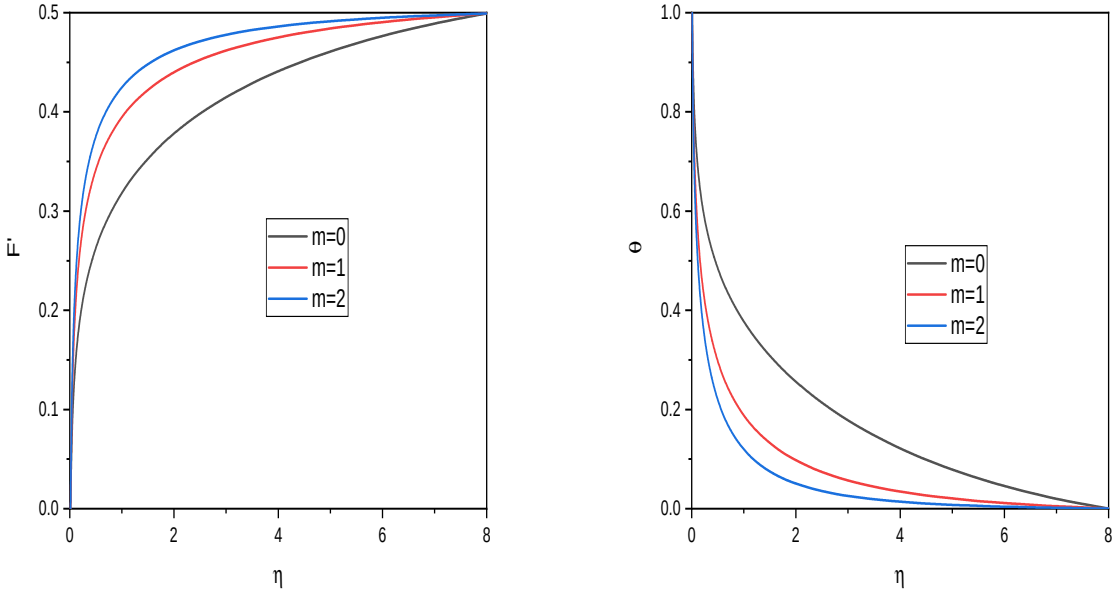

(a) (b)

Figure 8.5: "Effect of m on the velocity and temperature "

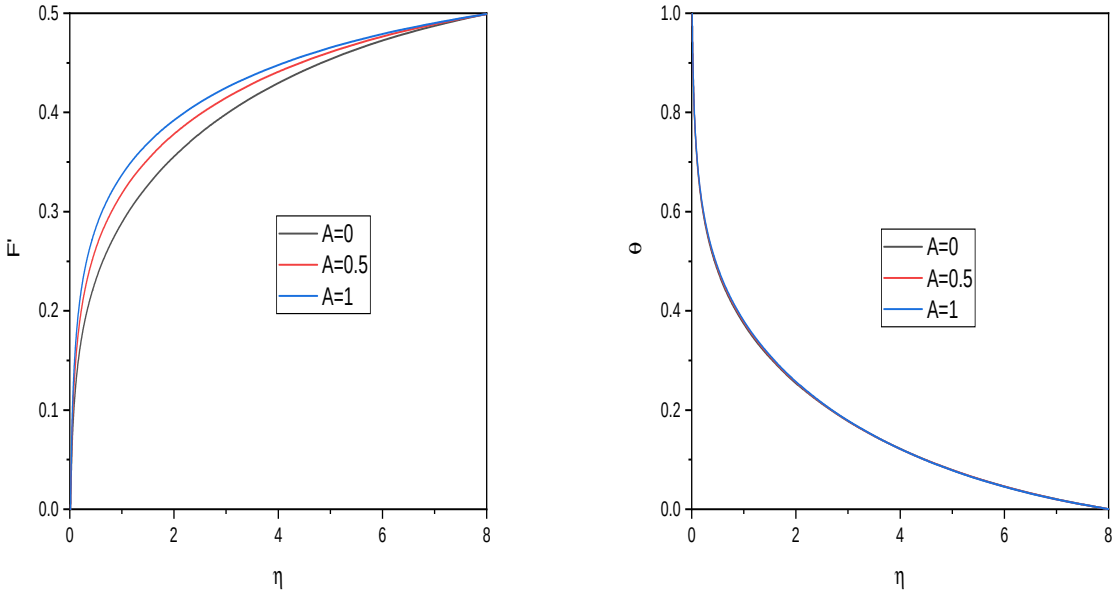

(a) (b)

Figure 8.6: "Effect of A on the velocity and temperature "

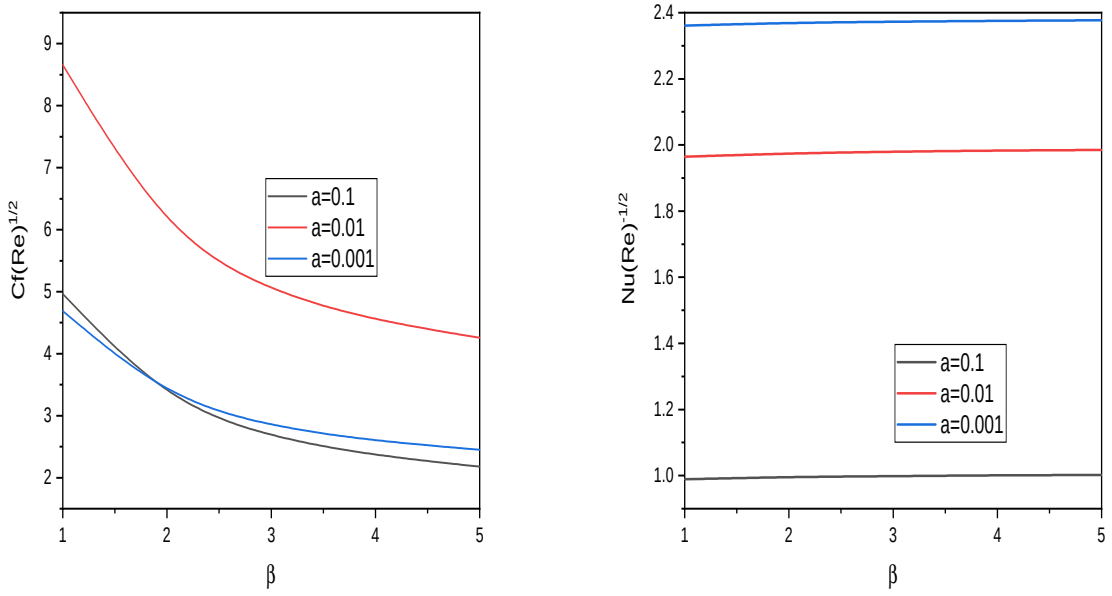

(a) (b)

Figure 8.7: "Effect of a on $C_f(Re)^{\frac{1}{2}}$ and $Nu(Re)^{\frac{-1}{2}}$"

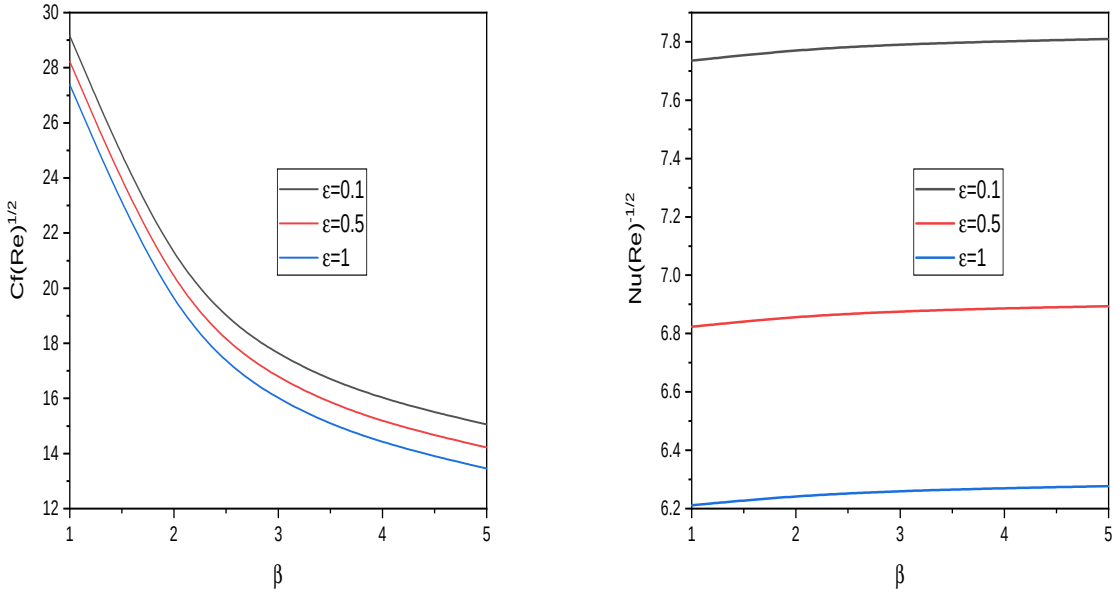

(a) (b)

Figure 8.8: "Effect of ϵ on $C_f(Re)^{\frac{1}{2}}$ and $Nu(Re)^{\frac{-1}{2}}$"

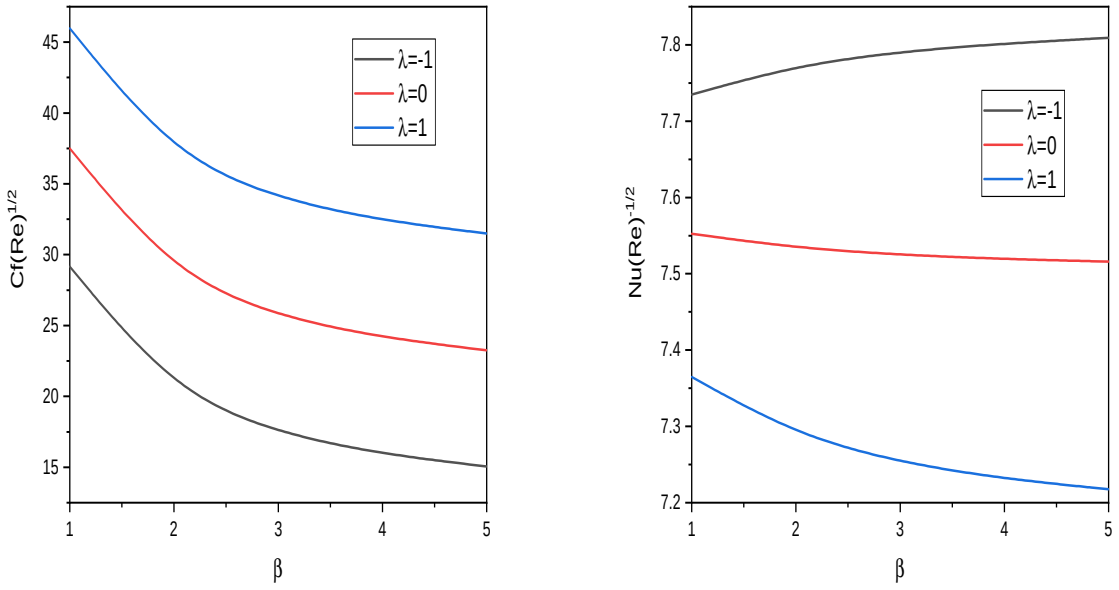

(a) (b)

Figure 8.9: "Effect of λ on $C_f(Re)^{\frac{1}{2}}$ and $Nu(Re)^{\frac{-1}{2}}$"

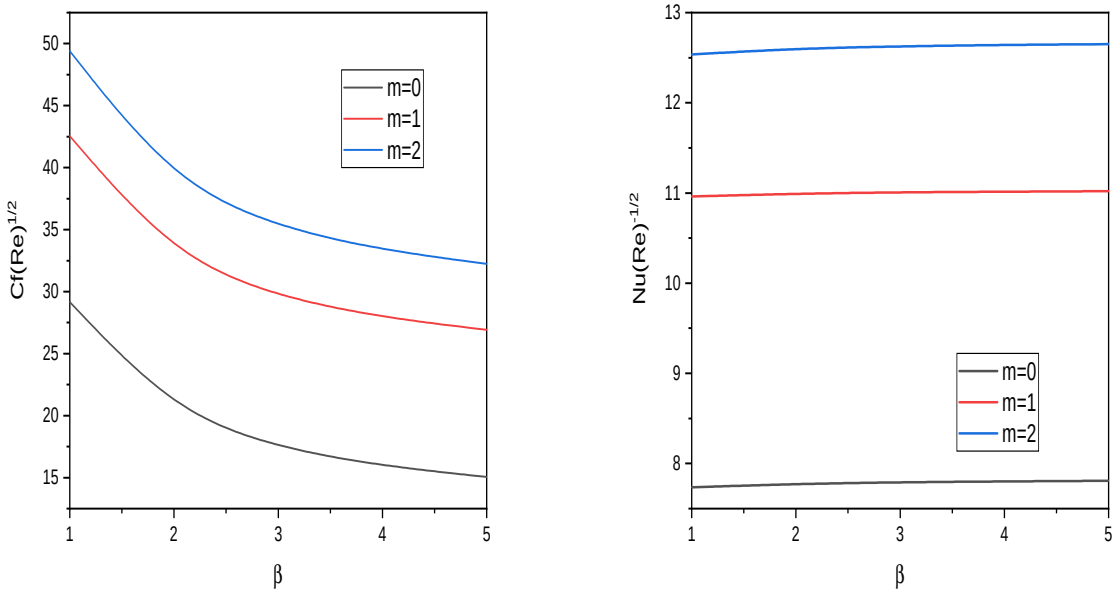

(a) (b)

Figure 8.10: "Effect of m on $C_f(Re)^{\frac{1}{2}}$ and $Nu(Re)^{\frac{-1}{2}}$"

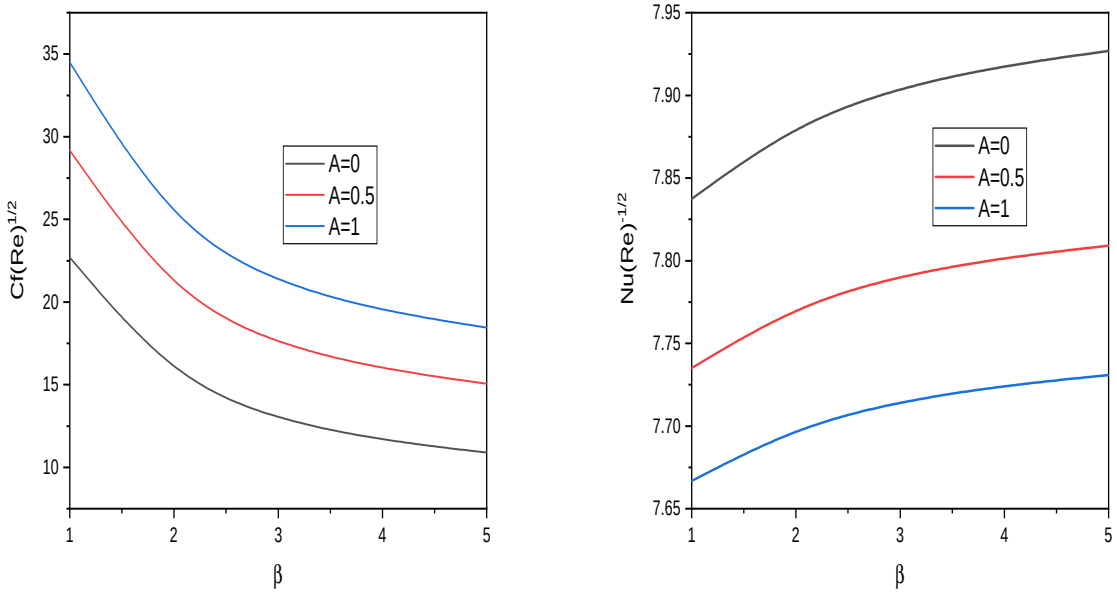

(a) (b)

Figure 8.11: "Effect of A on $C_f(Re)^{\frac{1}{2}}$ and $Nu(Re)^{\frac{-1}{2}}$"

Chapter 9

Cross Diffusion Effects on Mixed Convection of a Casson Fluid Flow Over a Thin Needle [1]

9.1 Introduction

Temperature gradients can cause mass flux, which is known as thermal diffusion, thermo-diffusion, or the Soret effect . The heat flux caused by a concentration gradient is known as the Dufour effect or diffusion-thermo effect. These impacts are usually regarded as a second-order effect and may become important in fields such as petrology, geosciences, hydrology, and so on. Waini et al. [43] investigated implications of Soret and Dufour on the stream of Al2O3-water nanoliquid through a narrow needle. Salleh et al.[44] scrutinized the consequences of Soret and Dufour on the convective stream near a moving slender needle. Rehman et al. [62] examined cross diffusive stream on moving tiny needle, focusing attention on the consequences of Soret and Dufour, heat absorption / generation, nonlinear heat radiation, thermal activation and chemical reaction properties. Reddy et al. [46] used the stream of hybrid (Al_2O_3-Cu/Ethylene glycol) Casson nanofluids over a moving tiny needle to analyze MHD, thermal radiation, and Dufour and Soret effects.

Literature reviews indicate that there is currently no published study on the investigation of Soret and Dufour effects in a mixed convection stream over a horizontal thin needle in Casson fluid. The purpose of this study is to determine how the heat transfer characteristics

[1] Communicated to "**Mathematics and Computers in Simulation**"

in a mixed convection are strongly explained by dimensionless parameters, specifically the needle size and mixed convection parameter.

9.2 Formulation of the Problem

Consider the laminar, steady, and mixed convection flow of Casson fluid over a horizontally moving thin needle. Assume that the uniform velocity of the fluid be $\bar{U_\infty}(\bar{x})$ and the moving velocity of the needle be $\bar{U_w}(\bar{x})$. Apart from the assumption of Chapter - 6, we assume the presence of Soret and DuFour effects in the medium.

The governing equations for the fluid flow are:

$$\frac{\partial(\bar{r}\bar{u})}{\partial\bar{x}} + \frac{\partial(\bar{r}\bar{v})}{\partial\bar{r}} = 0 \tag{9.1}$$

$$\bar{u}\frac{\partial\bar{u}}{\partial\bar{x}} + \bar{v}\frac{\partial\bar{u}}{\partial\bar{r}} = \bar{U}\frac{d\bar{U}}{d\bar{x}} + \nu\left(1+\frac{1}{\beta}\right)\frac{1}{\bar{r}}\frac{\partial}{\partial\bar{r}}\left(\bar{r}\frac{\partial\bar{u}}{\partial\bar{r}}\right) + g\beta_T(\bar{T}-T_\infty) + g\beta_C(\bar{C}-C_\infty) \tag{9.2}$$

$$\bar{u}\frac{\partial\bar{T}}{\partial\bar{x}} + \bar{v}\frac{\partial\bar{T}}{\partial\bar{r}} = \alpha\left(\frac{1}{\bar{r}}\frac{\partial}{\partial r}\left(\bar{r}\frac{\partial\bar{T}}{\partial\bar{r}}\right)\right) + \frac{D_s k_T}{c_s c_p}\frac{1}{\bar{r}}\frac{\partial}{\partial\bar{r}}\left(\bar{r}\frac{\partial\bar{C}}{\partial\bar{r}}\right) \tag{9.3}$$

$$\bar{u}\frac{\partial\bar{C}}{\partial\bar{x}} + \bar{v}\frac{\partial\bar{C}}{\partial\bar{r}} = D_m\left(\frac{1}{\bar{r}}\frac{\partial}{\partial r}\left(\bar{r}\frac{\partial\bar{C}}{\partial\bar{r}}\right)\right) + \frac{D_s k_T}{T_m}\frac{1}{\bar{r}}\frac{\partial}{\partial\bar{r}}\left(\bar{r}\frac{\partial\bar{T}}{\partial\bar{r}}\right) \tag{9.4}$$

where the quantities used in the above equations are already defined in Chapter - 2 and chapter - 6.

The boundary conditions are

$$\begin{aligned} \bar{u} = 0, \bar{v} = 0, \bar{T} = \bar{T_w}(\bar{x}), \bar{C} = \bar{C_w}(\bar{x}) \ \ at\ \bar{r} = \bar{R}(\bar{x}) \\ \bar{u} \to \bar{U}(\bar{x}), \bar{T} \to T_\infty, \bar{C} \to C_\infty \ \ at\ \bar{r} \to \infty \end{aligned} \tag{9.5}$$

The non-dimensional similarity variables are given by

$$\begin{aligned} x = \frac{\bar{x}}{L}, r = Re^{1/2}\frac{\bar{r}}{L}, R(x) = Re^{1/2}\frac{\bar{R}(\bar{x})}{L}, u = \frac{\bar{u}}{U_\infty}, \\ v = Re^{1/2}\frac{\bar{v}}{U_\infty}, U(x) = \frac{\bar{U}(\bar{x})}{U_\infty}, T = \frac{\bar{T}-T_\infty}{\Delta T}, T = \frac{\bar{C}-C_\infty}{\Delta C} \end{aligned} \tag{9.6}$$

Substituting Eq.(9.5) into Eq.(9.1) to (9.4), we get

$$\frac{\partial(ru)}{\partial x}+\frac{\partial(rv)}{\partial r}=0 \tag{9.7}$$

$$u\frac{\partial u}{\partial x}+v\frac{\partial u}{\partial r}=U\frac{dU}{dx}+\left(1+\frac{1}{\beta}\right)\frac{1}{r}\frac{\partial}{\partial r}\left(r\frac{\partial u}{\partial r}\right)+\lambda_T T++\lambda_C C \tag{9.8}$$

$$u\frac{\partial T}{\partial x}+v\frac{\partial T}{\partial r}=\frac{1}{Pr}\frac{1}{r}\frac{\partial}{\partial r}\left(r\frac{\partial T}{\partial r}\right)+D_f\frac{1}{r}\frac{\partial}{\partial r}\left(r\frac{\partial C}{\partial r}\right) \tag{9.9}$$

$$u\frac{\partial C}{\partial x}+v\frac{\partial C}{\partial r}=\frac{1}{Sc}\frac{1}{r}\frac{\partial}{\partial r}\left(r\frac{\partial C}{\partial r}\right)+Sr\frac{1}{r}\frac{\partial}{\partial r}\left(r\frac{\partial T}{\partial r}\right) \tag{9.10}$$

where λ is mixed convection parameter, $Pr=\dfrac{\nu}{\alpha}$ denotes the Prandtl number, $D_f=\dfrac{D_sK_T(C_w-C_\infty)}{C_sC_p\nu(T_w-T_\infty)}$ denotes the Dufour number, $Sr=\dfrac{D_sK_T(T_w-T_\infty)}{T_m\nu(C_w-C_\infty)}$ denotes the Soret number and $Sc=\dfrac{\nu}{D_s}$ denotes the Schmidt number.

The dimenaionless form of boundary conditions Eq.9.5 are

$$\begin{aligned} u=0,v=0,T=T_w(x),C=C_w(x)\ \ at\ r=R(x)\\ u\to U(x),T\to 0,C\to 0\ \ as\ r\to\infty \end{aligned} \tag{9.11}$$

Similarity Transformations are defined as:

$$\psi=xf(\eta),T(x)=x^{2m-1}\theta(\eta),\eta=x^{m-1}r^2 \tag{9.12}$$

Using Eq. (9.12) in the equation to the surface of the wall $\eta=a$, it can be written as $R=a^{1/2}x^{(1-m)/2}$ which characterizes shape and size of the needle.

Making use of above similarity variables in Eq.(9.8) to (9.10), we obtain

$$8\eta[1+\frac{1}{\beta}]f'''+8[1+\frac{1}{\beta}]f''+4ff''-4m(f')^2+m+\lambda_T\theta+\lambda_C\phi=0 \tag{9.13}$$

$$\frac{2\eta}{Pr}\theta''+\frac{2}{Pr}\theta'+D_f2\eta\phi''+2D_f\phi'+f\theta'-(2m-1)f'\theta=0 \tag{9.14}$$

$$\frac{2\eta}{Sc}\phi''+\frac{2}{Sc}\theta'+Sr2\eta\theta''+2Sr\theta'+f\phi'-(2m-1)f'\phi=0 \tag{9.15}$$

The modified conditions on boundary becomes

$$\begin{aligned} f^{'}(\eta) = 0, f(\eta) = 0, \theta(\eta) = 1, \phi(a) = 1 \quad at \quad \eta = a \\ f^{'}(\eta) \to \frac{1}{2}, \quad \theta(\eta) \to 0, \quad \phi(\eta) \to 0 \quad as \quad \eta \to \infty \end{aligned} \tag{9.16}$$

In additions to desired allotment for this model is Skin Friction C_f and the local Nusselt number Nu which are represented as:

$$\sqrt{Re}C_f = 8\sqrt{a}\left(1 + \frac{1}{\beta}\right) f^{''}(a), \frac{Nu}{\sqrt{Re}} = -2\sqrt{a}\theta^{'}(a), \frac{Sh}{\sqrt{Re}} = -2\sqrt{a}\phi^{'}(a) \tag{9.17}$$

9.3 Solution of the Problem

The combined Eqns. (9.13) to (9.15) and conditions on boundary (9.16) are linearized using the successive linearization method (SLM) [78] and the resulting linearized equations are solved by Chebyshev collocation method.

On applying the procedure explained in Chapter 2 to the equations Eqns. (9.13) to (9.15), we get the following linearized equations.

$$a_1 f_i^{'''} + a_2 f_i^{''} + a_3 f_i^{'} + a_4 f_i + a_5 \theta_i^{'} + a_6 \phi_i = r_1 \tag{9.18}$$

$$b_1 f_i^{'} + b_2 f_i + b_3 \theta_i^{''} + b_4 \theta_i{}' + b_5 \theta_i + b_6 \phi_i^{''} + b_7 \phi_i^{'} = r_2 \tag{9.19}$$

$$c_1 f_i^{'} + c_2 f_i + c_3 \theta_i^{''} + c_4 \theta_i{}' + c_5 \phi_i^{''} + c_6 \phi_i^{'} + b_7 \phi_i = r_3 \tag{9.20}$$

where

$$a_1 = 8\eta\left(1 + \frac{1}{\beta}\right), \quad a_2 = 8\left(1 + \frac{1}{\beta}\right) + 4\sum f_m,$$

$$a_3 = -8m\sum f_m', \quad a_4 = 4\sum f_m'',$$

$$a_5 = \lambda_T, \qquad a_6 = \lambda_C,$$

$$\begin{aligned} r_1 = -8\eta\left(1 + \frac{1}{\beta}\right)(\sum f_m''') - 8\left(1 + \frac{1}{\beta}\right)(\sum f_m'') + 4m(\sum f_m')^2 \\ -4(\sum f_m)(\sum f_m'') - \lambda_T(\sum \theta_m) - m - \lambda_C(\sum \phi_m) \end{aligned}$$

$$b_1 = -(2m-1)(\sum \theta_m), \quad b_2 = \sum \theta'_m, \quad b_3 = \frac{2\eta}{Pr}$$
$$b_4 = \frac{2}{Pr} + \sum f_m, \quad b_5 = -(2m-1)(\sum f'_m),$$
$$b_6 = 2\eta D_f, \quad b_7 = 2D_f,$$

$$r_2 = \frac{2\eta}{Pr}(\sum \theta''_m) - \frac{2}{Pr}(\sum \theta'_m) - 2\eta D_f(\sum \phi''_m) - 2D_f(\sum \phi'_m) - (\sum f_m)(\sum \theta'_m) + (2m-1)(\sum f'_m)(\sum \theta_m)$$

$$c_1 = -(2m-1)(\sum \phi_m), \quad c_2 = \sum \phi'_m, \quad c_3 = 2\eta Sr$$
$$c_4 = 2Sr, \quad c_5 = \frac{2\eta}{Sc}, \quad c_6 = \frac{2}{Sc} + \sum f_m$$
$$c_7 = -(2m-1)(\sum f'_m),$$

$$r_3 = -\frac{2\eta}{Sc}(\sum \phi''_m) - \frac{2}{Sc}(\sum \phi'_m) - 2\eta Sr(\sum \theta''_m) - 2Sr(\theta'_m) - (\sum f_m)(\sum \phi'_m) + (2m-1)(\sum f'_m)(\sum \phi_m)$$

As explained in Chapter - 2, using Chebyshev collocation method on the system of linearized equations. (9.18) t0 (9.20), we obtain the following equation in matrix form

$$A_{j-1}X_j = R_{j-1} \tag{9.21}$$

where A_{j-1} is a $3(N+1) \times 3(N+1)$ order matrix and X_j and R_{j-1} are $3(N+1) \times 1$ column matrix given by

$$A_{j-1} = \begin{pmatrix} A_{11} & A_{12} & A_{13} \\ A_{21} & A_{22} & A_{23} \\ A_{31} & A_{32} & A_{33} \end{pmatrix}, X_j = \begin{pmatrix} F_j \\ \Theta_j \\ \Phi_j \end{pmatrix}, R_{j-1} = \begin{pmatrix} r_{1,j-1} \\ r_{2,j-2} \\ r_{3,j-3} \end{pmatrix} \tag{9.22}$$

where

$$F_j = [f_i(\xi_0), f_i(\xi_1), ..., f_i(\xi_{N-1}), f_i(\xi_N)]^T,$$
$$\Theta_j = [\theta_i(\xi_0), \theta_i(\xi_1), .., \theta_i(\xi_{N-1}), \theta_i(\xi_N)]^T,$$
$$\Phi_j = [\phi_i(\xi_0), \phi_i(\xi_1), .., \phi_i(\xi_{N-1}), \phi_i(\xi_N)]^T,$$

$$A_{11} = a_1 D^3 + a_2 D^2 + a_3 D + a_4 I, A_{12} = O, A_{13} = O$$

$$A_{21} = b_1 I, A_{22} = b_2 D^2 + b_3 D, A_{23} = b_4 D^2 + b_5 D$$

$$A_{31} = c_1 I, A_{32} = c_2 D^2 + c_3 D, A_{33} = c_4 D^2 + c_5 D$$

$$r_1 = [r_1(\xi_0), r_1(\xi_1), ..., r_1(\xi_{N-1}), r_1(\xi_N)]^T,$$

$$r_2 = [r_2(\xi_0), r_2(\xi_1), ..., r_2(\xi_{N-1}), r_2(\xi_N)]^T,$$

$$r_3 = [r_3(\xi_0), r_3(\xi_1), ..., r_3(\xi_{N-1}), r_3(\xi_N)]^T$$

With the boundary conditions imposed in terms of the collocation points, the answer is given by

$$X_j = A_{j-1}^{-1} R_{j-1}$$

9.4 Results and Discussion

The seven dimensionless parameters: size of the needle (a), mixed convection parameter (λ_1, λ_2), casson fluid parameter (β), power index (m), Dufour number (Df), Soret number (Sr) on velocity and temperature profiles together with local Nusselt number $\frac{Nu}{\sqrt{Re}}$, Sherwood number $\frac{Sh}{\sqrt{Re}}$ and coefficient of local skin friction $\sqrt{Re}C_f$ are the focus of this study. A detailed numerical parametric analysis is conducted to assure a greater comprehension of the technical issue, and the findings are presented graphically (Figs. 9.1-9.12). Different values of a, λ_1, λ_2, β, m, Df, and Sr have been taken to analyze the effects numerically.

Figure 9.1 illustrates how the needle's size affects the velocity and temperature profiles. As shown in Fig.9.1(a), reducing a elevates the velocity. As a rises, the temperature and concentration are also increasing, as presented in Figs. 9.1(b) and 9.1(c).

The fluctuation of velocity, temperature, and concentration with the Casson fluid parameter β is shown in Fig.9.2. As the Casson fluid parameter increases, velocity increases, as illustrated in Fig. 9.2(a). As depicted in Figs. 9.2(b) and 9.2(c), the impact β on temperature and concentration profile is almost negligible.

The consequence of power index m on velocity, temperature, and concentration is given in Fig. 9.3. It is represented in Fig. 9.3(a) that the velocity improves as the power index parameter rises. The temperature and concentration profiles are also enhanced with a decrease in m, as depicted in Figs. 9.3(b) and 9.3(c).

The fluctuation of profiles of velocity, temperature, and concentration with mixed convection parameters λ_1 and λ_2 is given in the Figs. 9.4 and 9.5. As presented in Figs. 9.4(a) and 9.5(a), intensifying λ_1 and λ_2, increase velocity. The effect of λ_1 and λ_2 on temperature and concentration is negligible, as depicted in Figs. 9.4(b),9.4(c),9.5(b) and 9.5(c)

The impact of the Dufour number (Df) on velocity, temperature, and concentration is given in Fig. 9.6. It is detected from Figs. 9.6(a) and 9.6(c) that the impact of Df on velocity and concentration is almost negligible. As displayed in Fig. 9.6(b), the temperature profile enhances with intensifying the Dufour number.

Figure 9.7 presents the effect of the Soret number on velocity, temperature, and concentration. As displayed in Figs. 9.7(a) and 9.7(b), velocity and temperature profile relative to Sr are constant. The concentration increases as Sr rises as depicted in Fig. 9.7(c)

The impact of the size of the needle on the coefficient of skin friction $\sqrt{Re}C_f$, Nusselt number $\frac{Nu}{\sqrt{Re}}$, and Sherwood number $\frac{Sh}{\sqrt{Re}}$ are presented in Fig. 9.8. As depicted in Fig.9.8(a), the skin friction coefficient is improved by lowering a. As a increases, $\frac{Nu}{\sqrt{Re}}$ and $\frac{sh}{\sqrt{Re}}$ are also enhancing, as presented in Figs. 9.8(b) and 9.8(c)

The impact of m on the local rate of heat transfer $\frac{Nu}{\sqrt{Re}}$, the Sherwood number $\frac{Sh}{\sqrt{Re}}$, and the coefficient of local skin friction $\sqrt{Re}C_f$ are given in Fig. 9.9. It is understood from Fig. 9.9(a) that the $\sqrt{Re}C_f$ enhances as m rises.Figs. 9.9(b) and 9.9(c) demonstrate that a rise in m leads to an enhancement in $\frac{Nu}{\sqrt{Re}}$ and $\frac{Sh}{\sqrt{Re}}$.

The fluctuation of $\frac{Nu}{\sqrt{Re}}$, $\sqrt{Re}C_f$, and $\frac{Sh}{\sqrt{Re}}$ with mixed convection parameters λ_1 and λ_2 is given in the Figs. 9.10, 9.11. As presented in Figs. 9.10(a) and 9.11(a), the values of λ_1 and λ_2 increase the skin friction coefficient. Nusselt number and Sherwood number are enhanced by increases in λ_1 and λ_2, as seen in Figs.9.10(b), 9.11(b), 9.10(c), and 9.11(c).

The effect of Dufour number Df on $\frac{Nu}{\sqrt{Re}}$, $\sqrt{Re}C_f$, and $\frac{Sh}{\sqrt{Re}}$ is given in Fig. 9.12. It is noticed from Fig. 9.12(b) that the $\frac{Nu}{\sqrt{Re}}$ enhances as Df increases. Figs. 9.12(a) and 9.12(c) exhibit that the variation in the $\sqrt{Re}C_f$ independent of Df and $\frac{Sh}{\sqrt{Re}}$ is slightly increased.

Figure 9.13. presents variations of Soret number Sr on the $\frac{Nu}{\sqrt{Re}}$, $\sqrt{Re}C_f$, and $\frac{Sh}{\sqrt{Re}}$. The variation in the $\sqrt{Re}C_f$ is independent of Sr, as depicted in Figs. 9.13(a). As Sr increases, $\frac{Nu}{\sqrt{Re}}$ increases, as illustrated in Fig. 9.13(b). As Sr increases, $\frac{Sh}{\sqrt{Re}}$ decreases, as illustrated in Fig. 9.13(c).

9.5 Conclusion

This study examines the influence of Soret and Dufour on the mixed convection flow through a horizontal needle in Casson fluid. The flow equations are converted into a set of non-linear ordinary differential equations by appropriate transformations, and these equations are subsequently linearized using successive linearizations. The solution to the resulting equations is found via the Chebyshev spectral collocation technique.

- Temperature and concentration reduce, and skin friction coefficient, Nusselt number, Sherwood number, and velocity increase with increasing power index.
- A rise in Df leads to a rise in temperature and concentration profiles.
- An upsurge in Sr produces a rise in temperature and concentration distribution.
- The implications of Df and Sr on the Nusselt and Sherwood numbers are in reverse.

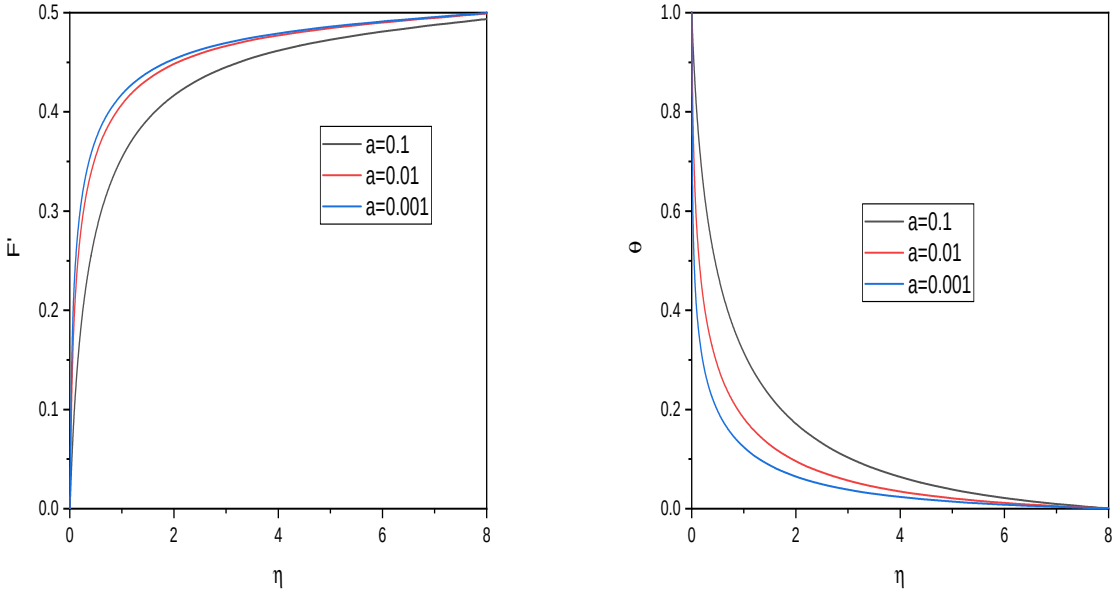

(a)

(b)

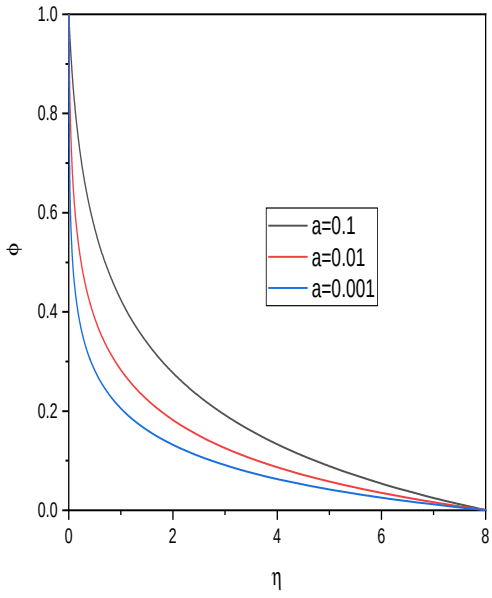

(c)

Figure 9.1: "Effect of a on the velocity,temperature and concentration profiles"

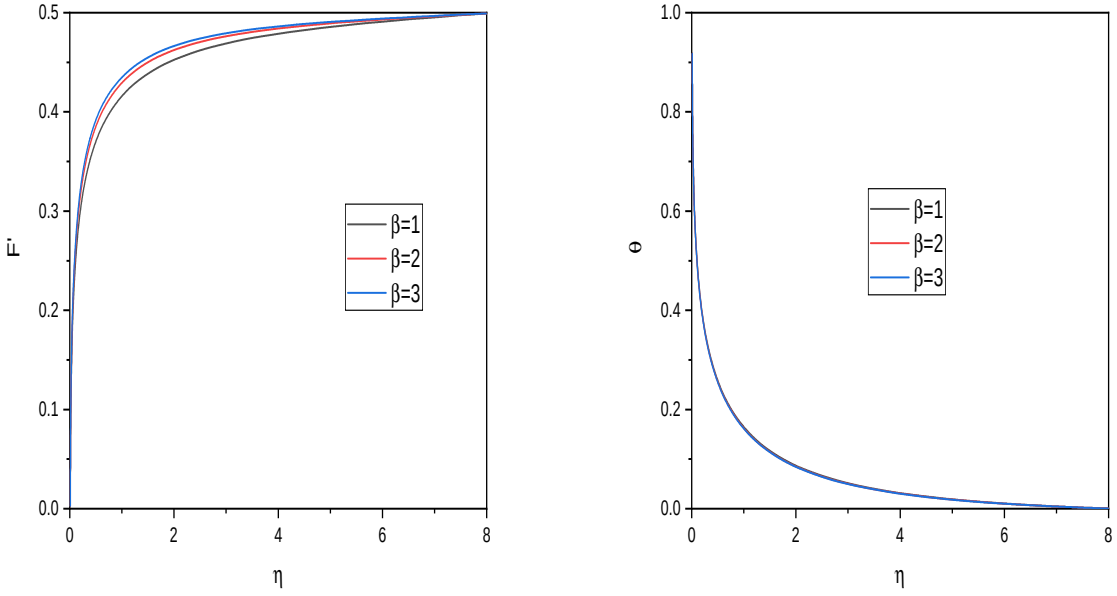

(a) (b)

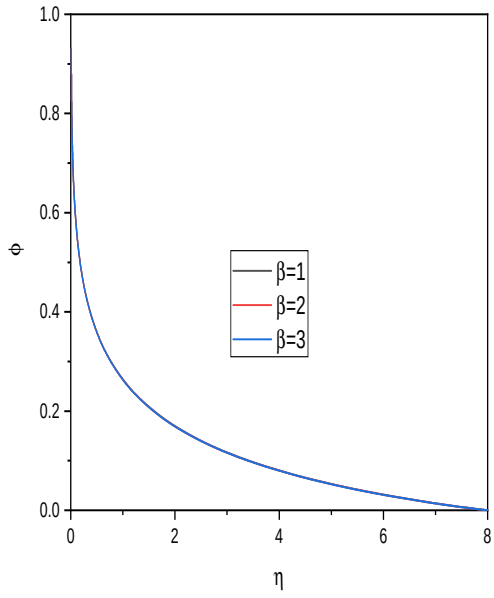

(c)

Figure 9.2: "Effect of β on the velocity,temperature and concentration profiles"

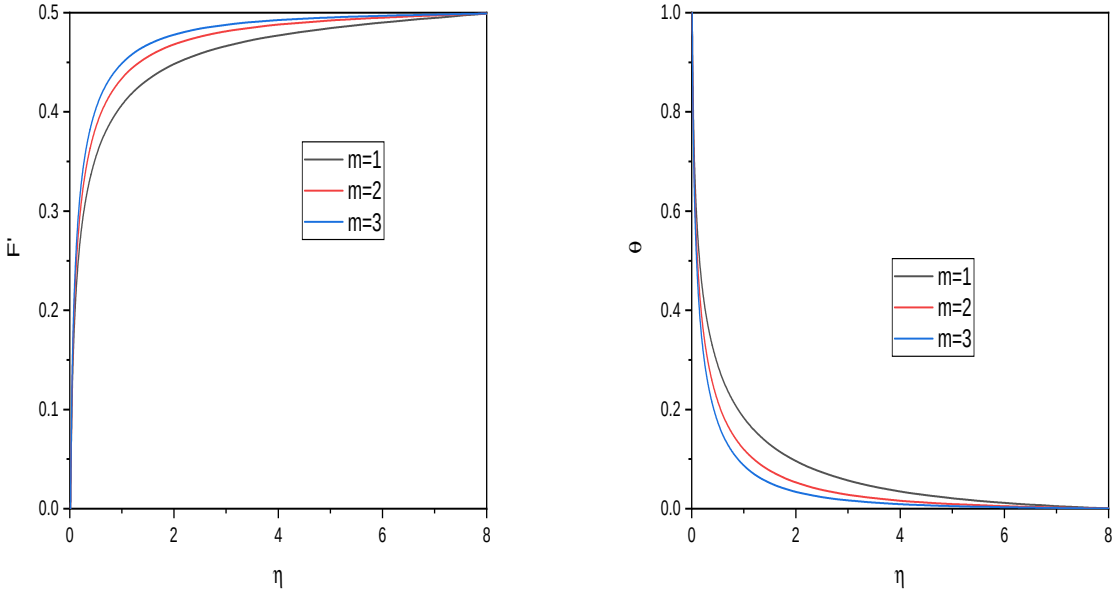

(a)

(b)

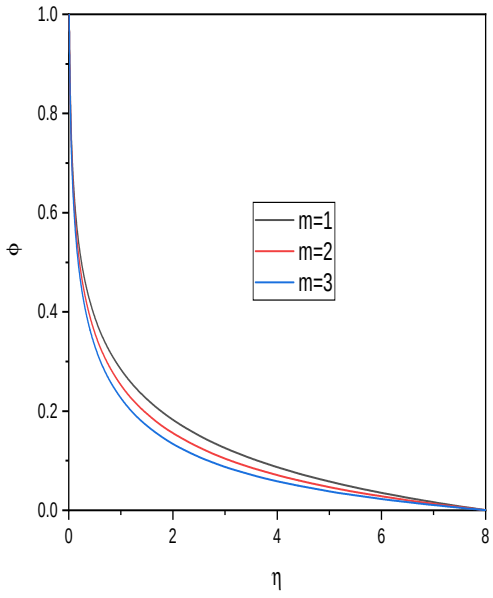

(c)

Figure 9.3: "Effect of m on the velocity,temperature and concentration profiles"

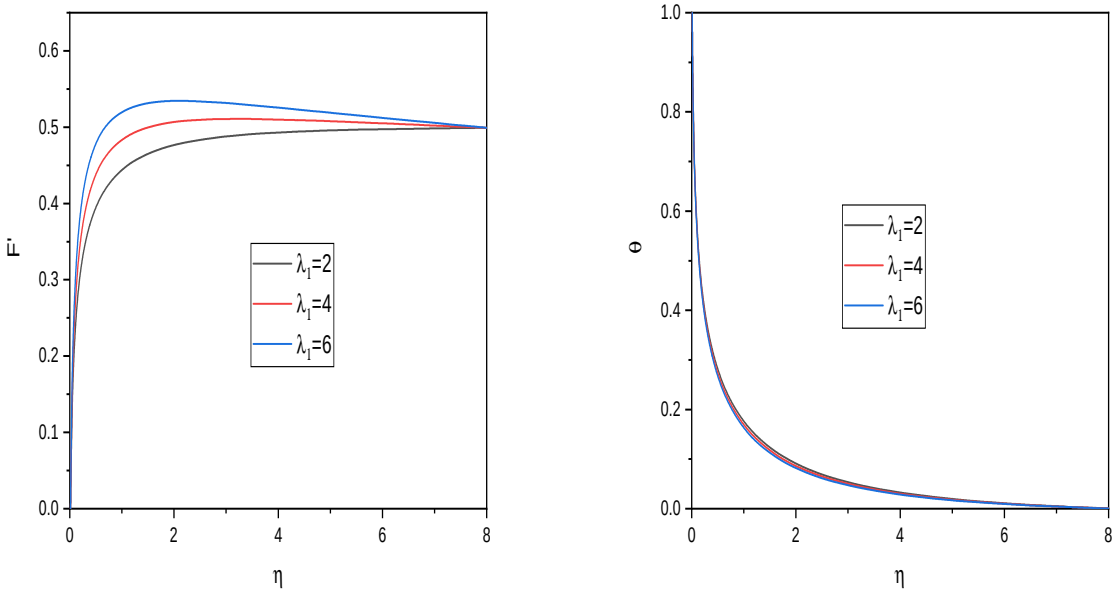

(a) (b)

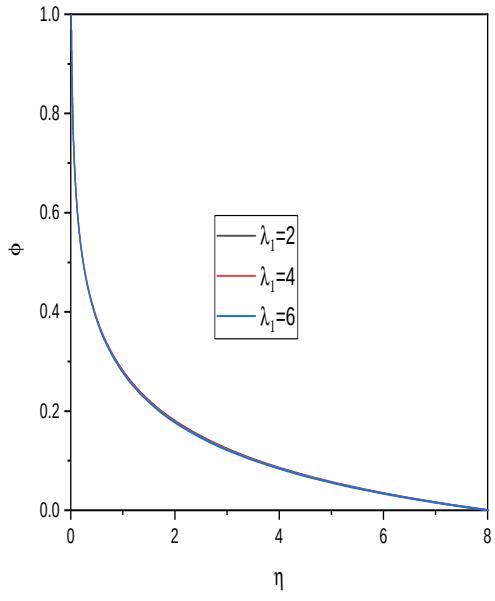

(c)

Figure 9.4: "Effect of $\lambda 1$ on the velocity,temperature and concentration profiles"

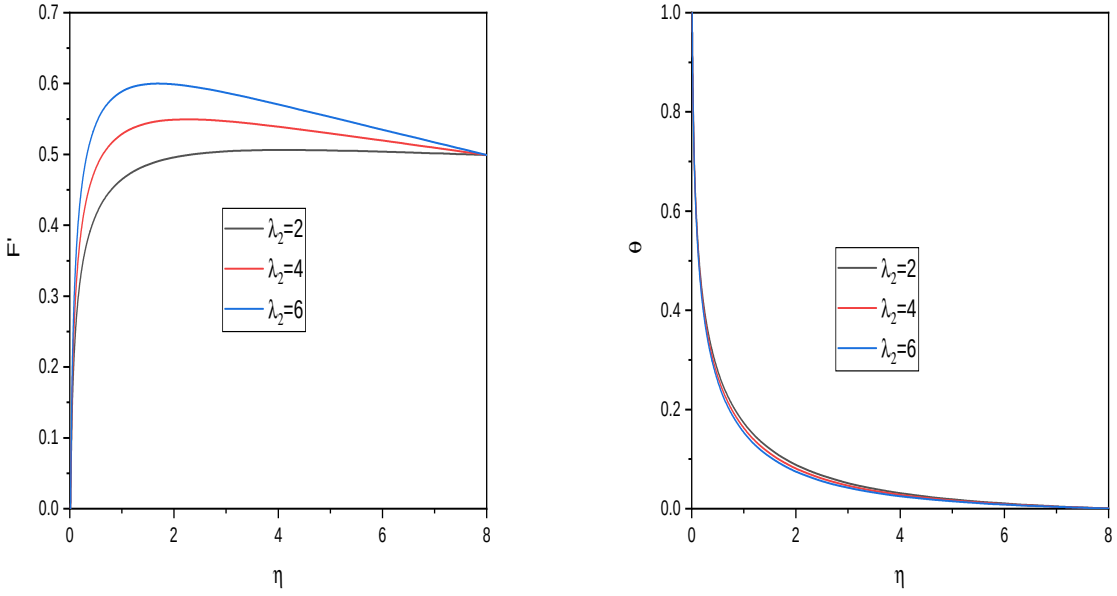

(a)

(b)

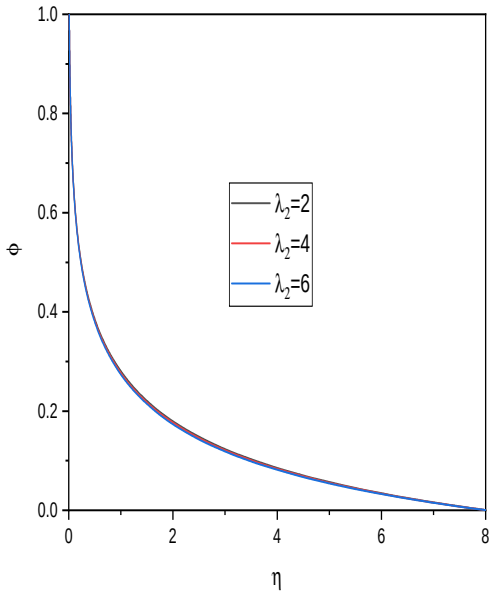

(c)

Figure 9.5: "Effect of $\lambda 2$ on the velocity,temperature and concentration profiles"

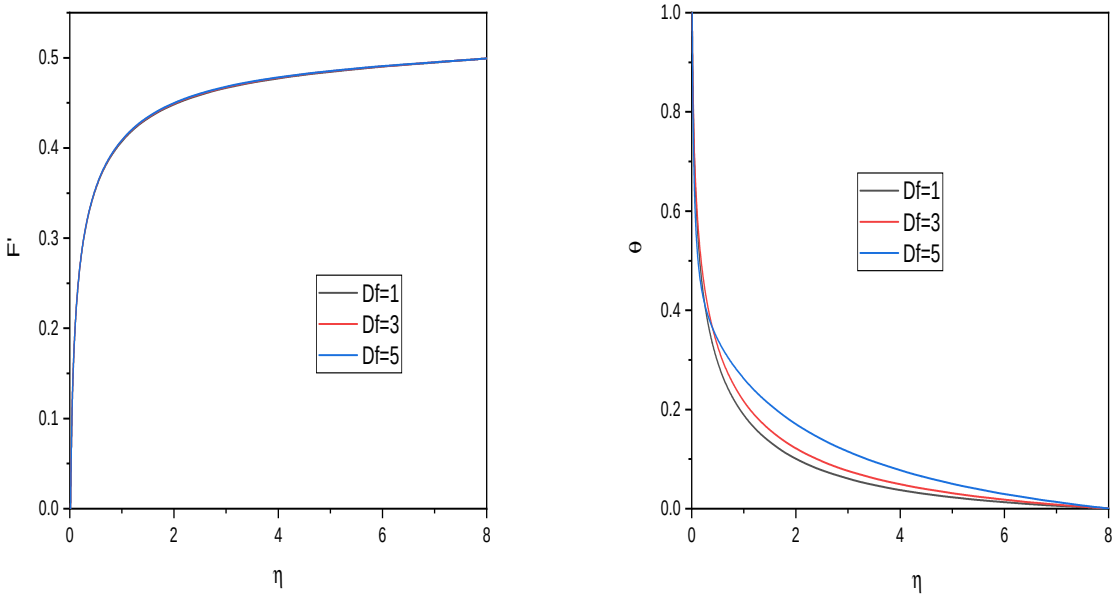

(a)

(b)

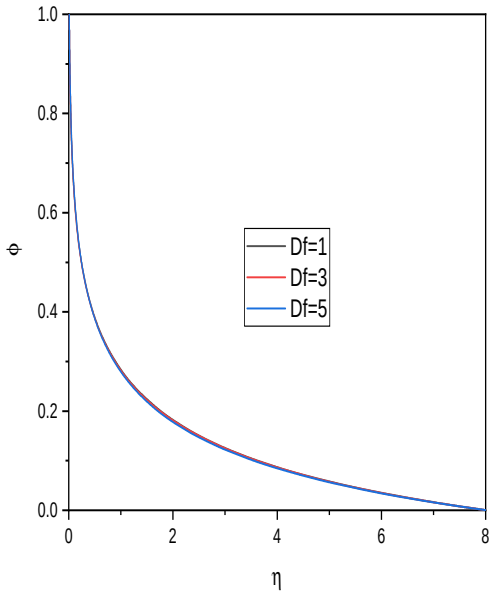

(c)

Figure 9.6: "Effect of Df on the velocity,temperature and concentration profiles"

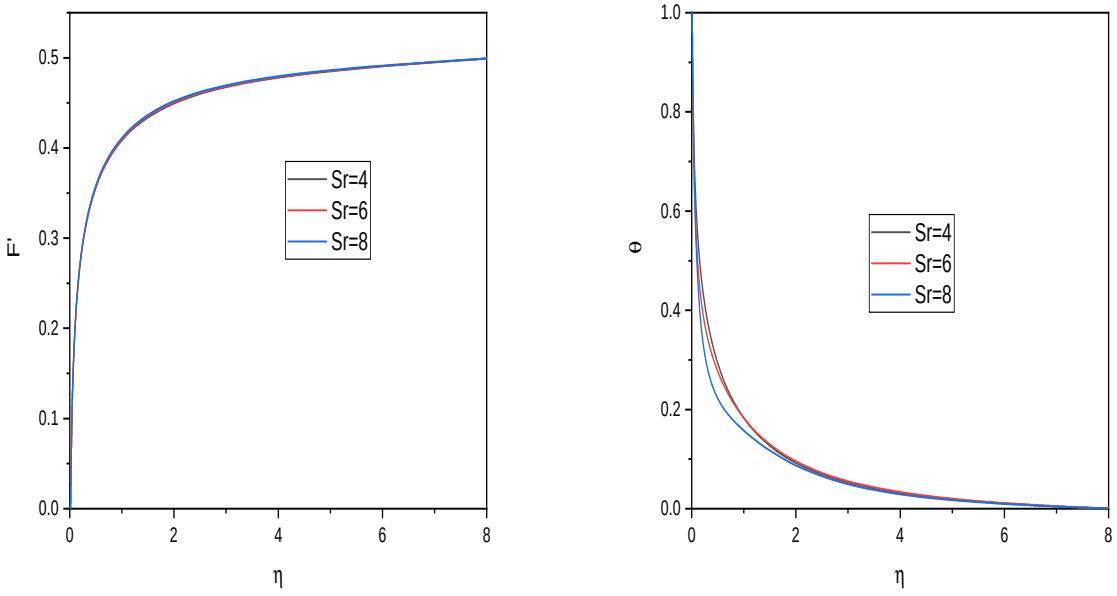

(a) (b)

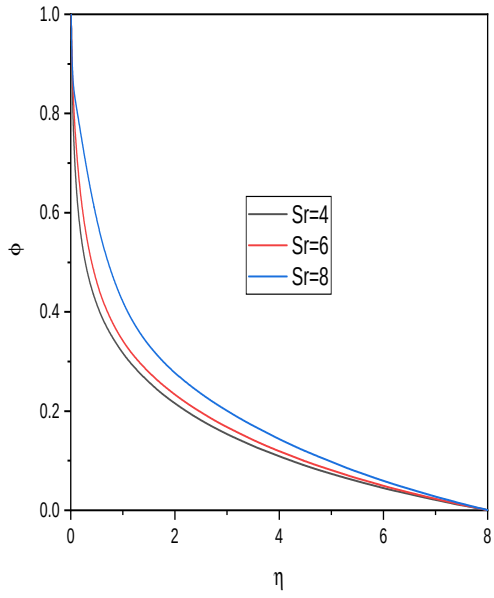

(c)

Figure 9.7: "Effect of Sr on the velocity,temperature and concentration profiles"

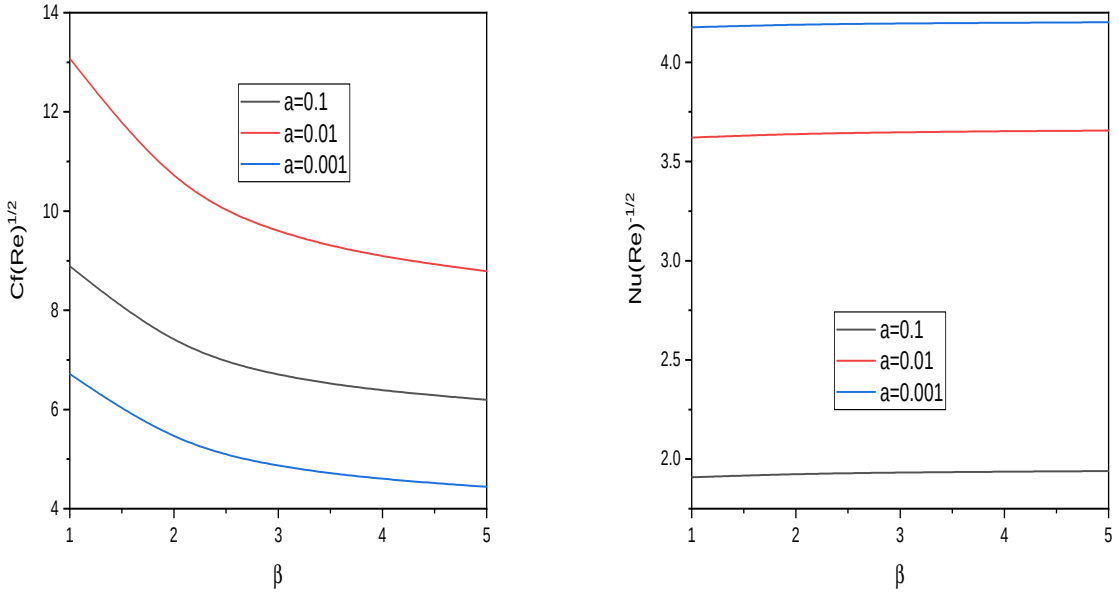

(a)

(b)

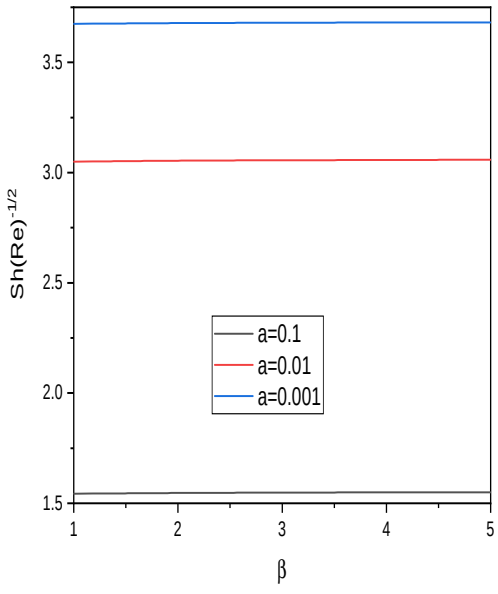

(c)

Figure 9.8: "Effect of a on the coefficient of skin friction, Nusselt number and Sherwood number"

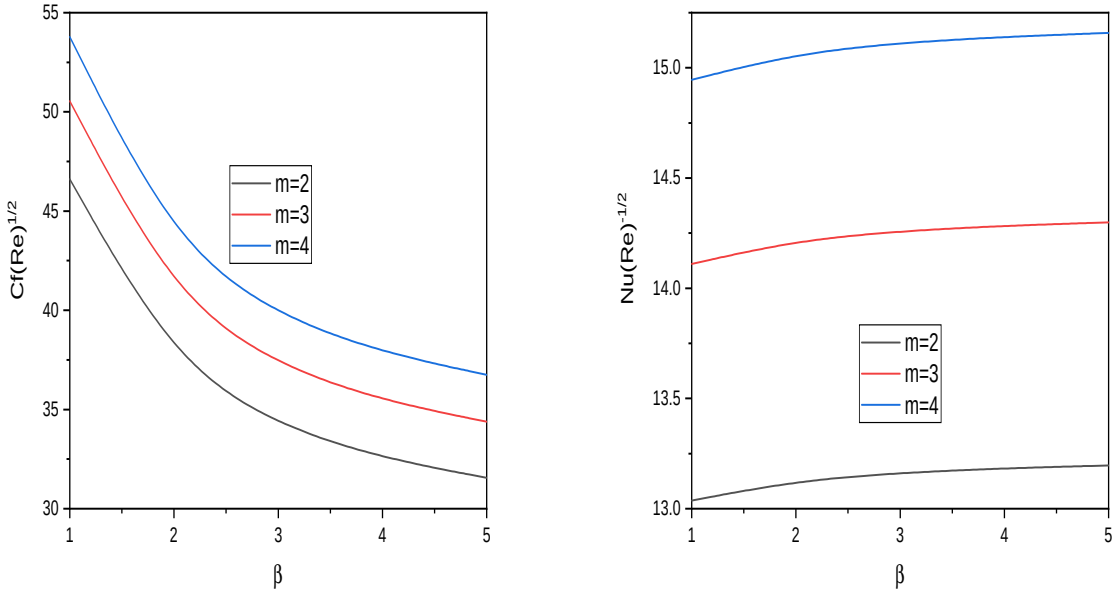

(a)

(b)

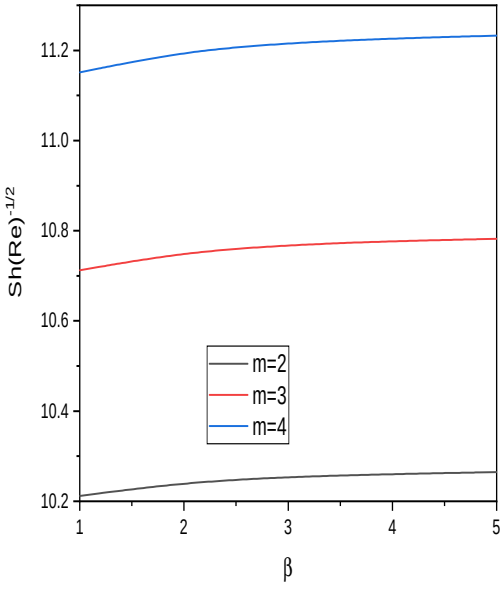

(c)

Figure 9.9: "Effect of m on the coefficient of skin friction, Nusselt number and Sherwood number"

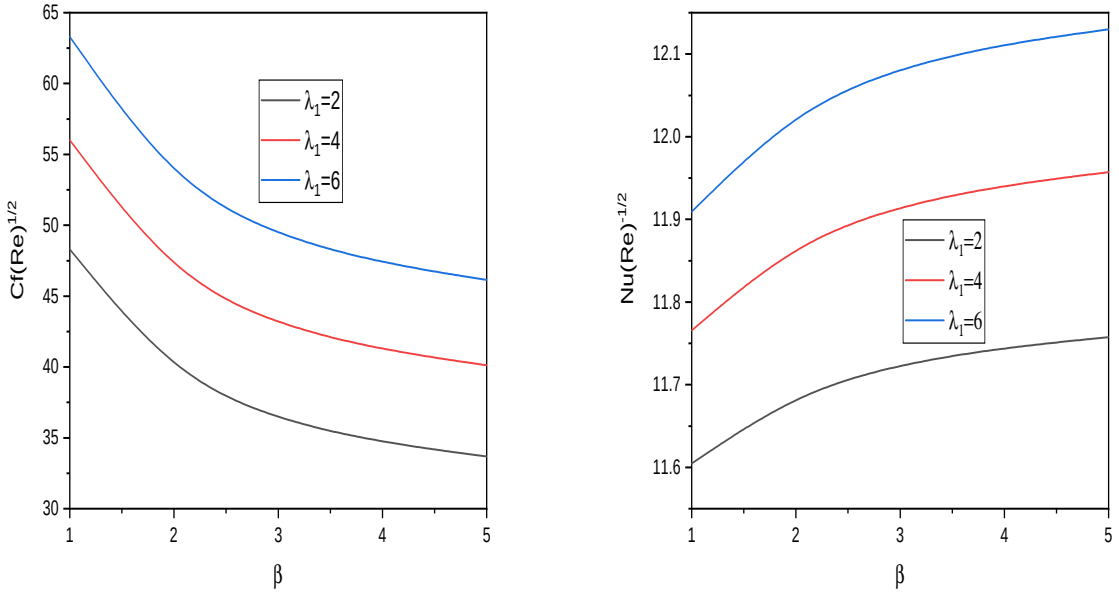

(a) (b)

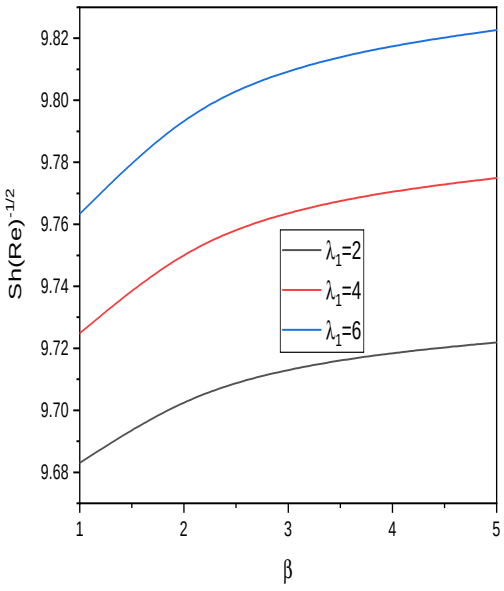

(c)

Figure 9.10: "Effect of λ_1 on the coefficient of skin friction, Nusselt number and Sherwood number"

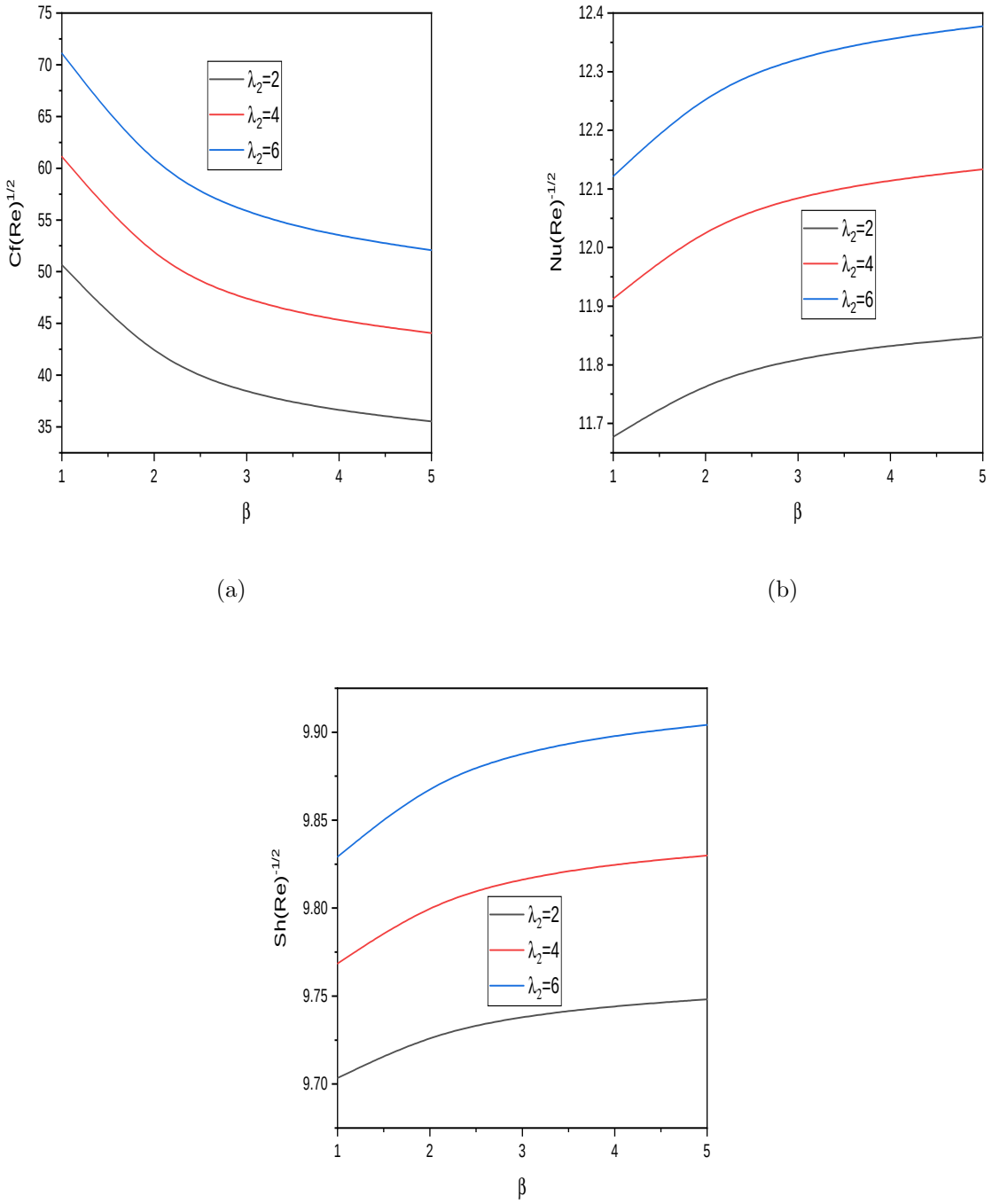

Figure 9.11: "Effect of λ_1 on the coefficient of skin friction, Nusselt number and Sherwood number"

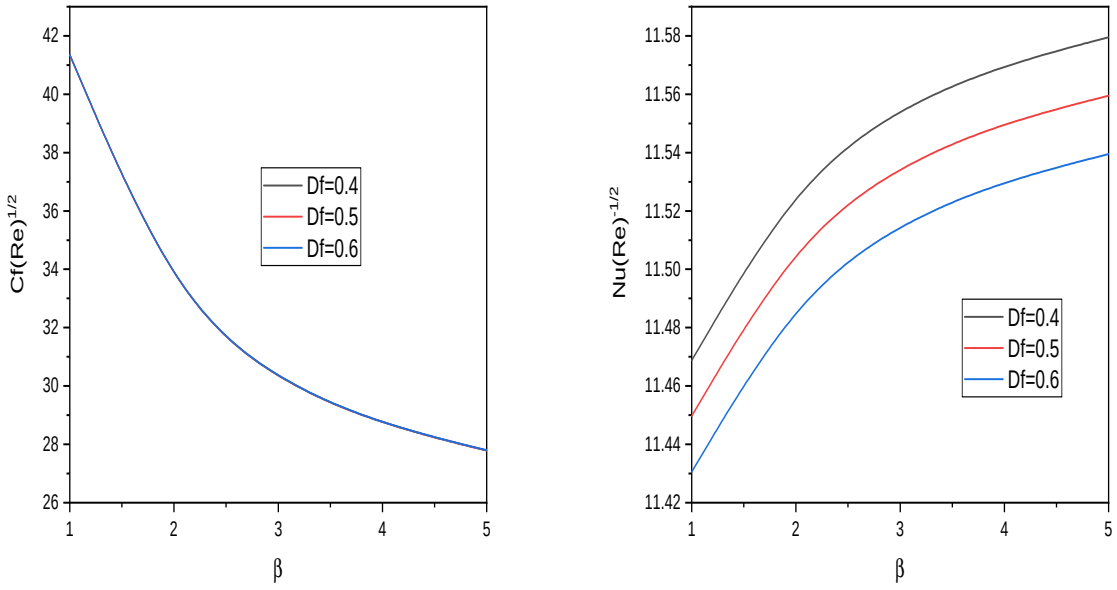

(a)

(b)

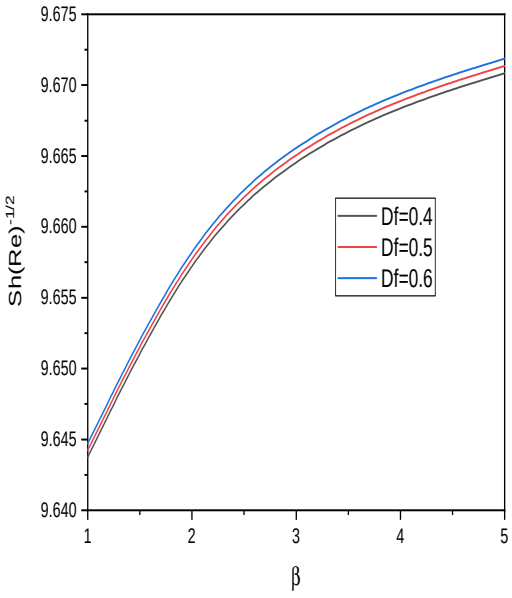

(c)

Figure 9.12: "Effect of Df on the coefficient of skin friction, Nusselt number and Sherwood number"

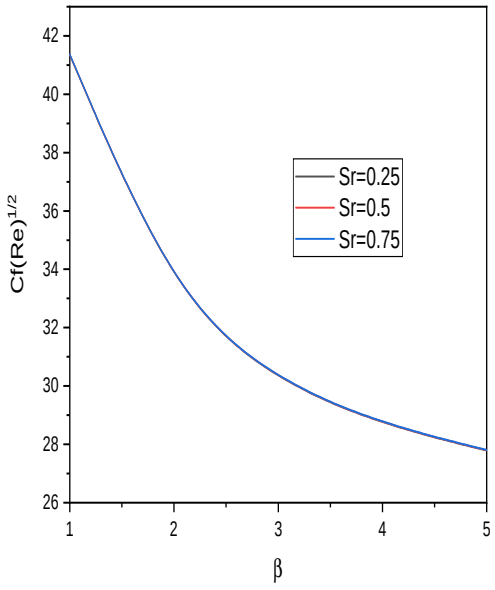

(a)

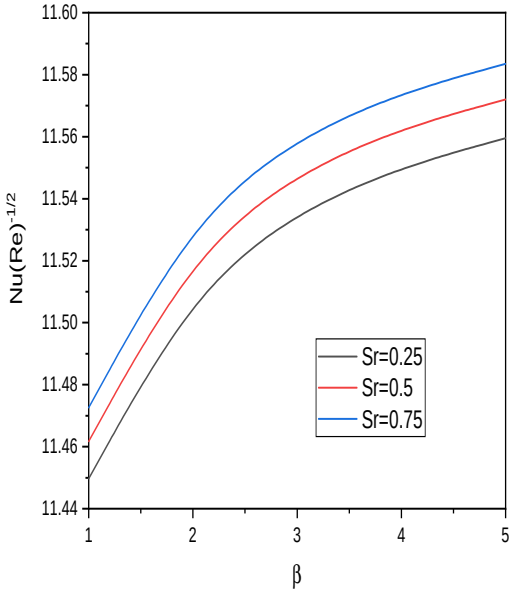

(b)

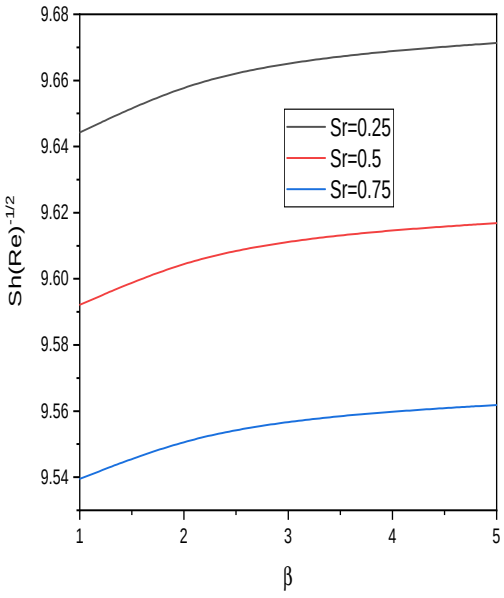

(c)

Figure 9.13: "Effect of Sr on the coefficient of skin friction, Nusselt number and Sherwood number"

Part IV

SUMMARY AND CONCLUSIONS

Chapter 10

Summary and Conclusions

In this thesis, incompressible Casson fluid flow over a horizontal, thin needle is considered. The equations governing the flow in Chapters 2 through 9 are transformed into a system of nonlinear ordinary differential equations using suitable transformations. The non-linear ordinary differential equations were linearized by using the successive linearization method. The solution to the resulting equations is obtained by the Chebyshev collocation method.

The natural convection flow past a thin needle in a Casson fluid is studied in Part II. The objective of this part is to study the effects of variable properties such as Soret and Dufour, radiation, viscous dissipation, and chemical reactions on velocity, temperature, concentration, skin friction coefficients, the Nusselt number, and the Sherwood number. The important observations made in this study are listed below:

- As the needle size decreases, the velocity profile increases, and as the Casson fluid parameter increases, it decreases.
- The velocity rises and the heat transfer rate reduces with an improvement in the viscosity parameter.
- A rise in the thermal conductivity parameter leads to an increase in velocity, temperature, and heat transfer rate.
- The velocity reduces and temperature, and concentration improve with the increase in size of the needle.
- A rise in Df steers to a rise in temperature and concentration profiles.

- An upsurge in Sr produces a rise in temperature and concentration distribution.
- Skin friction coefficient, local heat, and mass transfer coefficients reduce with enhanced needle size.
- The implications of Df and Sr on the Nusselt and Sherwood numbers are in reverse.
- While the concentration, temperature, and velocity of the flow rise as the needle size increases, the skin friction coefficient, heat transfer coefficient, and Sherwood number decrease.
- With improved concentration distribution, the chemical reaction parameter decreases, and with an increased chemical reaction parameter, the Sherwood number rises.
- The temperature rises as the radiation parameter is improved, whereas the Nusselt number rises as the radiation parameter is reduced.

Part III deals with mixed convection flow past a thin needle in a Casson fluid. Examining the effects of magnetic, heat source, chemical reaction, variable properties, Soret, and Dufour on velocity, temperature, concentration profiles, skin friction coefficients, heat, and mass transfer rates are the objectives of this section. The main observations of these studies are

- As the needle size decreases, the velocity, coefficient of skin friction, and Nusselt number enhance in both cases, while the temperature drops.
- Increasing λ causes the velocity to increase in the aiding case and decrease in the opposing case. While the influence of the mixed convection parameter on temperature is insignificant,.
- For both assisting and opposing scenarios, when the power index grows, velocity increases and temperature declines.
- As size of the needle reduces, velocity and the coefficient of skin friction improve, whereas temperature, the Nusselt number, and the Sherwood number decrease.
- Intensifying the magnetic parameter decreases the velocity, whereas the effect of the magnetic parameter on temperature and concentration is negligible.
- Temperature and velocity both improve as needle size grows, while the Nusselt number and the coefficient of skin friction both drop.

- Temperature rises and skin friction coefficient, Nusselt number, and velocity decrease with increasing thermal conductivity parameter.
- Temperature reduces and skin friction coefficient, Nusselt number, and velocity increase with increasing power index.
- Increasing the variable viscosity parameter and decreasing the Nusselt number leads to improvements in velocity and the coefficient of skin friction.
- With increasing needle size, temperature, concentration, Nusselt number, and Sherwood number increase, while velocity and the coefficient of skin friction decrease.
- Temperature and concentration reduce, and skin friction coefficient, Nusselt number, Sherwood number, and velocity increase with increasing power index.
- A rise in Df steers to a rise in temperature and concentration profiles.
- An upsurge in Sr produces a rise in temperature and concentration distribution.
- The implications of Df and Sr on the Nusselt and Sherwood numbers are in reverse.

The work presented in the thesis can be extended to analyze the various effects like MHD, Hall effect, Hall and ion slip, binary chemical reaction, etc. Further, this work can be extended by studying the analysis in various non-Newtonian fluids, like Jeffrey fluids and Power-law fluids. This work can also be extended to porous media.

The transverse curvature introduces nonsimilarity into the flow and thermal fields. For example, flow over a needle of very large diameter is similar to flat plate boundary layer flow. As the curvature increases, or the diameter of the needle decreases, the work presented in the thesis can be extended by taking nonsimilar effects into account.

In the recent past, the study of stability analysis has attracted the curiosity of many researchers. Thus, the work presented in the thesis can be extended to study the stability of boundary layer flows in Newtonian and/or non-Newtonian fluids.

Bibliography

[1] Casson, N. "A flow equation for pigment-oil suspensions of the printing ink type." In: Rheology of disperse systems, Mill CC (Ed.) Pergamon Press, Oxford, 22 (1959), 84–102.

[2] Prandtl, L., "Uber Flussigkeitsbewegungen bei sehr kleiner Reibung, in Verhandlungen des III. Internationalen Mathematiker Kongresses", 484–491, Heidelberg, Germany, 1904.

[3] Eckeret, E.R.G., Drake, R.M., "Analysis of heat and mass transfer", McGraw Hill, Newyork, 1972.

[4] Cebeci,T. and Bradshaw,P., "Physical and computational aspects of convective heat transfer", New York: Springer-Verlag, 1984.

[5] Bejan, A., "Convection Heat Transfer", John Wiley., New York, 2004

[6] Soret, C., "Influence de la temperature sur la distribution des sels dans leurs solutions", C.R. Acad. Sci., Paris, 91:289–291, 1880.

[7] WM Kays and Crawford ME. Convective heat and mass transfer, Vol. 4, McGraw-Hill New York, 1980.

[8] Herwig H, and Wickern G (1986) The effect of variable properties on laminar boundary layer flow. Wärme-und Stoffübertragung 20(1): 47-57.

[9] ZG Makukula, P Sibanda, and SS Motsa, A novel numerical technique for two dimensional laminar flow between two moving porous walls, Mathematical Problems in Engineering, 2010:15, 2010.

[10] SS Motsa and P Sibanda, A new algorithm for solving singular ivps of lane-emden type, Proceedings of the 4^{th} International Conference on Applied Mathematics, Simulation and Modelling, pages 176–180, 2010.

[11] ZG Makukula, SS Motsa, and P Sibanda, On a new solution for the viscoelastic squeezing flow between two parallel plates, J. of Adv. Research in Appl. Math, 2:31–38, 2010.

[12] ZG Makukula, P Sibanda, and SS Motsa., A note on the solution of the von karman equations using series and chebyshev spectral methods., Boundary Value Problems, 471793, 2010.

[13] S Shateyi and SS Motsa. Variable viscosity on magnetohydrodynamic fluid flow and heat transfer over an unsteady stretching surface with hall effect., Boundary Value Problems, 2010:1–20, 2010.

[14] FG Awad, P Sibanda, SS Motsa, and OD Makinde. Convection from an inverted cone in a porous medium with cross-diffusion effects., Computers and Mathematics with Applications, 61:1431–1441, 2011.

[15] C. Canuto, MY Hussaini, A Quarteroni, and TA Zang, Spectral methods fundamentals in single domains, Springer, Berlin, 2006.

[16] C Canuto, MY Hussaini, A Quarteroni, and TA Zang. Spectral methods: evolution to complex geometries and applications to fluid dynamics, Springer Science & Business Media, 2007.

[17] WS Don and A Solomonoff. Accuracy and speed in computing the chebyshev collocation derivative. SIAM J. Sci. Comput., 16:1253–1268, 1995.

[18] LN Trefethen., Spectral methods in MATLAB, SIAM.

[19] Lee, L.L., "Boundary layer over a thin needle", Phys. Fluids 10, 820–822, 1967

[20] Narain, J.P. and Uberoi, M.S., "Forced heat transfer over a thin needle", J. Heat Transf. Transactions of the ASME 94, 240-242, 1972.

[21] Narain, J.P. and Uberoi, M.S., "Free-convection heat transfer from a thin vertical needle", Phys. Fluids 15,928–929, 1972.

[22] Narain, J.P. and Uberoi, M.S., "Combined forced and free-convection over thin needles", International Journal of Heat and Mass Transfer 16.8 (1973): 1505-1512.

[23] Soid, S.K., Ishak, A., and Pop, I., Boundary layer flow past a continuously moving thin needle in a nanofluid, Applied Thermal Engineering, Vol 114, 2017, pp. 58-64.

[24] Qasim, M., Riaz, N., and Lu, D. Flow over a Needle Moving in a Stream of Dissipative Fluid Having Variable Viscosity and Thermal Conductivity. Arab J Sci Eng 46, 7295–7302 (2021). https://doi.org/10.1007/s13369-021-05352-w

[25] Prashar, P., Ojjela, O., and Kambhatla, P.K. Numerical investigation of boundary layer flow past a thin heated needle immersed in a hybrid nanofluid. Indian J Phys 96, 137–150 (2022).

[26] Nazar, T., Bhatti, M.M. and Michaelides, E.E. Hybrid (Au-TiO2) nanofluid flow over a thin needle with magnetic field and thermal radiation: dual solutions and stability analysis. Microfluid Nanofluid 26, 2 (2022).

[27] Souayeh, B., Reddy, M.G., Sreenivasulu, P., Poornima, T., Rahimi-Gorji, Md. e,f, Alarifi I.M., Comparative analysis on non-linear radiative heat transfer on MHD Casson nanofluid past a thin needle, Journal of Molecular Liquids 284, 163–174, 2019.

[28] Ibrar, N., Reddy, M. G., Shahzad, S.A., Sreenivasulu, P. and Poornima, T., Interaction of single and multi-walls carbon nanotubes in magnetized-nano Casson fluid over radiated horizontal needle. SN Appl. Sci. 2, 677 (2020).

[29] Hamid A., Terrific effects of Ohmic-viscous dissipation on Casson nanofluid flow over a vertical thin needle: buoyancy assisting & opposing flow. Journal of Materials Research and Technology, 9(5), 11220–11230, 2020.

[30] Bilal, M.; Urva, Y. Analysis of non-Newtonian fluid flow over a fine rotating thin needle for variable viscosity and activation energy. SN Appl. Sci. 2020, 2, 677.

[31] Naveen Kumar, R., Punith Gowda, R J, Madhukesh, J K, Prasannakumara B C, and G K Ramesh, Impact of thermophoretic particle deposition on heat and mass transfer across the dynamics of Casson fluid flow over a moving thin needle, Physica Scripta, 96(7), (2021) : 075210

[32] Prashar, P., Ojjela, O., Kambhatla, P.K.: Impact of needle size and distinct flow conditions on thermal performance of TiO2–MWCNTs hybrid nanofluid flow past thin needle using Casson fluid model. Z Angew Math Mech. 103, (2023) : e202100456

[33] Akinshilo, A.T., Mabood, F., legbusi, A.O., Heat generation and nonlinear radiation effects on MHD Casson nanofluids over a thin needle embedded in porous medium, International Communications in Heat and Mass Transfer 127, 105547, 2021.

[34] Herwig H, and Wickern G (1986) The effect of variable properties on laminar boundary layer flow. Wärme-und Stoffübertragung 20(1): 47-57.

[35] Animasaun I L, Adebile E A, and Fagbade, A I (2016) Casson fluid flow with variable thermo-physical property along exponentially stretching sheet with suction and exponentially decaying internal heat generation. J Nigerian Math Society 35(1):1-17

[36] Mondal R K, Reza-E-Rabbi S, Gharami P.P, Ahmmed S F and Arifuzzaman S M (2019). A simulation of Casson fluid flow with variable viscosity and thermal conductivity effects. Mathematical Modelling of Engineering Problems 6(4):625-633.

[37] Sivaraj R, Benazir A J, Srinivas S, and Chamkha A J (2019) Investigation of cross-diffusion effects on Casson fluid flow in existence of variable fluid properties. Eur. Phys. J. Spec. Top. 228:35–53.

[38] Prasad K V, Vaidya H, Rajashekhar C, Khan S U, Manjunatha G and Viharika J U (2020) Slip flow of MHD Casson fluid in an inclined channel with variable transport properties, Communications in Theoretical Physics. 72(9): 095004

[39] Govindaraj N, Iyyappan G, Singh A K, Shukla P, and Roy S A (2022) computational study on the MHD Casson fluid flow with thermal radiation and variable physical properties under the influence of Soret and Dufour effects. Heat Transfer. 51: 5857- 5873.

[40] Eckert E. R. G. and Drake, R. M., "Analysis of Heat and Mass Transfer". McGraw Hill, New York, 1972

[41] Soret, C., "Influence de la temperature sur la distribution des sels dans leurs solutions", C.R. Acad. Sci., Paris, 91:289–291, 1880.

[42] Shojaei, A., Amiri, A. J., Ardahaie, S. S., Hosseinzadeh, K. and Ganji, D. D. Hydrothermal analysis of non-Newtonian second grade fluid flow on radiative stretching cylinder with Soret and Dufour effects. Case Stud. Therm. Eng. 13, 100384 (2019).

[43] Waini, I., Ishak, A., and Pop, I. Dufour and Soret effects on Al2O3- water nanofluid flow over a moving thin needle: Tiwari and Das model. Int. J. Numer. Methods Heat Fluid Flow (2020).

[44] Salleh, S N A., Bachok, N M Arifin, F M Ali, Influence of Soret and Dufour on forced convection flow towards a moving thin needle considering Buongiorno's nanofluid model, Alexandria Engineering Journal (2020) 59, 3897–3906

[45] Rehman, M.I.U., Chen, H., Hamid, A., Aayyum, S., Raizah, Z, Eid M. R., snf Din E.S.M.T.E Soret and Dufour influences on forced convection of Cross radiative nanofluid flowing via a thin movable needle. Sci Rep 12 (2022), 18666.

[46] Reddy, V.S.; Kandasamy, J.; Sivanandam, S. Impacts of Casson Model on Hybrid Nanofluid Flow over a Moving Thin Needle with Dufour and Soret and Thermal Radiation Effects. Math. Comput. Appl. 2023, 28, 2.

[47] Khan MI, Waqas M, Hayat T, Alsaedi A., A comparative study of Casson fluid with homogeneous-heterogeneous reactions. Journal of colloid and interface science, 498, 85–90. pmid:28319844, 2017

[48] Afridi MI, Qasim M. Entropy generation and heat transfer in boundary layer flow over a thin needle moving in a parallel stream in the presence of nonlinear Rosseland radiation. Int J Therm Sci, 123: 117–128, 2018.

[49] Sulochana C, Ashwinkumar GP, Sandeep N (2018) Boundary layer analysis of persistent moving horizontal needle in magnetohydrodynamic ferrofluid: A numerical study. Alexandria engineering journal, 57(4), 2559–2566.

[50] Raju SS, Kumar KG, Rahimi-Gorji M, Khan I, Darcy–Forchheimer flow and heat transfer augmentation of a viscoelastic fluid over an incessant moving needle in the presence of viscous dissipation. Microsystem Technologies, 25(9), 3399–3405, 2019.

[51] Upreti H, Kumar M. Influence of non-linear radiation, Joule heating and viscous dissipation on the boundary layer flow of MHD nanofluid flow over a thin moving needle. Multidiscip Model Mater, 16: 208–224, 2020.

[52] Nayak, MK, Mabood, F, Makinde, OD. Heat transfer and buoyancy-driven convective MHD flow of nanofluids impinging over a thin needle moving in a parallel stream influenced by Prandtl number. Heat Transfer. 2020; 49: 655–672.

[53] Khan A, Kumam W, Khan I, Saeed A, Gul T, Kumam P, and Ali I., Chemically reactive nanofluid flow past a thin moving needle with viscous dissipation, magnetic effects and hall current. PLoS ONE 16(4): e0249264, 2021.

[54] Sultana, J., Ferdows,M., Shamshuddin, MD and Zaimi, K. “Effects of Solar Radiation and Viscous Dissipation on Mixed Convective Non-Isothermal Hybrid Nanofluid over Moving Thin Needle”. Journal of Advanced Research in Micro and Nano Engineering 3 (1):1-11, 2021.

[55] Ali B, Jubair S, Fathima D, Akhter A, Rafique K, Mahmood Z. MHD flow of nanofluid over moving slender needle with nanoparticles aggregation and viscous dissipation effects. Science Progress. 2023;106(2).

[56] Wang, C.Y.: Mixed convection on a vertical needle with heated tip. Phys. Fluids A 2 (1990), pp. 622–625.

[57] S. Ahmad, N.M. Arifin, R. Nazar, I. Pop, Mixed convection boundary layer flow along vertical thin needles: Assisting and opposing flows, International Communications in Heat and Mass Transfer, 35(2) (2008), pp.157-162

[58] Ahmad, S., et al. "Mixed convection boundary layer flow along vertical moving thin needles with variable heat flux." Heat and mass transfer 44.4 (2008): pp.473-479.

[59] Trimbitas, R., Grosan, T., and Pop, I. "Mixed convection boundary layer flow along vertical thin needles in nanofluids", International Journal of Numerical Methods for Heat and Fluid Flow (2014).pp.579-594.

[60] Salleh, S.N.A.; Bachok, N.; Arifin, N.M.; Ali, F.M.; Pop, I.: Stability analysis of mixed convection flow towards a moving thin needle in nanofluid. Appl. Sci. 8 (2018), pp. 1–16.

[61] Qasim, M.; Afridi, M.I.: Effects of energy dissipation and variable thermal conductivity on entropy generation rate in mixed convection flow. J. Therm. Sci. Eng. Appl. 10 (2018), 044501.

[62] Rehman, M.I.U., Chen, H., Hamid, A., Aayyum, S., Raizah, Z, Eid M. R., snf Din E.S.M.T.E Soret and Dufour influences on forced convection of Cross radiative nanofluid flowing via a thin movable needle. Sci Rep 12 (2022), 18666.

[63] Raza J, Rohni AM, Omar Z (2016) Multiple solutions of mixed convective MHD casson fluid flow in a channel. J Appl Math., Volume 2016, Article ID 7535793

[64] Kataria, H. R., and Patel, H. R., Radiation and chemical reaction effects on MHD Casson fluid flow past an oscillating vertical plate embedded in porous medium, Alexandria Engineering Journal,Vol. 55 (1), 2016, Pages 583-595

[65] Ahmed, N., Khan, U., Khan, S. I., Bano, S., Mohyud-Din, S. T., Effects on magnetic field in squeezing flow of a Casson fluid between parallel plates, Journal of King Saud University - Science, Volume 29, Issue 1, 2017, 119-125,

[66] Jain, S., and Parmar, A., Multiple slip effects on inclined MHD Casson fluid flow over a permeable stretching surface and a melting surface. Int. J. Heat Technol. 36, 585–594 (2018).

[67] Senapati, M., Swain, K. and Parida, S. K. Numerical analysis of three-dimensional MHD flow of Casson nanofluid past an exponentially stretching sheet. Karbala Int. J. Mod. Sci. 6(1), 13.

[68] Raghunath, K. and Obulesu, M. Unsteady MHD oscillatory Casson fluid flow past an inclined vertical porous plate in the presence of chemical reaction with heat absorption and Soret effects. Heat Transf. 51(3), 1–19, (2021).

[69] Saeed A, Algehyne EA, Aldhabani MS, Dawar A, Kumam P, Kumam W (2022) Mixed convective flow of a magnetohydrodynamic Casson fluid through a permeable stretching sheet with first-order chemical reaction. PLoS ONE 17(4): e0265238.

[70] Rasheed, H. U. , Islam S, Zeeshan, Khan W, Khan J, Abbas T. Numerical modeling of unsteady MHD flow of Casson fluid in a vertical surface with chemical reaction and Hall current. Advances in Mechanical Engineering. 2022;14(3).

[71] Umavathi, J. C., Prakasha, D. G., Alanazi, Y. M., Lashin, M. A. M., Al-Mubaddel, F.S., Raman Kumar, and Punith Gowda, R. J., Magnetohydrodynamic squeezing Casson nanofluid flow between parallel convectively heated disks. Int. J. Mod. Phys. B., Vol. 37(4), Article ID2350031 (2023)

[72] Arruna Nandhini, C., Jothimani, S. and Chamkha, A.J. Effect of chemical reaction and radiation absorption on MHD Casson fluid over an exponentially stretching sheet with slip conditions: ethanol as solvent. Eur. Phys. J. Plus 138, 68 (2023).

[73] Mythili, D.,and Sivaraj, R., Influence of higher order chemical reaction and non-uniform heat source/sink on casson fluid flow over a vertical cone and flat plate, J. Mol. Liq., 216, 466 - 475 (2016).

[74] Makinde, O. D.,and Rundora, L., Unsteady mixed convection flow of a reactive casson fluid in a permeable wall channel filled with a porous medium, Defect Diffus., 377, 166 - 179, (2017),

[75] Zia, Q., Ullah, I., Waqas, Alsaedi, M. A., and Hayat, T.,Cross diffusion and exponential space dependent heat source impacts in radiated three-dimensional (3d) flow of casson fluid by heated surface, Results Phys, 8, 1275 - 1282 (2018),

[76] Goud, B. S., Kumar, P. P., and Malga, B. S., Effect of heat source on an unsteady mhd free convection flow of Casson fluid past a vertical oscillating plate in porous medium using finite element analysis, Partial Differential Equations in Applied Mathematics, 2, 100015 (2020),

[77] Awais, M., Raja, M. A. Z., Awan, S. E., Shoaib, M., and Ali, H. M., Heat and mass transfer phenomenon for the dynamics of casson fluid through porous medium over shrinking wall subject to lorentz force and heat source/sink, Alex. Eng. J., 60(1), 1355 - 1363, (2021).

[78] Motsa S.S, and Shateyi S. "Successive Linearisation Solutiony of Free Convection Non-Darcy Flow with Heat and Mass Transfer." Advanced topics in mass transfer 19 (2011): 425-438.

[79] Canuto, C., Hussaini, M. Y., Quarteroni, A., and Zang, T. A., Spectral Methods in Fluid Dynamics, Springer-Verlag, Berlin, 1988.